EFFECT OF TEMPERATURE ON THE WIDE ANGLE X-RAY DIFFRACTION OF NANOCRYSTALLINE TRIACYLGLYCEROLS

by

Xiyan Deng

Submitted in partial fulfillment of the requirements
for the degree of Master of Science

at

Dalhousie University
Halifax, Nova Scotia
December 2014

TABLE OF CONTENTS

LIST OF TABLES

LIST OF FIGURES

ABSTRACT

The peak position of wide angle x-ray diffraction patterns of nanocrystalline triacylglycerols is affected by the temperature. To observe this effect quantitatively, pure triacylglycerols and triacylglycerol mixtures were crystallized in a desired polymorph in capillaries or a Couette system. The crystallized samples were kept at different temperatures and shear rates. The detailed WAXD patterns were obtained using in-house x-ray and synchrotron x-ray sources. When the temperature increased, the d-spacing for the peaks with small d-spacing increased as well. However, the d-spacing for other peaks remained unchanged or just had a very small change. The relationship between differences of d-spacing for the peaks with small d-spacing and temperature can be used to estimate the real sample temperature, especially under higher shear rate. This provides a new way to monitor and control the temperature of the system under study and the effect of high shear rate on nanocrystalline triacylglycerol crystallization.

LIST OF ABBREVIATIONS USED

ANL	Argonne National Laboratory
APS	Advanced Photon Source
CCC	Tricaprin
CCD	Charge-Coupled Device
DCL	Double Chain Length Structure
DSC	Differential Scanning Calorimetry
FA	Fatty acid
FOT	Fiber Optic Temperature Sensor
FWHM	Full Width at Half Maximum
GUI	Graphical User Interface
LD	Lamellar Distance
LLL	Trilaurin
LS	Liquid Signal
MMM	Trimyristin
NMR	Nuclear Magnetic Resonance
PPP	Tripalmitin
SAXD	Small Angle x-ray Diffraction
SF	Solid Fraction
SR-XRD	Synchrotron Radiation x-ray Diffraction
SS	Solid Signal
SSS	Tristearin
TAG	Triacylglycerols

TCL	Triple Chain Length Structure
TEC	Thermoelectric Cooler
WAXD	Wide Angle x-ray Diffraction
XRD	x-ray Diffraction
3L7M	30% trilaurin: 70% trimyristin triacylglycerol mixture by weight
5L5M	50% trilaurin: 50% trimyristin triacylglycerol mixture by weight
5L5S	50% trilaurin: 50% tristearin triacylglycerol mixture by weight
7L3M	70% trilaurin: 30% trimyristin triacylglycerol mixture by weight
3M7P	30% trimyristin: 70% tripalmitin triacylglycerol mixture by weight
5M5P	50% trimyristin: 50% tripalmitin triacylglycerol mixture by weight
7M3P	70% trimyristin: 30% tripalmitin triacylglycerol mixture by weight
3P7S	30% tripalmitin: 70% tristearin triacylglycerol mixture by weight
5P5S	50% tripalmitin: 50% tristearin triacylglycerol mixture by weight
7P3S	70% tripalmitin: 30% tristearin triacylglycerol mixture by weight
6B4P	60% tributyrin: 40% tripalmitin triacylglycerol mixture by weight
6B4S	60% tributyrin: 40% tristearin triacylglycerol mixture by weight
γ	shear rate
q	reciprocal lattice spacing ($Å^{-1}$)
T	temperature of crystallization (K)
θ	incident angle of x-rays
ΔG	change in Gibbs energy (J)
λ	wavelength of x-rays (Å)
d	The lamellar spacing of crystal planes

ACKNOWLEDGEMENTS

Firstly I would like to gratefully acknowledge my supervisor Dr. Gianfranco Mazzanti, for his encouragement, guidance, inspiration, and patience for not only my project, but also my life. I also want to thank my advisory team Dr. Jan Haelssig and Dr. Benedict Newling (University of New Burnswick) for their guidance and assistance for my thesis. To my research colleagues, Omar Qatami, Amro Alkhudair, Pavan Batchu, Pranav Arora, Mohit Kalaria, Liangle Lin, Rong Liu and Yujing Wang, your very insightful discussions made this work possible and enjoyable. I am grateful to Ray Dube for the assistance of experiment setup and the undergraduate project member Shenglin Yao for all the related assistance. I also want to thank DND-CAT staffs in Argonne National Laboratory, especially Steven Weigand and James Rix, for their help in experiment setup and operation of x-ray beamline.

Deepest thanks to my parents, who give birth to me, raise me, teach me and support me, for their endless love to me. It is my parents that make all the wonderful things happen in my life. Words cannot express how much I love you both.

My appreciation goes to my friends and other family members for their kindness and generous supports. One page is not enough to name you all.

CHAPTER 1 INTRODUCTION

With the development of society, people have never lost their interest in finding novel methods to prepare food. People expect food to bring more pleasure to their lives. Therefore, food scientists and technologists devote themselves to advance the science of food and ensure a safe and abundant food supply. The food industry is doing its best to satisfy the need of providing good texture and taste of food products. The understanding of food ingredients and the methods to modify and manipulate the ingredients to get better food are more and more important. Luckily, food science provides us with a large platform to achieve better food.

Dietary fat is one of the main nutrients for humans. Dietary fat provides people with energy storage resources. More importantly, it provides essential fatty acids to help regulate body functions and carry the fat-soluble vitamins. From the point of view of food, dietary fat is also an important ingredient in many daily foods, such as chocolate, margarine, butter, spreads and baked products. Dietary fat provides a creamy texture and special mouth feel of the products. It also plays a critical role in food structures. Fat crystallization, the formation of solid fat crystals, always occurs during the industrial manufacturing and the storage of the fat-based foods. It has a great impact in the texture, shelf life and food quality of the fat-based foods (Metin and Hartel, 2005). In order to improve the quality and the ability of fat-based foods to meet the current market demands, a better understanding of the fat crystallization process of dietary fat from physics, chemistry and biochemistry is needed (Sato et al., 1999).

Many researches show that the sensorial attributes of many common fat-based foods are derived from the network structure of the crystalline fat (Narine and Marangoni, 1999,

Wright et al., 2000, Mazzanti et al., 2005). Many sensorial attributes, such as texture, spread ability and mouthfeel, are dependent on the mechanical strength of the fat crystal network (Narine and Marangoni, 1999). Some factors play an important role in determining the crystallized fat structure, such as the solid fat content, microstructure of the crystal and the types of polymorph. The processing conditions, such as crystallization temperatures, shear rates and cooling rates, have great effects on the fat crystallization.

The complexity of natural fats in the fat-based foods limits the accuracy of manufacturing and results in uncertain quality of the products. This research aims to observe the behaviour of nanostructure during the lipid crystallization process under several constant temperatures and shear rates using x-ray diffraction techniques. It was noticed in previous studies that the peak position of wide angle x-ray diffraction (WAXD) patterns is affected by the temperature (Mazzanti, unpublished). In order to observe this effect quantitatively, crystallization of different kinds of triacylglycerols (TAGs) and their mixtures, which are normally the main or critical components of the food products, are studied at different controlled temperatures and shear flow. This thesis describes how different WAXD peaks change their position as the temperature changes and provides a new attempt to study the change of sample temperature when a shear rate is applied. It is particularly interesting that the anisotropy of the nanocrystals is evident by these changes. The findings of this research should help future studies of academic researchers and the food industry to develop a deeper knowledge of lipid crystallization, leading to better products and manufacturing procedures.

1.1 Objectives

The general research aim of our lab is to gain a better and wider understanding of the

characteristics of the triacylglycerols crystallizing under different temperatures and shear rates.

The specific objectives of this Thesis are:

- To study how different WAXD peaks of the pure triacylglycerol crystals change their position as the temperature changes.
- To observe how different WAXD peaks of triacylglycerol mixture crystals with difference proportions change their position when the temperature changes.
- To investigate how the WAXD peaks of triacylglycerol crystals change their position under shear when the temperature changes under different shear rates.
- To compare the change of WAXD peaks of triacylglycerol crystals with and without shear.
- To utilize WAXD vs. temperature as an intrinsic thermometer to study the thermomechanical increase of temperature at high shear rates.

CHAPTER 2 LITERATURE REVIEW

2.1. Fat Crystallization

In the food industry, fat crystallization has been applied in two ways: one is to process fat crystal containing products, such as chocolates and margarine; the other one is to separate specific fats and liquid materials from natural resources (Sato, 2001). Fat molecules rearrange themselves to form a solid crystalline lattice from a supersaturated liquid or solution. Fat crystallization is a kinetic process in which the lipid melt must be significantly supercooled to start crystallization.

As shown in Figure 2-1, triacylglycerol (TAG) molecules crystallize from the melt via mass and heat transfer to form crystals which then aggregate to particles, larger clusters, until a three dimensional space filling network forms (Acevedo and Marangoni, 2010).

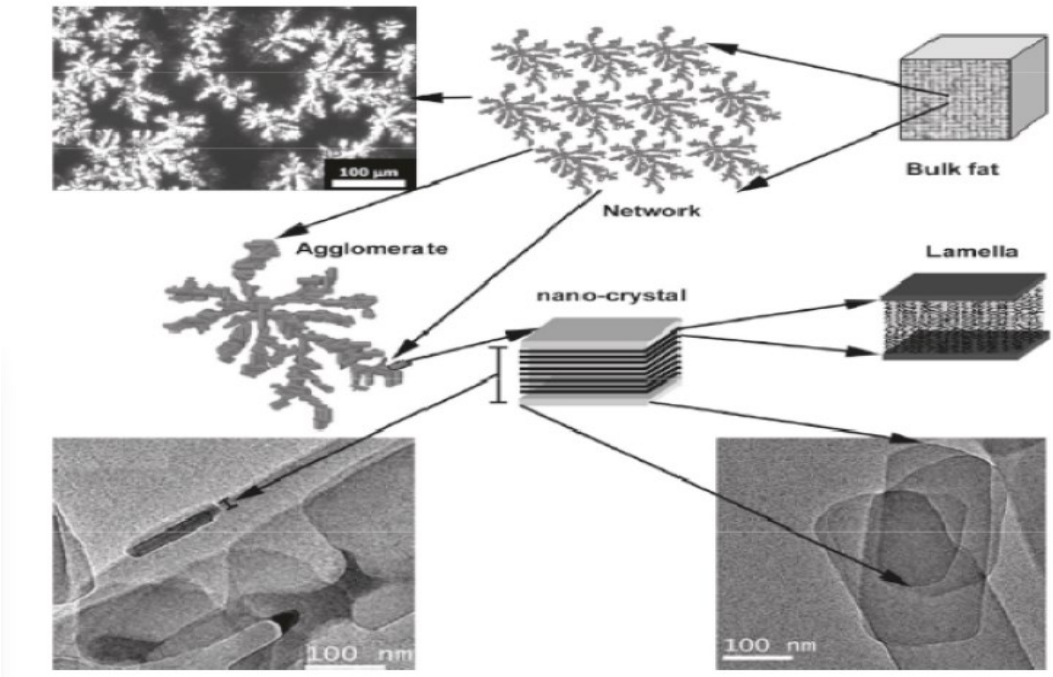

Figure 2 - 1 Schematic representation of the different levels of structure in a bulk fat (Acevedo and Marangoni, 2010).

2.1.1 Triacylglycerols

Triacylglycerol molecules (TAG), which have a complex polymorphism, are the main component of edible fats. Triacylglycerols constitute more than 95% of the edible fat composition. They are composed by three fatty acids esterified to one glycerol unit. There are several kinds of TAGs. One is called monoacid TAGs or simple TAGs, which means that there is just one type of fatty acids attached to the glycerol unit, such as trilaurin and tristearin. The other is called mixed-acid TAGs or mixed TAGs. Two or three types of fatty acids are attached to the glycerol unit. FA can be saturated (no C=C double bonds) or unsaturated (C=C double bonds).

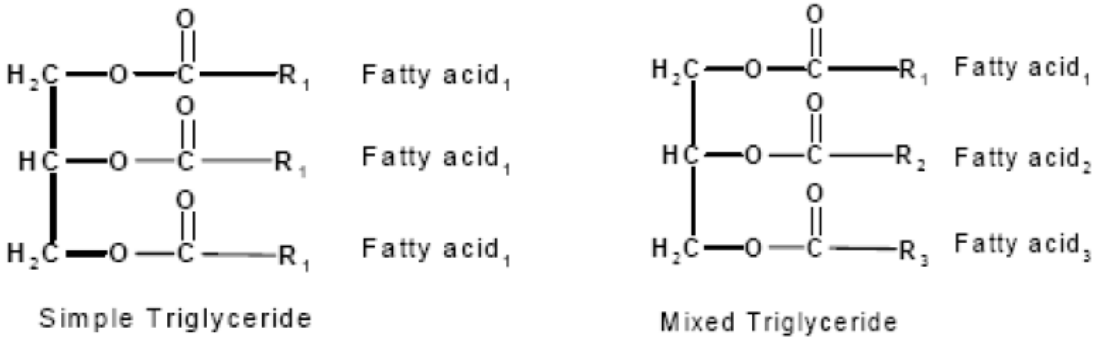

Figure 2 - 2 The structure of typical saturated triacylglycerol molecules (Metin and Hartel, 2005)

2.1.2 Polymorphism

Polymorphism is the ability of a molecule to crystallize in more than one crystalline form. The crystalline form is dependent on the arrangement within the crystal lattice (Metin and Hartel, 2005). Polymorphic forms are crystalline phases with different structural characteristics, but with identical chemical compositions when melted in their liquid state. In lipids, differences in hydrocarbon chain packing and the tilt angle of the packing are the cause of different polymorphs. The formation of one polymorph or another is mainly

influenced by the molecular structure and the external factors, such as temperature, pressure, impurities and shear rate. The rate of crystallization can also affect polymorph formation (Sato, 2001).

2.1.2.1 Polymorphic Types and Sub-Cell Structures

The chain length structure produces a repetitive sequence of the acyl chains involved in a unit cell lamella along the long-chain axis. This plays an important role in the phase behavior of different types of TAGs in a solid phase. A double chain length (DCL) structure is formed when the chemical properties of the three fatty acids are the same or similar. A triple chain length (TCL) structure is formed when the chemical properties of one or two of the three fatty acids are largely different from others (Sato, 2001).

A special sub-cell structure is defined as a lateral cross-sectional packing mode of the hydrocarbon chains of TAGs (Vand and Bell, 1951; Hagemann and Rothfus, 1993; van Langevelde et al. 1999). The subcells are described by a capital letter and a symbol. The letter indicates the symmetry (e.g., O for orthorhombic, T for triclinic, M for Monoclinic) and the symbol indicates either a parallel (//) or perpendicular ($\perp$) position between the zigzag planes of the different chains. In crystalline fat there are 10 types of sub-cell structures that have been revealed. Among these five sub-cell structures are predominant: H, $O_{\perp}$, $O'_{//}$, $T_{//}$, and $M_{//}$.

In the hexagonal (H) subcell structure, the two-dimensional lattice is hexagonal and gives a broad 0.41 nm wide-angle x-ray diffraction pattern. The carbon atoms rotate several degrees and form disordered conformations of hydrocarbon chains. This is why the chain packing of the hexagonal (H) subcell structure is loose and the specific chain-chain interactions are lost. In the orthorhombic perpendicular ($O_{\perp}$) subcell structure, the two

dimensional lattice is rectangular. This means a tightly packed lattice with specific chain-chain interactions. This subcell structure is characterized by strong wide angle x-ray diffraction patterns at 0.37 nm and 0.41 nm. The triclinic parallel subcell structure (T//) has an oblique two-dimensional lattice. There is strong specific chain-chain interaction because of the tightly packed chains. This T// subcell structure is characterized by a strong wide-angle XRD pattern at 0.46 nm and week patterns at 0.39 nm and 0.38 nm. Two sub-cells of O'// and M// contain the zigzag aliphatic chains and are arranged in a parallel manner. There are several other sub-cell structures and some of them belong either to O⊥ or to T// (Sato and Ueno, 2005).

Natural fats display complex polymorphisms during crystallization because they contain a huge number and variety of fatty acids. There are three main fat crystal polymorphs: α (hexagonal sub-cell) is an unstable form; β′ (orthorhombic perpendicular sub-cell) is a metastable form and hydrocarbon chains that are inclined with respect to the basal plane by about 108 degrees; and β (triclinic sub-cell) is the most stable form and has a triclinic parallel sub-cell with the hydrocarbon chains inclined at about 128 degrees (Takeuchi et al., 2003).

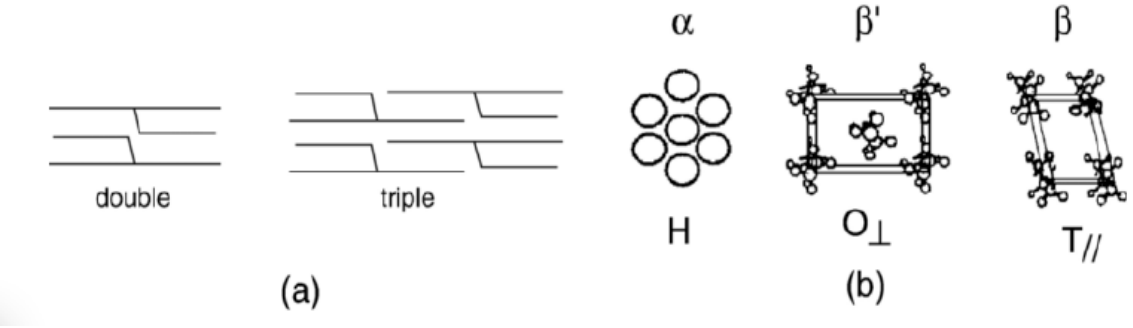

Figure 2 - 3 (a). Chain-length packing structure in TAG. (b). The polymorph sub-cell structure (Himawan et al., 2006).

2.1.2.2. Polymorphic Transition

Since the β polymorph is the most stable form, all other forms of crystals tend to transform to β in the end. Figure 2-4 shows the difference of the Gibbs energy of formation of the three major polymorphic forms (α, β′, and β). The hypothetical transition starts from the initial free energy G of the liquid to the three main polymorphic types. The transition depends on the energy barrier $\Delta G*(\alpha)$, $\Delta G*(\beta')$, and $\Delta G*(\beta)$ also the free energy of formation $\Delta G_f(\alpha)$, $\Delta G_f(\beta')$, and $\Delta G_f(\beta)$. ΔG should be negative for a spontaneous transformation. A higher degree of undercooling below the melting point is required to form a more stable polymorphic form like β, while a lower degree of undercooling is enough to form a metastable form like α (Rousset, 2002).

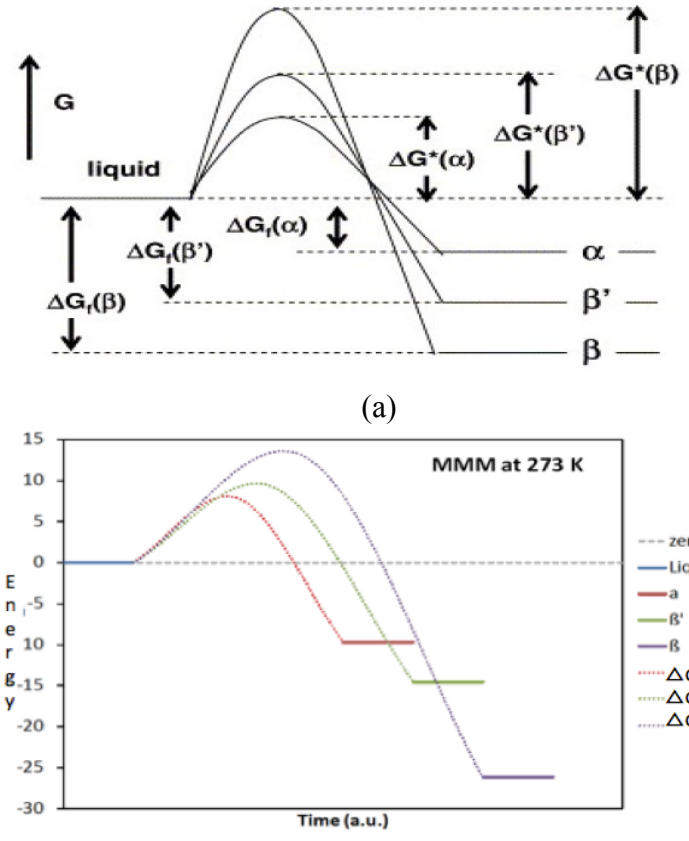

Figure 2 - 4 Energy barrier diagram for the 3 main polymorphic forms of a TAG at a given condition below their melting temperatures. (a) General concept (Rousset, 2002), (b) Calculated specifically for trimyristin at 273 K.

The polymorphic transitions happen monotropically from less stable polymorphic forms to more stable polymorphic forms (Ostwald's step rule) because TAG molecules tend to form the most stable subcell and arrange to accomplish the most efficient space-filling close-packing (Marangoni & Wesdorp, 2013). Figure 2-5 shows that the polymorphic transition within the solid phase could occur from α to β' and β or from α to β directly. And all polymorphic forms can be crystallized directly from a hypothetical liquid crystal structure (Sato, 1993). The recrystallization of a more stable phase from the melting of a less stable phase can reduce the total activation energy of polymorphic transition if the liquid retains some organization (Sato, 1993). The transition of β' to β sometimes takes place in the solid state. The hydrocarbon chain packing changes to T// with end group panes (1/3, 0, 1) from O⊥ with end groups (1,1,1). The overall packing is improved and the stability relation between β' and β can be explained (Larsson, 1972).

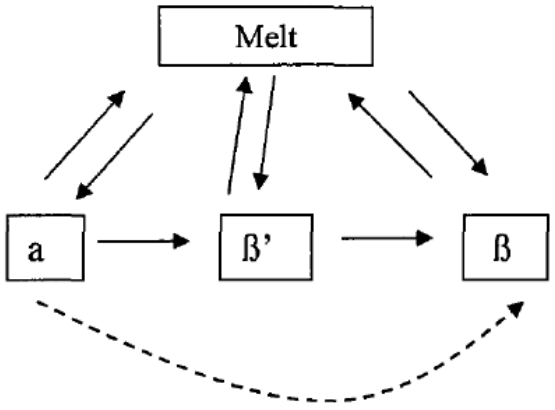

Figure 2 - 5 Polymorphic transition pathway in fat (Marangoni and Wesdorp, 2013)

2.1.2.3 Basic Methods for Studying the Polymorphism of Fats

There are many methods we can use to study the polymorphism of fats, such as DSC, x-ray diffraction and NMR. DSC analysis is the basic tool providing the data of temperatures,

enthalpy and entropy values of melting, crystallization, and polymorphic transitions. DSC analysis is a prerequisite for isolation of individual polymorphic forms and determination of their thermal properties and stability. XRD gives us the chance to study the molecular structural information. Small-angle diffraction patterns tell us the lamellar distance (long spacing) while wide-angle diffraction patterns reveal the subcell structure (short spacing) of the crystals. SAXD patterns give information about the number of phases formed and the amount of each phase formed as crystallization proceeds. WAXD patterns give information about the lateral distances between hydrocarbon chains in a crystal, which are characteristic of a particular polymorph. NMR is also a powerful tool for studying the molecular conformations of the TAGs in a crystalline state. Adam-Berret et al. proved that TD-NMR could evaluate triacylglycerol polymorphism, independently from temperature and chain length. T2 measurements are known to be a method for the determination of different properties of TAGs (Adam-Berret et al, 2008). Cross-polarization and magic-angle spinning NMR (CP/MAS NMR), is helpful for studying the molecular conformations of the TAGs in a crystalline state (Arishima et al, 1996).

2.1.3 Mechanisms of Crystallization

Three different events are involved during lipid crystallization. They are the induction of crystallization, also called nucleation, crystal growth and crystal perfection or crystal ripening (Vazque, et al, 2001). Because of the continuous variation of the thermodynamic conditions in a crystallization process, such as supersaturation or supercooling, these events occur simultaneously and at different rates.

In order to study crystallization, several mechanistic models have been developed. The Fisher-Turnbull model describes the nucleation and molecular diffusion by establishing the

dependence of nucleation rate on the activation free energy. The Avrami model is famous for describing the mechanism of crystal growth and the overall crystallization rate (Toro-Vazquez et al, 2001). The application of these mechanistic models to simple and complex lipids has given us lots of helpful information to study and understand TAG crystallization (Metin and Hartel, 2005).

In this study it was necessary to have a basic understanding of these mechanisms, to be able to develop temperature-time protocols that produced the target polymorphic forms that were sought.

2.1.3.1. Nucleation

When the temperature of a liquid fat decreases under the melting point of the highest melting TAG in the mixture, the melt becomes supersaturated. This undercooling or supercooling below the melting temperature of the crystallizing species forms the thermodynamic driving force for changing from liquid to solid. The occurrence of supercooling or supersaturation is a requirement to develop nucleation (Marangoni and Rousseau, 1999). This thermodynamic drive brings the molecules into a "liquid structure," until a critical size of monomers aggregates and then thermodynamically stable solid nuclei are formed (Toro-Vazquez, 2002). A nucleus is the smallest crystal that can exist in a solution in equilibrium at a certain temperature. The formation of a nucleus from the liquid phase requires the molecules to organize into a crystal lattice. Fats usually have to be undercooled by at least 5°C to 10°C before they start to crystallize. For a few degrees below the melting point, the melt exists in a metastable region and the molecules begin to aggregate into tiny clusters called embryos. Embryos continuously form and breakdown, but do not persist to form stable nuclei. The energy of interaction between TAG molecules

has to be greater than the thermal energy of the molecules in the melt to overcome Brownian effects. As the undercooling is increased, stable nuclei of a specific critical size are formed (Marangoni and Wesdorp, 2013).

The nucleation rate is the major determining factor in the number and size of crystals formed, their polymorphic form, and the ultimate distribution of crystalline solids (Metin and Hartel, 2005). There are three most common types of nucleation: primary homogeneous nucleation, primary heterogeneous nucleation and secondary nucleation.

Homogeneous Nucleation

The primary homogeneous nucleation occurs in pure solutions where the foreign interfaces are absent and may occur in a melt when there is significant undercooling. The accretion of molecules in the liquid phase is the base of the homogeneous nucleation.

Depending on temperature and supersaturation, an accumulation process occurs and continues until a stable nucleus forms. Firstly, single molecules get together to form dimers. By adding a molecule, dimers become trimers and eventually the nuclei form.

The creation of a solid-liquid interface requires energy, leading to an increase in the free energy of the system; however, the creation of a nucleus also causes a decrease in the free energy of the system (Marangoni and Wesdorp, 2013). The balance of these two energies determines the critical size of a nucleus, and its mathematical expression is known as the Gibbs-Thomson equation.

Heterogeneous Nucleation

In practice, nucleation often occurs in the presence of foreign particles or interfaces. The presence of foreign particles, such as dust particles or vessel walls, reduces the free energy

required for nucleation. Foreign particles reduce the effective surface free energy because the foreign surface makes the crystal-melt interfacial tension lower and the foreign surface also provides some energy needed to overcome the formation of the crystal surface (Metin and Hartel, 2005). Therefore, primary heterogeneous nucleation requires a much lower driving force (supersaturation or subcooling) than homogeneous nucleation. Heterogeneous nucleation is likely the result of interaction at the interface between the solid particle and the fluid that is supersaturated (Marangoni and Wesdorp, 2013).

Secondary Nucleation

Secondary nucleation is the process where new crystal nuclei form contacts with existing crystals or crystal fragments (Metin and Hartel, 2005). It normally proceeds once some primary homogeneous or heterogeneous nucleation has happened.

Secondary nucleation is affected by many parameters. They include the driving force of crystallization, temperature, foreign matter, agitation, the size and number of existing crystals, and the roughness of crystal surface. When crystal slurry is agitated in a vessel, the crystals contact with vessel walls, other crystals and the stirrer may lead to fractures of the existing crystal structure and finally the formation of secondary nuclei (Metin and Hartel, 2005). Secondary nucleation may also occur when microscopic crystalline elements are separated from an existing crystal surface.

Like primary homogeneous and heterogeneous nucleation, secondary nucleation also depends on the crystallization driving force (supersaturation or subcooling). At higher supersaturation there are more stable nuclei being formed (Marangoni and Wesdorp, 2013).

2.1.3.2 Crystal Growth

Once nuclei have formed and reached the critical size, they grow by incorporating other TAG molecules from the liquid phase. The correct configuration and the correct location on the crystal surface are determinants of the binding into a lattice when a new TAG molecule migrates from the liquid phase to the existing nuclei (Marangoni & Wesdorp, 2013).

For crystal growth to take place, the TAG molecules must migrate from the liquid phase to the crystal surface. A growth unit, which is either an individual molecule or a cluster of molecules, migrates to the surface of crystal until there is an appropriate site for incorporation into the lattice. Crystal growth keeps going as long as the driving force for crystallization exists. There is a release of latent heat when the growth unit has been incorporated. This energy diffuses away from the growing surface and makes the temperature of the whole system increase if the system is isolated. When the whole system is either fully crystallized or it reaches phase equilibrium, no further overall crystal growth can occur (Metin and Hartel, 2005). If the system is kept isothermal, the heat will be removed until the system reaches phase equilibrium.

The rate of crystal growth depends on several factors. They include the degree of supercooling, the structure of the crystal surface, the rate of the molecular diffusion to the crystal surface, the nature of the surface of crystal-melt and the difference between the rate of the attachment and the detachment of the molecule on the interface (Fisher and Kurz, 1992). The crystal growth is also affected by lipid composition, temperatures, and shear rates (Mazzanti et al., 2005).

2.2 Principles of X-Ray Diffraction

An x-ray beam is an electromagnetic wave characterized by an electric field whose strength varies sinusoidally with time at any one point in the beam (Cullity, 1956).

X-ray diffraction is widely used in structure analysis. X-ray diffraction can be used to determine the structure of a compound and phase, identify a phase by comparison with a data base, follow the formation and reactivity of a phase, observe changes in lattice constants under stress/change and obtain a microscopic image of phases in a heterogeneous sample. Bragg's law established a relationship between nanostructural distances and the measurable x-ray diffraction angle (Bragg, 1913). Thus, by using x-rays of known wavelength λ and measuring θ, the spacing d of various planes in a crystal can be determined (Cullity, 1956).

The x-ray used for XRD has just one wavelength after passing the monochromator. When a beam of x-rays passes through the sample and hits a crystal, most of the x-rays go through, but some x-rays are scattered by the crystals in the sample, due to interaction with the electrons of the atoms. When scattered, the single beam of x-rays is split and the x-rays come out of the sample in several beams at different angles to the sample. The beams can form constructive or destructive interference, depending on the scattering angles. The detected position and strength of these constructive interferences is called the diffraction pattern.

Each polymorphism and phase diffracts x-rays differently and has a different x-ray diffraction pattern. The pattern of a mixture is made up by all the patterns of each compound. Viewed as different sets of planes in the crystal, the geometry of the x-ray diffraction is shown in Figure 2-6. For a given set of lattice plane with an inter-plane distance of *d*, the condition for a diffraction peak can be written as: (Bragg, 1913)

$$n\lambda = 2d\sin\theta \quad (1)$$

where λ is the wavelength of the x-ray, θ is the scattering angle and n is an integer representing the order of the diffraction peak. In the Bragg law, firstly, the incident beam, the normal to the reflecting plane, and the diffracted beam are always coplanar. Secondly, the angle between the diffracted beam and the transmitted beam is always 2θ (Cullity, 1956).

It is more convenient to use the reciprocal lattice spacing q rather than the diffraction angle 2θ when analyzing x-ray diffraction data. According to Bragg's law,

$$q = 4\pi/(n\lambda)*\sin\theta \quad (2)$$

Therefore, $q = 2\pi/d$. Because the value of q is independent of wavelength λ, the x-ray diffraction patterns taken at different wavelengths can be compared directly.

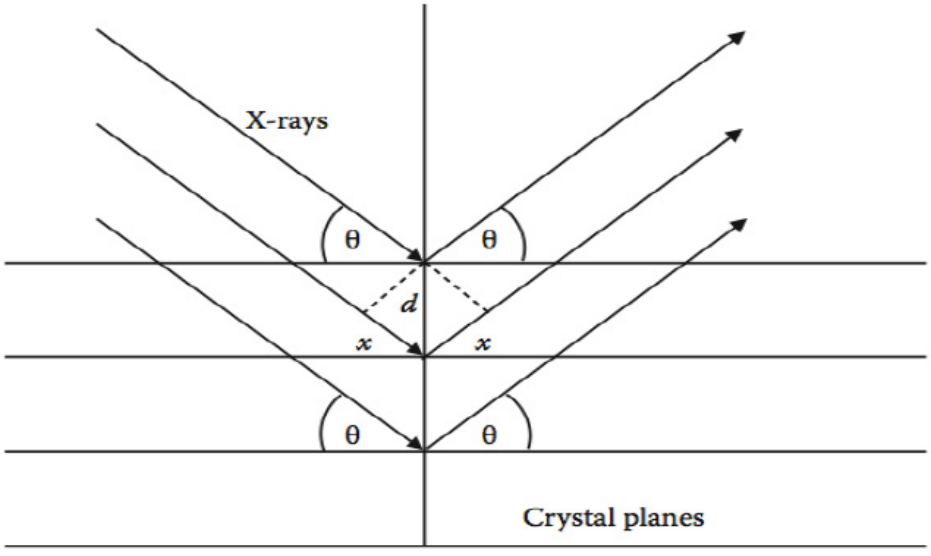

Figure 2 - 6 Geometry of the reflection of x-rays from crystal planes used in the derivation of Bragg's law (Marangoni & Wesdorp, 2013).

2.2.1 Miller Indices

Miller indices, a workable symbolism for the orientation of a plane in a lattice, are defined as the reciprocals of the fractional intercepts which the plane makes with the

crystallographic axes. If the Miller Indices of a plane are (*hkl*), then the plane makes fractional intercepts of 1/*h*, 1/*k*, 1/*l* with the axes, and if the axial lengths are a, b and c, the plane makes actual intercepts of a/*h*, b/*k*, c/*l* (Cullity and Stock, 2001).

The Miller indices are very useful in calculating the separation of the planes (Marangoni and Wesdorp, 2013). The value of d, the distance between adjacent planes in the set (*hkl*), may be found from the following equations (Cullity and Stock, 2001).

Hexagonal: $\frac{1}{d^2} = \frac{4}{3}\left(\frac{h^2+hk+k^2}{a^2}\right) + \frac{l^2}{c^2}$ (3)

Orthorhombic: $\frac{1}{d^2} = \frac{h^2}{a^2} + \frac{k^2}{b^2} + \frac{l^2}{c^2}$ (4)

Triclinic: $\frac{1}{d^2} = \frac{1}{V^2}(S_{11}h^2 + S_{22}k^2 + S_{33}l^2 + 2S_{12}hk + 2S_{23}kl + 2S_{13}hl)$ (5)

In the equation, V is the volume of the unit cell.

$V=abc\sqrt{1 - cos^2\alpha - cos^2\beta - cos^2\gamma + 2cos\alpha\ cos\beta\ cos\gamma}$ (6)

$S_{11}=b^2c^2\sin^2\alpha$, (7)

$S_{22}=a^2c^2\sin^2\beta$, (8)

$S_{33}=a^2b^2\sin^2\gamma$, (9)

$S_{12}=abc^2(\cos\alpha \cos\beta - \cos\gamma)$ (10)

$S_{23}=a^2bc (\cos\beta \cos\gamma - \cos\alpha)$ (11)

$S_{13}=ab^2c (\cos\gamma \cos\alpha - \cos\beta)$ (12)

These equations will be used later to estimate the changes in (a,b,c) and crystal volume due to the temperature change.

2.2.2 Wide Angle X-Ray Diffraction (WAXD)

WAXS or WAXD can be used to determine the crystal structure, crystallinity and to study the molecular orientation in a crystal. Compared to the small-angle x-ray diffraction

(SAXD), Wide-angle x-ray diffraction is the same technique except the distance from sample to the detector is much shorter and the diffraction maxima at larger angles are observed (Bower, 2002).

In lipid crystallization, the wide-angle x-ray diffraction ("short-spacing" region) patterns give information about the lateral distances between two hydrocarbon chains in a crystal. The number and position of the peaks permit the identification of the different polymorphic forms of TAGs, which was discovered by Malkin in 1934 (Marangoni and Wesdorp, 2013). In the small-angle region (or "long spacing" region), the position of the peaks provides information on the size of the TAG chain length and the angle of tilt of the TAG chains relative to the normal. It gives the information about the number of phases formed and the amount of each phase formed as crystallization proceeds (Acevedo and Marangoni, 2010).

Vand & Bell (1951) succeeded in determining the hydrocarbon chains of a TAG. Jensen & Mabis (1963) determined the structure of β form tricaprin (CCC) which has an asymmetric "tuning-fork" conformation and got the cell parameters of β-CCC. Larsson (1965) present the crystal structure of β-LLL and Gibon et al. (1984) further refined the β-LLL structure. Skoda et al. (1967) and De Jong & Van Soest (1978) also contributed to the determination of the unit cell of β-SSS. Van Langevelde et al. (1999) summarized the cell parameters of different β mono-acid even-numbered triacylglycerols which were determined by different researchers. They also present the cell parameters for β form PPP and transformed the experimental cells of β-CCC, β-LLL and β-PPP to the same reference axes, which made the comparison of homologous series of triacylglycerols possible. With the cell parameters present in the paper published by Van Langevelde et al. we can estimate the changes in density due to the temperature using the Miller indices equations of triclinic crystal cell

(Van Langevelde et al, 1999).

The nucleation and growth processes determine the type of polymorphic structure formed, but also determine the size of the nano-platelets and the 'perfection' of the crystals formed (Acevedo et al, 2011). The thickness of the nanoplatelets can be estimated from the widening of the SAXD peaks (Mazzanti et al, 2005). On the other hand, an increase in the correlation length in the 'a' and 'b' directions reduces the width of the WAXD scattering peaks.

2.2.3 Temperature Effect on the X-Ray Diffraction Peaks

As a powerful tool, x-ray techniques, including wide/small angle x-ray scattering and wide/small angle x-ray diffraction, are widely used in different research areas. In the membrane science, WAXS analysis and molecular modeling were carried out for interpreting d-spacings in 6FDA-based polyimide (Shimazu et al, 2000). Koberl et al. (1998) characterized the polymorphic behavior of glycolipid model membranes as a function of temperature using wide and small angle synchrotron x-ray scattering (Koberl et al, 1998).

Sirelli et al. (2006) studied the structural changes in the crystalline and amorphous phases of polyethylene terephthalate (PET) samples using wide angle x-ray diffraction. The crystallite sizes in the a and b directions slightly increased. The results indicated a growth in the crystal lateral dimensions, while in the c direction practically no variation was observed. Due to the thermal expansion, the volume of unit cell had a discrete increase and its density decreased (Sirelli et al. 2006).

In lipid crystallization, many scientists have studied the effect of temperature and other important factors on lipid crystallization using x-ray techniques. Mazzanti et al. (2005)

discovered that the small angle x-ray diffraction peak positions of palm oil at 22 °C were higher than at 17 °C for the same shear rate. Mazzanti et al. (2005) also found the peak positions of Small-angle x-ray were correlated to compositional variation of crystals in milk fat. (Mazzanti et al., 2004). MacMillan and Roberts (2002) found that in situ small-angle x-ray scattering (SAXS) polymorphisms change in cocoa butter samples was correlated with temperature, and these findings were later expanded by Himawan (2006) and by Mazzanti (2007). However, for triacylglycerols and edible fats, the wide angle x-ray diffraction variation with temperature has not been methodically studied.

2.3 Crystallization under Shear

2.3.1 Shear Effect on Fat Crystallization

Shearing, as a regular industrial manufacturing process, is widely used in the food industry during the fat crystallization process. One of the famous examples is the production of chocolate. The quality of chocolate is highly dependent on the proper application of tempering and shearing. Stapley et al. (1999) found the higher melting polymorphic form predominated when the shear rate was high enough and the temper time was long enough in the crystallization of chocolate. Also, shearing is one of the factors affecting the consistency and spreadability of butter and margarine (Mazzanti, 2005). Therefore, understanding the effect of shear on fat crystallization plays an important role in process and equipment design for the entire food industry.

Studies show shear flow increases the speed of crystalline orientation and reduces the phase transition time of polymorphic forms when it is applied to crystallizing lipid systems (Mazzanti et al, 2003). Shear can also alter the phase composition of the final product. Mazzanti et al. (2004) also reported the existence of a new phase (phase X) of

cocoa butter, which was not observed under static conditions previously, as well as the previously unreported existence of the phase IV structured under shear.

Dhonsi and Stapley (2006) tested shear rates ranging from 1 to 50 s^{-1} at four different isothermal temperatures on the tempering of cocoa butter. At 23 °C, induction times were shear dependent, with higher shear rates producing higher melting samples, suggestive of higher melting polymorphs.

Mazzanti et al. (2005) studied the shear effect on the crystallization of palm oil in a Couette cell using a synchrotron beamline and found that shear induced the acceleration of the phase transition from α to β′. The α nuclei form many distinct small crystallites and can easily transform to β′ form. The increased shear rate could promote the crystallization of the higher melting fraction and affect the composition of the crystallites.

The effect of shear on solid fat content (SFC) was also studied by Mazzanti's research group using Rheo-NMR system. The viscous heat generation produced by the shear energy may lead to the lower SFC at higher shear rate. A combination of direct and indirect methods had been developed to estimate the temperature increase due to viscous heating (Mazzanti et al. 2008). Above a limiting value, the increase in shear starts delaying the onset of crystallization, perhaps due to generation of viscous heat. Shear is also likely to produce a significant enhancement of heat transfer and to foster crystallite collisions (Mazzanti et al, 2005).

2.3.2 Studies on Shear Effect on the X-Ray Diffraction

Mudge and Mazzanti (2009) studied crystallization of cocoa butter, and applied shear rates between 45 and 720 s^{-1} which were shown to have accelerated phase transitions compared to static experiments. A shear rate of 720 s^{-1} delayed phase transitions, likely due to viscous

heating of the sample (Mudge and Mazzanti, 2009).

Mazzanti et al. (2009) found that the applied shear affected the composition trajectory of the crystallization by changing the lamellar thickness calculated from the peak positions. At higher shear rates the values of d tended to be larger and the values of d are 0.03 nm larger under shear than under static conditions. The application of shear favors the crystallization of longer molecules belonging to the higher melting point fraction. Higher levels of shear reduce the concentration gradient across the boundary layer, and may also cause an increase in temperature due to viscous heating (Mazzanti et al, 2009).

Shear flow affects the kinetics of crystallization and modifies the composition of the solid and liquid phases obtained during crystallization. Synchrotron x-ray diffraction patterns were captured and showed the integrated intensity, average thickness, and average lamellar spacing of the crystalline nanoplatelets were modified by the shear rate step. Thickness and crystalline orientation increased, evidently after the shear rate step-up (Mazzanti et al. 2011).

The shear flow also affects the temperature of the fat samples and crystallization process due to the viscous heating effect. Because the viscosity of most liquids and soft materials is highly temperature dependent, viscous heating is a common source of error under high shear rates. For example, under high shear rates the temperature set for the sample holder does not match the actual temperature of the sample. The heat produced by the intermolecular friction under high shear rate is unavoidable. In practice, the temperature of the sample during crystallization of triacylglycerols cannot be measured directly because the gap between the sample tube and the rotating shaft is too small to insert any temperature measuring devices, and an immersed measuring device would distort the flow (Wang and Mazzanti, 2011).

Devices have been developed to study the crystallization behaviour of triacylglycerols using Rheo-NMR and Rheo-XRD (Mudge and Mazzanti, 2009; Mazzanti and Mudge, 2008; Mazzanti et al, 2008). If the temperature of samples can be estimated through the changes of x-ray diffraction peaks, it provides a great chance to combine these two systems together to get a more complete picture of the crystallization of triacylglycerols under shear flow.

CHAPTER 3 EXPERIMENTAL METHODS AND MATERIALS

3.1 Materials

3.1.1 Sample Preparation

Trilaurin (LLL), trimyristin (MMM), tripalmitin (PPP) and tristearin (SSS) were purchased from Sigma-Aldrich Chemical Co. and had a purity of at least 99%. No further purification was carried out.

The binary mixtures (dry blends) were prepared by mixing the weighted samples in composition on a weight per weight basis. For example, the LLL: MMM ratios were 30:70, 50:50 and 70:30, denoted as 3L7M, 5L5M and 7L3M. In this research, 3L7M, 5L5M, 7L3M, 3M7P, 5M5P, 7M3P, 3P7S, 5P5S, 7P3S and 5L5S were prepared.

The samples mentioned above were melted at approximately 100 °C using a hot plate (Cole-Parmer, USA). 20-30 μL of sample was transferred to the x-ray capillary (Charles Supper Co., 1.5 mm diameter, 10 μm wall) by using a preheated disposable capillary tube with a wire plunger (Drummond Scientific Company, Wiretrol® II, Cat. Number 5-000-2010, 5 μL and l0 μL) and sealed by fire.

Cocoa butter and the commercial product, 99% dark chocolate, were also used in this research. Cocoa butter was stored at -20 °C in the fridge for a long time and it was crystallized in the β form. 99% dark chocolate was purchased in the local supermarket and the chocolate was crystallized in β form (V phase). The solid cocoa butter and 99% dark chocolate were chopped into tiny pieces and put into the capillaries without melting and sealed by fire.

For the experiments with shear flow, 6B4P and 6B4S were prepared as samples. Since the amount of sample needed in the mini Couette Cell was much larger than the capillary cell,

in this case BBB acted as a solvent to dissolve PPP and SSS. These samples were also prepared by mixing the weighted samples in composition on a weight per weight basis. The BBB: PPP ratio and the BBB: SSS ratio was 60:40. The samples were melted and placed in the sample tubes, which fitted the mini Couette cell.

3.2 In-House Wide Angle X-Ray Diffraction Measurements

The in-house WAXD experimental set up is shown in Figure 3- 1. The x-ray generator had a Commercial GeniX x-ray source (Xenocs Corporation, Sassenage, France), which produced 0.7093 Å wavelength Mo Kα radiation. The x-rays were focused by a mirror and then collimated by two sets of scatterless slits which were aligned on a small diameter vacuum fly-path.

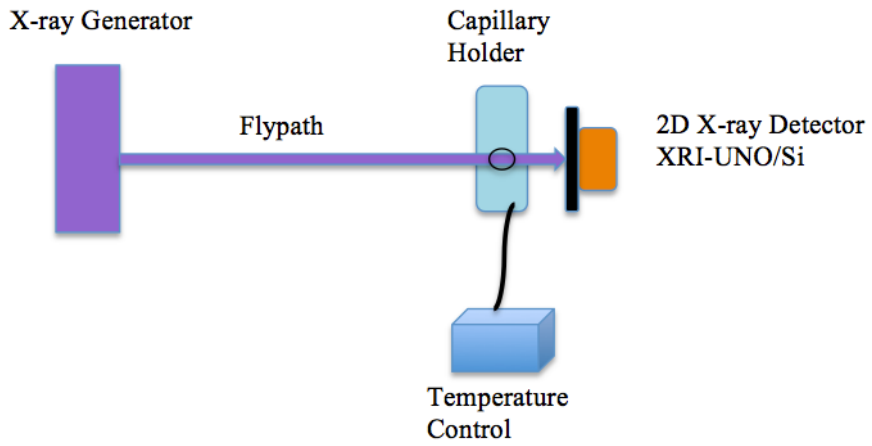

Figure 3 - 1 In-house XRD set up.

The x-ray beam was projected to the sample capillary right after it passed the fly-path. The beam size at the sample was approximately 0.4 mm x 0.5 mm.

The detector used in our in-house x-ray experimental set up was XRI-UNO/Si 2D x-ray detector (XRAY-IMATEK, Barcelona, Spain). The detector was built as a single chip

array of silicon sensors and its active area was 14 mm × 14 mm. The pixel size (ps) was 0.055 mm ×0.055 mm. The detector camera was controlled and all the images were collected by software named 'XRI-UNO'.

There was an enclosure around the whole x-ray system to isolate the surroundings and minimize the danger of x-ray exposure.

3.2.1 Centering the Diffraction Patterns

The detector needs to be moved to the center position where both x-axis and y-axis are 0 before putting the sample capillary into the capillary holder. The center location is used to calculate the distance from the sample holder to the detector. This centering allows the better calculation of the scattering vector q and d-spacing. A short x-ray exposure (10 s) was taken and the beam spot was captured by the detector. In ImageJ program, the beam spot was located in a 256×256 pixel image and the center position should be (128, 128). The detector was moved to -22.02 mm horizontally and the final center location should take this -22.02/0.055 pixel into account. The XY coordinate in pixels for the center for in this WXRD experiment was (-270.06, 127.11).

3.2.2 Detector Distance Calibration

The distance from sample holder to the detector was calibrated using Al_2O_3 that has known d-spacings. A radial plot of Al_2O_3 was obtained by using the ImageJ plug-in program XR2D (developed by Mazzanti and Idziak), which gave the pixel location (cpx) of each diffraction pattern. No matter what the detector distance was, the angular location difference between each diffraction pattern was kept constant. According to Bragg's law,

$$\lambda = 2d\sin\theta \quad (13)$$

$$\theta=\sin^{-1}(\lambda/2d) \quad (14)$$

$$y_d=p_s*c_{px}/\tan(2\theta) \quad (15)$$

Since λ was constant (0.7093 Å), a measured detector distance (y_d) and known Al_2O_3 d-spacings were used to calculate the p_s*c_{px} values of each pattern. The difference between each patterns of calculated p_s*c_{px} values, and similarly experimental p_s*c_{px} values could be obtained. Using Excel solver, the difference between calculated and experimental values was minimized by changing the y_d value and the c_{px} value. The final y_d value was the calibrated distance, and c_{px} was the refined center point. In this WAXD experiment, the distance from the sample to the detector was 130.36 mm.

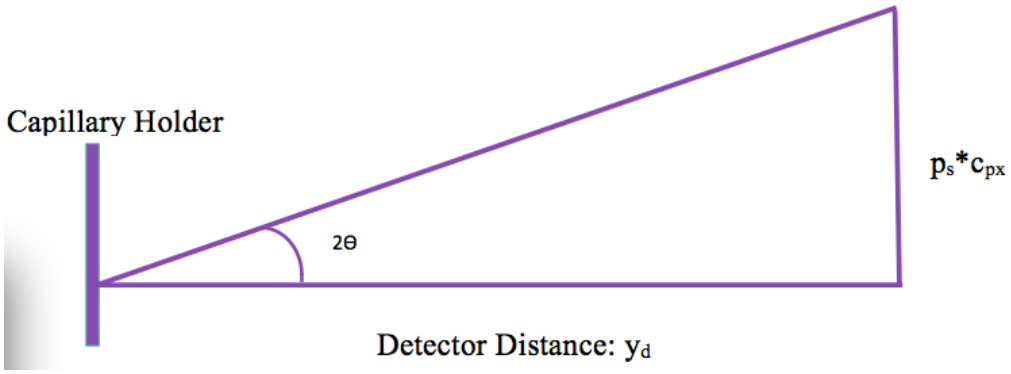

Figure 3 - 2 Explanation of distance calibration.

3.2.3 Experimental Procedure

The sample was first melted at high temperature to erase the crystal memory and then tempered to crystallize in the capillary. After getting the expected polymorphic form, the sample was kept at different temperatures according to the melting temperature shown in Table 3-1. Since the intensity of the in-house x-ray was low, a long exposure time was necessary to acquire images with good resolution and the sample was kept for 100 minutes at each temperature. Instead of taking a single image for a long exposure time, an

image was taken every 75 seconds and there were approximately 80 images for each temperature. In this way partial images were saved and the previous acquisition would not be lost if an interruption occurred in the experiment.

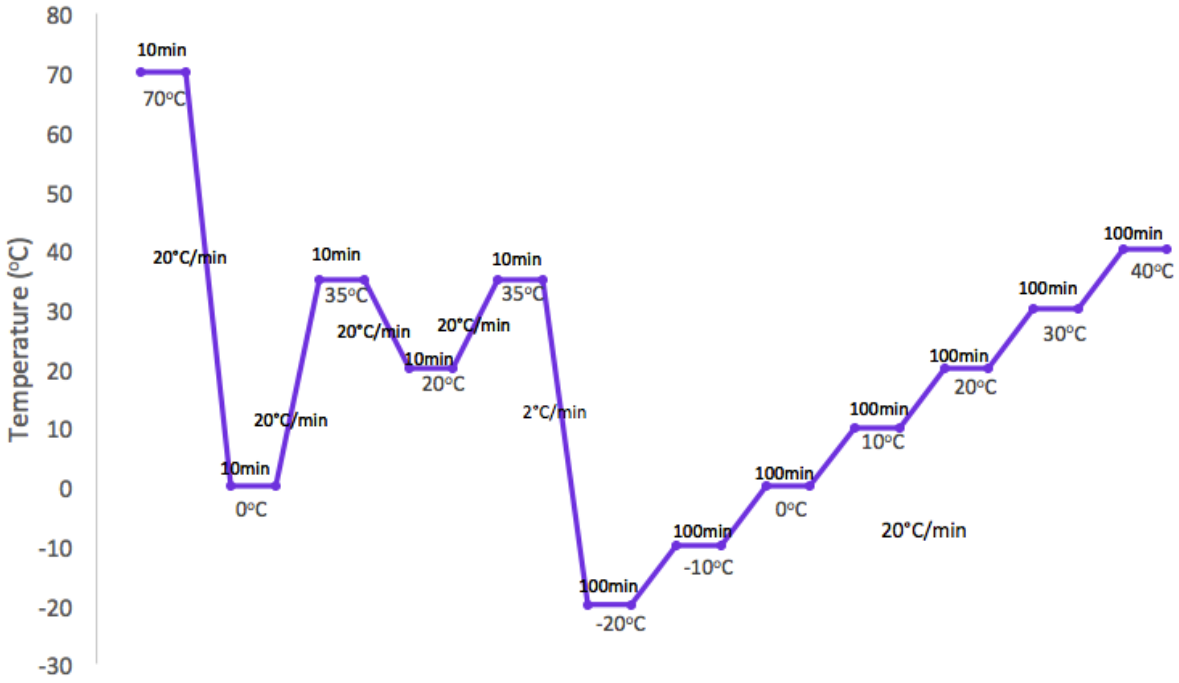

Figure 3 - 3 Temperature - time profile of in-house WXRD experiment for β LLL

Taking LLL as an example, the temperature profile is shown in Figure 3-3.

There are three parts in a temperature profile: melting temperature, cooling rate and final temperature, and the corresponding holding time at each temperature. All the samples were initially melted at 70°C or 80°C for 10 min to make a homogeneous liquid mixture. For β polymorph, the liquid sample was cooled down at a cooling rate of 20°C/min to 0°C where the crystallization takes place. The samples were heated up at a heating rate of 20°C/min to a temperature a little bit higher than the α form melting point to melt the α form crystals. And then the same procedure was done to melt the β' form crystals. After getting the β form crystallized triacylglycerol by cooling down the sample at a cooling rate of 2°C/min, the sample was kept from -20 °C to the temperature set according to its β

form melting point which is shown in Table 3-1. After tempering to get β polymorph, SSS was also crystallized at -20°C, 0°C, 20°C, 40°C, 20°C, 0°C for 5 times to test the reversibility of the WAXD peaks. For α polymorph, all the three samples (MMM, PPP, SSS) were crystallized by cooling down at a cooling rate of 20°C/min to -20°C and then the samples were kept from -20 °C to the temperature set according to their α form melting points which are shown in Table 3-1. For β' polymorph, the tempering procedure to melt the α form crystals was the same as that for β polymorph. The sample was cooled down at a cooling rate of 20°C/min and kept from -20 °C to the temperature set according to its β' form melting point.

Table 3 - 1 The melting point of each polymorphic form for LLL, MMM, PPP and SSS (Takeuchi et al, 2003).

	α	β'	β
LLL	15.6°C	35.1°C	45.7°C
MMM	32.6°C	45.9°C	57.1°C
PPP	44.7°C	55.7°C	65.9°C
SSS	54.7°C	64.3°C	72.5°C

For cocoa butter and 99% dark chocolate, the sample capillaries were placed into the capillary holder when the temperature was 20°C to avoid melting. And then the sample capillaries were cooled down at a cooling rate of 20°C/min and kept from -20 °C to 20°C since the melting point of Phase V cocoa butter is 33.8°C.

Table 3 - 2 The melting point of each phase for cocoa butter (Garti and Widlak. 2012).

Phase	I	II	III	IV	V	VI
M.P.	17.3°C	23.3°C	25.5°C	27.5°C	33.8°C	36.3°C

A LabView program developed by Dr. Gianfranco Mazzanti and Dr. Stefan Idziak, and upgraded by Pavan K. Batchu, was used to control the temperature of the capillary cell. This program has a graphical user interface (GUI), which permits the user to input the temperature profile. LabView program also allows the user to create a log file to record

the time, actual temperature and set point temperature of the capillary cell for each temperature cycle. The capillary holder is isolated to minimize the temperature interference from the ambient environment.

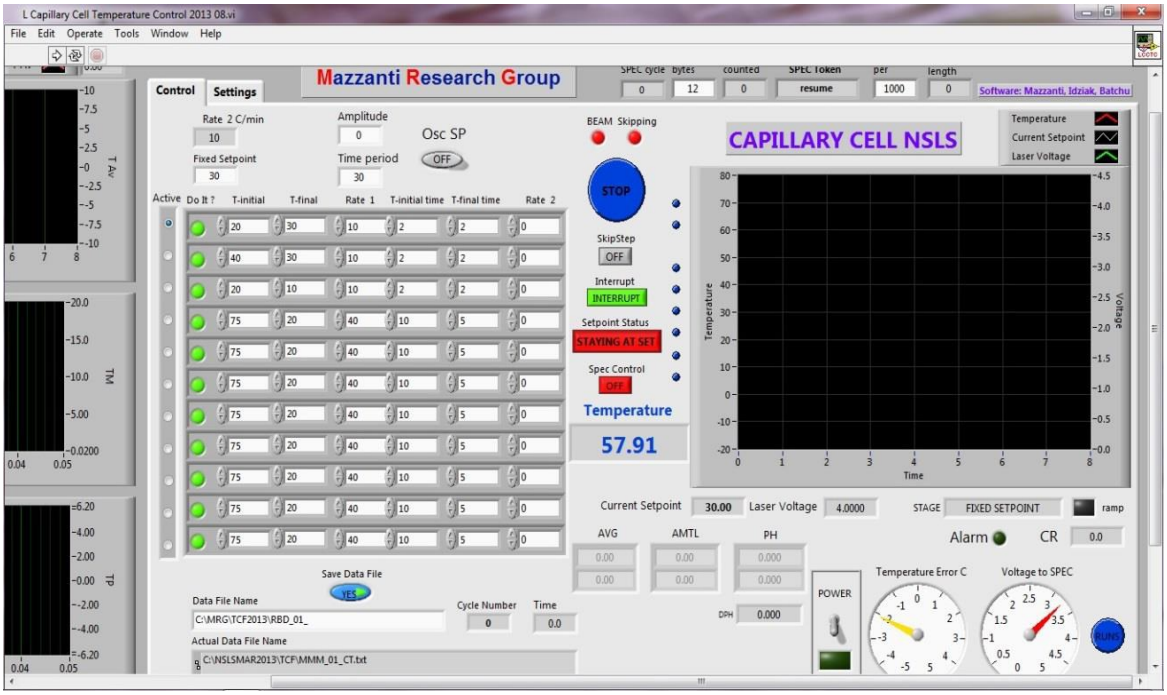

Figure 3 - 4 A GUI interface of the capillary cell temperature control program (Provided by Pavan K. Batchu)

Normalizing images

Since the number of images taken at different temperatures varies, it is necessary to normalize the images to get reliable results. The images, which were taken at the same temperature, were opened as a stack (a series of images that share a single window) of 8-bit raw images with size 256 X 256 pixels in ImageJ software. The images were added together to form a single image by using Z project, then converted to 32-bit, multiplied by 1000 and divided by the number of images added together. At last the image was saved as a 16-bit image which is suitable for creating the radial plot.

Creating radial plots

The XR2D plug-in program for ImageJ, which was developed by Stefan Idziak, Gianfranco Mazzanti, Maochen Hannah Wang and Kisun Park, is used to create the radial plots for further analysis in Igor Pro. The XR2D plug-in program was used to reduce the XRD 2D images to 1D plots of intensity as function of scattering vector q. It also allows for contrast manipulation and the definition of a region of interest (ROI).

The radial plots were created by taking a radial average of intensity at increasing value of q or pixel values on a diffraction pattern. The radial plot provides information about the peak position, the x-ray scattering intensity and the full width at half maximum (FWHM).

Normalized images of one sample were first opened as a stack of 16 bit unsigned images of size 256 X 256 pixels. The parameters used to extract radial plots from the images were $\lambda = 0.7093$ Å, distance = 130.36 mm, centreX = -270. 06 and centreY = 127.11 pixels. The ROI boundaries x Left = 6.0, x Right = 249. 0, y Up = 6.0 and y Down = 249.0 were used for each image stack. This ROI was chosen to exclude noise outside the specified boundary, produced by the edges of the silicon chip. The analysis of images was performed using just the pixels within this specified boundary. A starting radius corresponding to $q = 1.1$ Å^{-1} and an ending radius for $q = 1.85$ Å^{-1} were chosen to create the radial plot because this region included all of the necessary data. The radial plot information was saved in "text image format" (standard tab delimited ASCII text file) for further analysis.

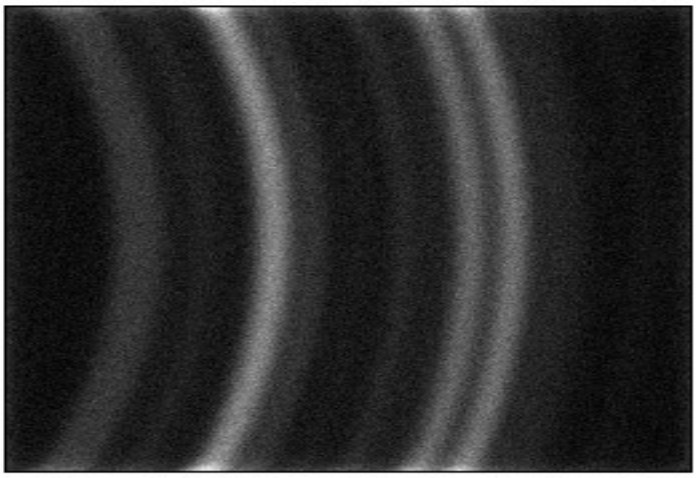

(a)

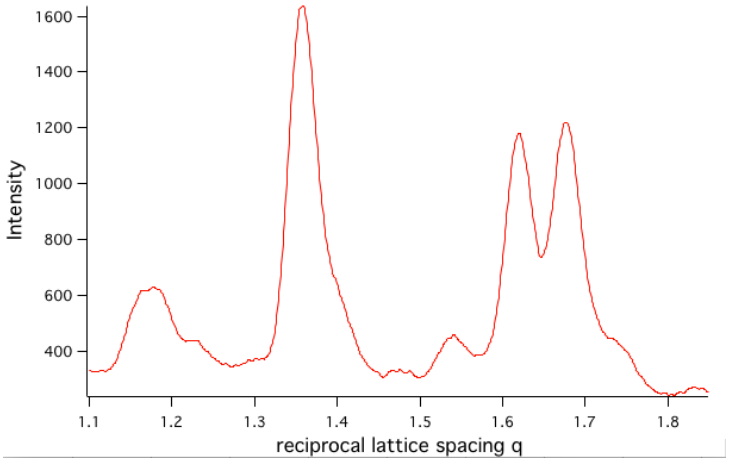

(b)

Figure 3 - 5 (a) Original x-ray image and (b) radial plot of 3L7M

3.2.4 Data Processing

3.2.4.1 Peak Fitting by Igor Pro

Igor Pro 6.0, produced by Wavemetrics Inc., is scientific data analysis software designed for curve fitting and peak fitting. All the peak fittings in this research were done by using Igor Pro.

Baseline calibration

The peak fitting will only be accurate if the background is accounted for. There are five

different baseline options provided by the Igor Pro 6.0 peak fitting program: Constant, Linear, Cubic, logCubic and logPoly5. Linear or cubic background functions were chosen to fit be the baselines.

Peak fitting

Multi-peak Fit 2, a package of Igor Pro, was used to fit the WAXD peaks in this research. There is a function named "auto locate peaks" which can automatically locate any positive positioned peak in one curve file. However, the type of baseline needed to be first set as "linear" or "cubic" manually, and also the type of each peak had to be defined. All the peaks started with the Gauss type and were changed to other kinds of function manually if needed. Using this Multi-peak Fit 2 program, the peaks were fitted by minimizing the error with a fixed baseline and defined peak types. The "peak results" functionality reported several parameters such as peak location, amplitude, area, and FWHM.

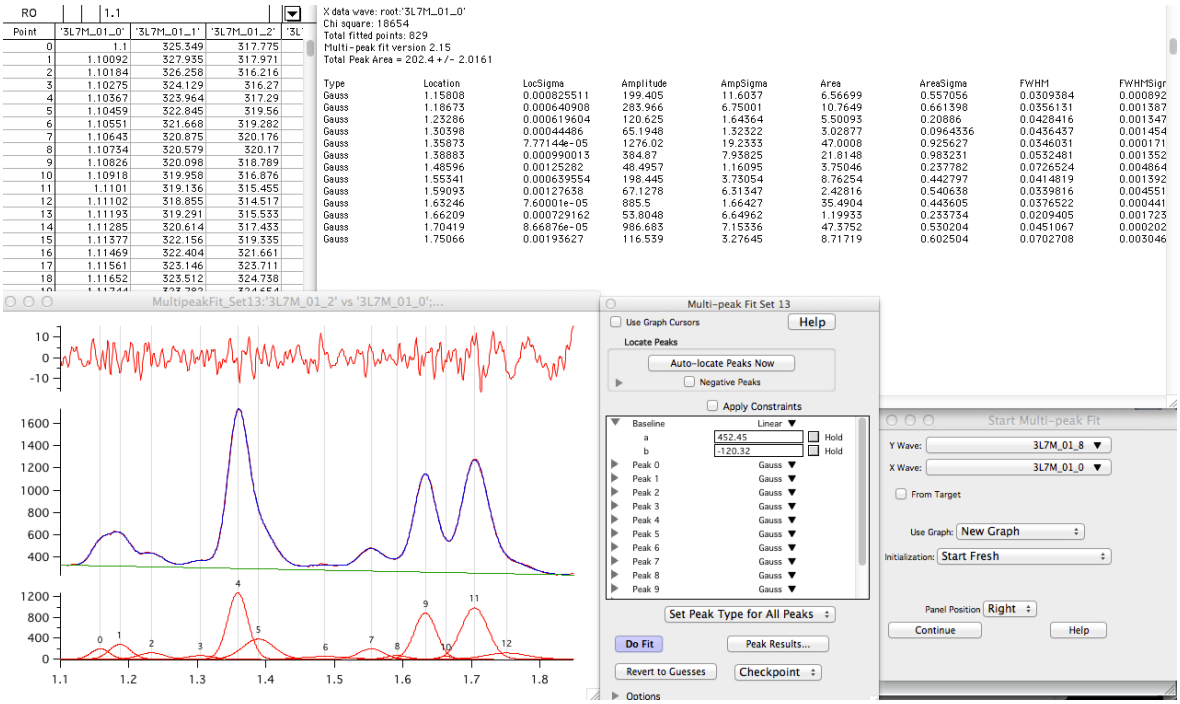

Figure 3 - 6 User interface for Igor Pro Multi-peak fit displaying a curve plot corresponding to WAXD of 3L7M.

3.2.4.2 Types of function (Voigt, Gauss, Lorentzian)

Three kinds of function (Voigt, Gauss, Lorentzian) were used in fitting the WAXD peaks in this research.

The Gauss distribution with a characteristic bell shape is defined by two parameters: the frequency from line center (x) and variance (σ^2), expressed as:

$$G(x;\ \sigma) = \frac{1}{\sigma\sqrt{2\pi}} exp[-\frac{1}{2}(\frac{q-q0}{\sigma})^2] \quad (16)$$

Where

q is the reciprocal lattice spacing

σ is the standard deviation of the distribution function.

The Lorentzian distribution is a continuous symmetric probability distribution with a width characterized by its full width at half maximum (γ). The Lorentzian probability function is defined as:

$$L(q - q0;\ \gamma)\ = \frac{\gamma}{\pi((q-q0)^2+\gamma^2)} \quad (17)$$

The Voigt profile is a convolution of a Lorentzian and a Gauss profile. The Voigt profile can be expressed as:

$$V(x;\ \sigma,\gamma)\ = \int_{-\infty}^{\infty} G(x';\ \sigma)L(x - x';\ \gamma)dx' \quad (18)$$

3.2.4.3 Calculation of d-spacing

The d-spacing of each WAXD peak was calculated in Microsoft Excel according to the Bragg's Law from the reciprocal lattice spacing q obtained by Igor Pro:

$$d = 2\pi/q \quad (19)$$

3.2.4.4. Uncertainty of the experiment data

The first kind of uncertainty of the experiment data is the sigma of the location obtained from the peak fitting by Igor Pro, as shown in Figure 3-7. The sigma of the location shows the error range of the peak locations due to uncertainties in the fit.

The second kind of uncertainty is observed when experiments are repeated with the same sample, and the third kind when they are repeated with another sample of the same material. The third kind includes and is expected to be larger than the third kind.

There is a fourth kind of uncertainty, which is associated with different samples and different peaks. Overall, this fourth kind of uncertainty is expected to be the largest one. The statistical evaluation of these uncertainties will be discussed along with the results, since the methods depend on the magnitude of the variations observed in the data.

MultipeakSet4_TD

Fit completed 6:22 PM Sunday, March 2, 2014
Y data wave: root:'5L5S_01_4'
X data wave: root:'5L5S_01_0'
Chi square: 24032
Total fitted points: 829
Multi-peak fit version 2.15
Total Peak Area = 290.22 +/- 6.0339

Type	Location	LocSigma	Amplitude	AmpSigma	Area	AreaSigma	FWHM	FWHMSigma
Gauss	1.16598	0.000277604	94.5471	7.18212	2.52778	0.300537	0.0251165	0.00120768
Gauss	1.19574	0.000401809	398.968	5.32308	24.2902	0.661959	0.0571952	0.000880009
Gauss	1.29161	0.000641666	178.238	10.9694	17.6168	1.5768	0.0928526	0.00290278
Gauss	1.37412	4.65826e-05	1695.49	13.369	70.066	0.771367	0.0388223	0.000129477
Gauss	1.41835	0.000849998	355.41	11.9866	26.7088	1.50471	0.070598	0.00234088
Gauss	1.48393	0.000471284	102.326	4.53342	3.91237	0.288623	0.0359187	0.00123513
Gauss	1.57142	0.000573317	270.36	13.5793	38.1701	3.04856	0.132632	0.00446123
Gauss	1.64091	7.23283e-05	1026.92	5.00045	40.6966	0.366758	0.0372298	0.000174161
Gauss	1.69233	0.00135169	674.465	45.2601	31.266	3.15668	0.0435492	0.0015159
Gauss	1.72607	0.00146034	614.976	40.3697	29.0483	3.27237	0.0443743	0.00213828
Gauss	1.77433	0.00125094	131.342	7.24454	5.92044	0.590737	0.0423467	0.00201562

Figure 3 - 7 The location, amplitude, area and FWHM information of the fitted WAXD peaks provided by Igor Pro (5L5S).

3.3 Synchrotron Wide Angle X-Ray Diffraction Measurements

3.3.1 Synchrotron X-Ray Beamline Information

The synchrotron wide angle x-ray diffraction measurements were performed at beamline 5-ID-D of the Advanced Photon Source (APS) at the Argonne National Laboratory (ANL) located in Argonne, Illinois. The x-rays at beamline 5-ID-D are generated by the 3.3 Undulator (Undulator A). The energy range of x-rays at beamline 5-ID-D is between 6-17.5 keV. A Si (111) monochromator is used to further adjust the wavelength of the incoming radiation to a certain value. In this experiment, the wavelength was adjusted to 0.7293 Å and the beam size was 0.08860 mm × 0.08860 mm. The distance from Sample to detector was 255.9 mm and the calibration was performed using the geometry calibration standard LaB6 SRM660a ("Argonne National Laboratory").

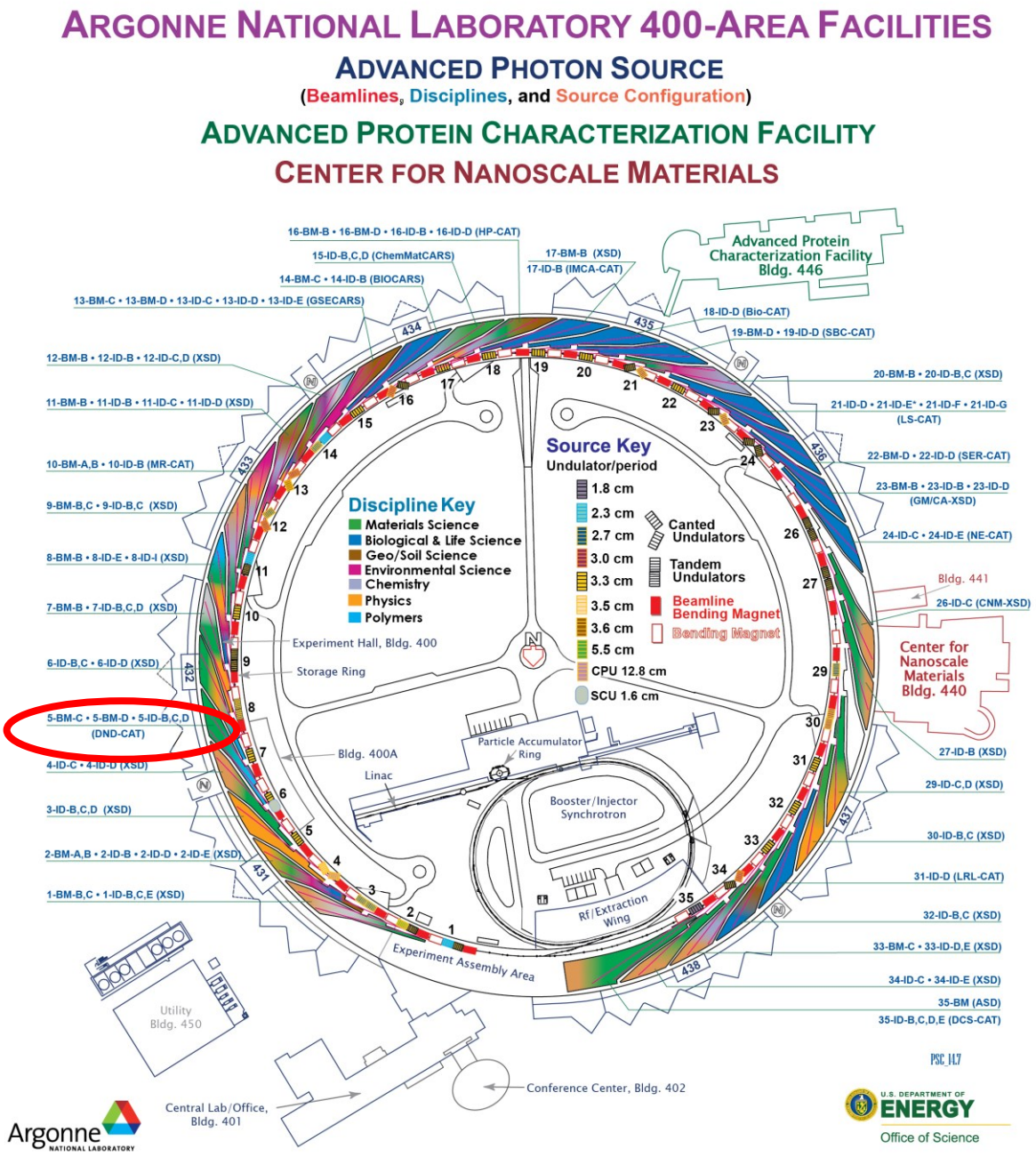

Figure 3 - 8 Floor plan of the Advanced Photon Source (APS) at ANL showing storage rings and beam lines. x-rays originating from Sector 5 - Insertion Device Beamline are further split into three beam lines 5-ID-B, 5-ID-C and 5-ID-D ("Argonne National Laboratory").

3.3.2 Experimental Setup

3.3.2.1 Temperature Control System

A schematic diagram of the experimental system is shown in Figure 3-9. The temperature control system used in this research comprised a temperature controller, a water bath, a heat exchanger, a Galden reservoir, a peristaltic pump (Cole-Parmer Instrument Company®, Model: Masterflex® Tubing Pump) for Galden fluid, three fiber optic thermistors, and a temperature sensor (Neoptix).

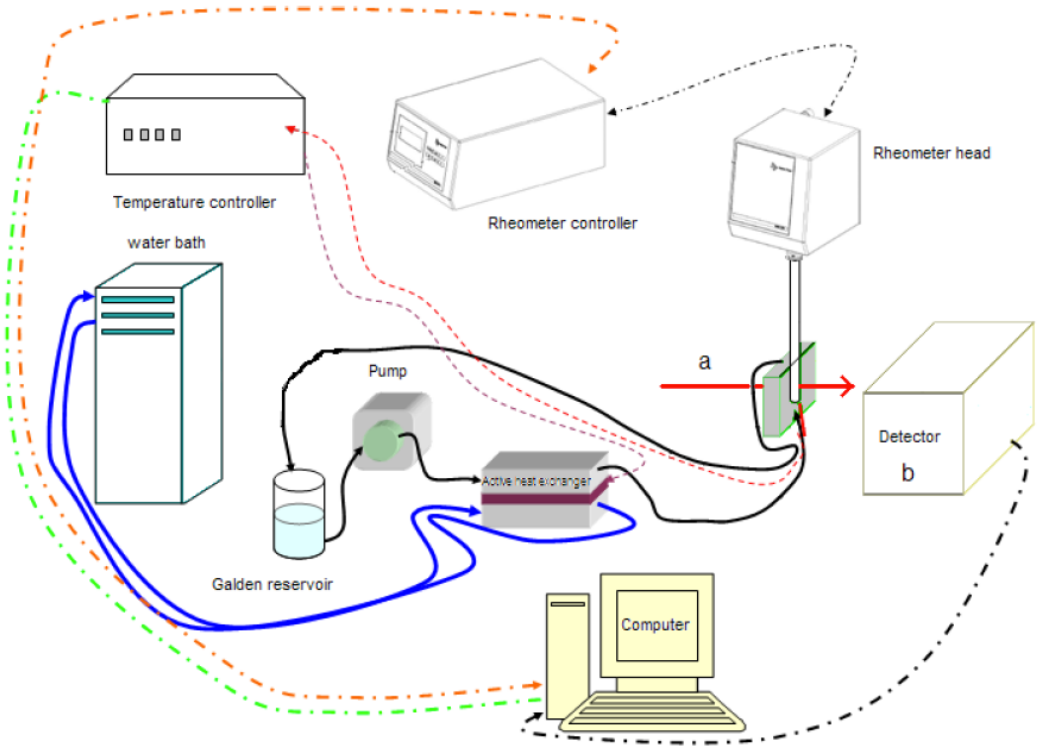

Figure 3 - 9 Schematic figures of the temperature control system configuration (Li, 2011).

Temperature controller

The temperature controller connected to the computer allows communication between the software and the temperature control system. In this experiment, it was controlled via LabVIEW, which was programmed by Dr. Gianfranco Mazzanti. The LabVIEW gave commands to the temperature control system and recorded the set and real temperature.

Water Bath

The water was connected to the heat unit for transferring the thermal energy. The temperature of the water bath was set at 0°C. The pipes between the water bath and the heat unit were insulated for minimizing thermal loss.

Active heat exchanger

The active heat exchanger was connected to the temperature controller and followed its commands to heat or cool down the Galden. There were six thermoelectric elements built in the heat unit for heat transfer between the water and Galden fluids. These thermoelectric elements controlled the temperature of the Couette system precisely. The thermoelectric elements were assembled with Bismuth Telluride semiconductor material and thermally conductive Aluminum Oxide ceramics (Wright et al., 2000). They were connected in the system in parallel with a 24-volt power supply. They were manufactured by Laird Technologies inc., MO, US.

Galden heat transfer fluid system

Galden heat transfer fluid is a perfluorinated polyether without hydrogen. Galden HT135 (Solvay-Solexis) was chosen in this research because its low viscosity and wide operating temperature range, which was from -50 to 125°C with a boiling point at 135°C. This permitted it to act as the heat transfer liquid in our experiment temperatures (-20 to 80°C). The Galden fluid was kept in a stainless steel thermos. A glass condenser was installed on the top to avoid evaporation of the Galden and pressurization of the system. The Galden fluid was pumped by a peristaltic pump (Cole Parmer, US), went through the heat exchanger and finally reached the sample holder. The Galden fluid went back to the container after flowing though the outside cylinder

of the sample holder. The three Two Reflex fiber optic sensors (Neoptix, QC, Canada) were placed at the Galden inlet and outlet in the magnet cell, the Galden in and the Galden out of the sample holder to measure the temperature of Galden fluid. The pipes between the heat exchanger to the sample holder were insulated to minimize the thermal loss. A 15 kΩ thermistor (Oven Industries, US) was used to monitor the Galden temperature at the outset of the active heat exchanger and to provide the signal for the temperature controller.

Fiber optic temperature sensor

Fiber Optic Temperature Sensor was chosen for three reasons. First of all, there is no metal part in the sensor. It means there is no electrical power going through it. Second, the Fiber Optic Temperature sensors could be located at the bottom and the upper side of the sample holder to detect the temperature of Galden fluid because of the small size of the sensors. Third, it is readable from a computer. The computer reads the temperature as a voltage signal (0 to 10 V), and then converts it to temperature (-20 to 100°C).

3.3.2.2 Couette System Configuration

The Rheo-XRD system was composed of a mini Couette cell, an Anton Paar DSR301 Rheometer head held by a controllable support, Rheometer control box, and connected to the temperature control system. The Rheometer control box was connected to the computer with the manufacturer's software Rheoplus® to control the rheometer head to provide different shear rates. The rheometer head was equipped with a powerful, synchronous EC motor and high-precision air bearing technology. A long shaft made of

titanium with a Teflon end was connected to the Rheometer head to spin at a given shear rate to provide shear effect.

The mini Couette cell used in this research is shown in Figure 3-10. It was composed by a sample tube and the Galden tube which was made by Lexan because it allowed x-rays to go through. The red colour indicates the shaft connected to the Rheometer head to provide shear to the samples. The yellow part indicates the sample gap between the shaft and the wall of the sample tube. The Galden went in from the bottom of the Galden tube. After the whole Galden tube was filled with Galden, the Galden came out from the upper side. There were two fiber optic temperature sensors to test the temperature of Galden in and Galden out.

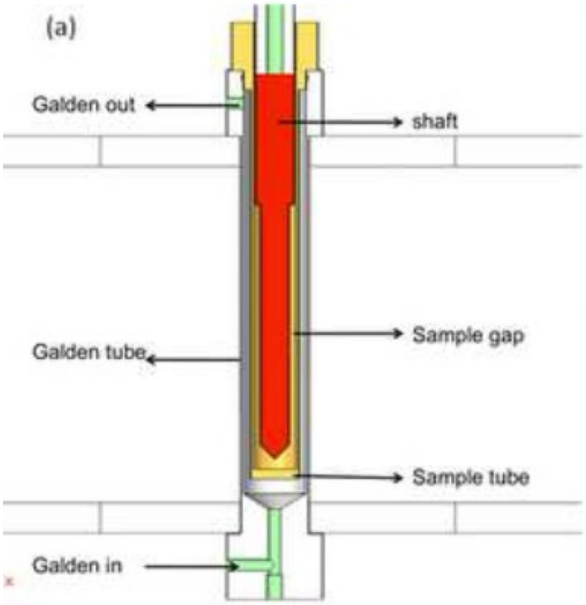

Figure 3 - 10 The mini-Couette cell used in APS. (Provided by Cendy Wang.)

3.3.3 Experimental Procedure

6B4P was initially melted at 80°C for 10 min to make a homogeneous liquid mixture. The liquid sample was cooled down at a cooling rate of 20°C/min to -5°C. The crystallized 6B4P was kept at 0°C, 10°C, 20°C, 30°C, 40°C and 50°C. No shear was

applied for 6B4P in this experiment.

6B4S was initially melted at 80°C for 10 min to make a homogeneous liquid mixture. The liquid sample was cooled down at a cooling rate of 20°C/min to -5°C. The crystallized 6B4S was kept at 0°C, 10°C, 20°C, 30°C, 40°C and 50°C with a constant shear rate. Two rotational speeds, 40 r/s and 50 r/s, were applied for 6B4P in this experiment.

When the temperature was stable, the WAXD patterns were captured by custom Rayonix fast frame-transfer CCD detector. An image was also taken every 1 second and the exposure time was 1 second. In total 120 images were captured at each temperature and shear rate.

3.3.4 Data Processing

The WAXD peak information, including the intensity and peak position, was saved in a text file at the same time when the WAXD pattern of the sample was saved and could be retrieved by Igor Pro directly. A starting radius of $q = 0.6$ Å^{-1} and an ending radius of $q = 2.0$ Å^{-1} were chosen to do the multi-peak fitting because this region included all of the necessary data. The data processing procedure which followed afterwards is the same as Part 3.2.4 in this thesis.

CHAPTER 4 RESULTS AND DISCUSSION – I - EFFECT OF TEMPERATURE ON WAXD OF PURE TRIACYLGLYCEROLS

4.1 Effect of Temperature on d-Spacing of WAXD Peaks

4.1.1 Effect of Temperature on d-spacing of β Form WAXD Peaks

The polymorph WAXD patterns fitted using the software Igor Pro were almost the same as the β form in the literature. The β form crystal is arranged in a triclinic subcell packing and it is identified by a very strong reflection at 4.6 Å, and the other two strong reflections at 3.85 Å and 3.7 Å (Kellens et al, 1990).

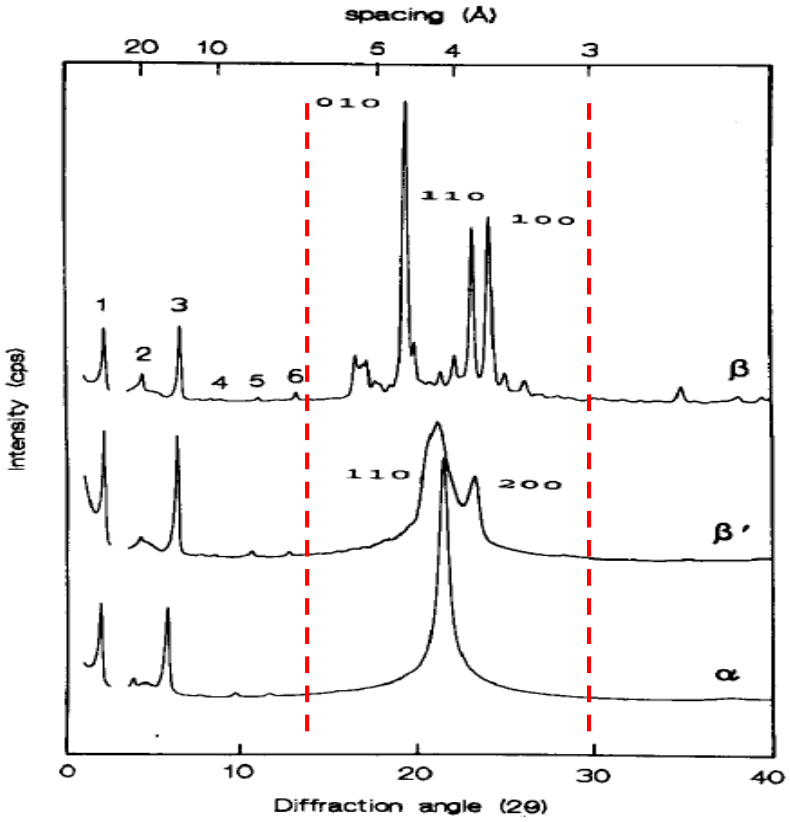

Figure 4 - 1 β, β' and α form WAXD Peaks in the literature (Kellens et al, 1990)

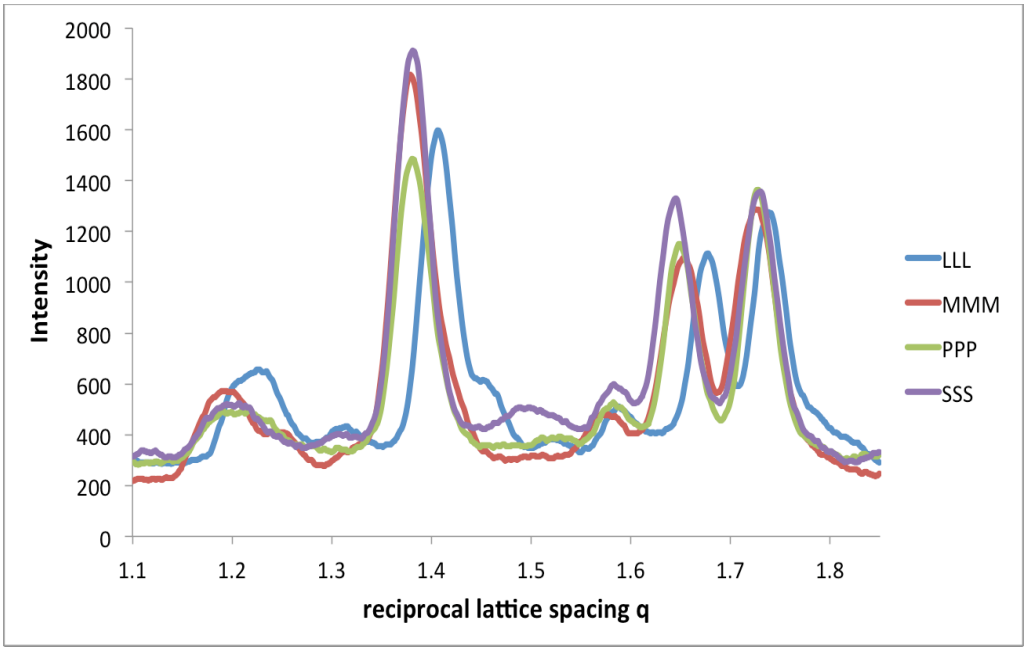

Figure 4 - 2 Radial plot for the four pure triacylglycerol samples (LLL, MMM, PPP and SSS) at -20°C

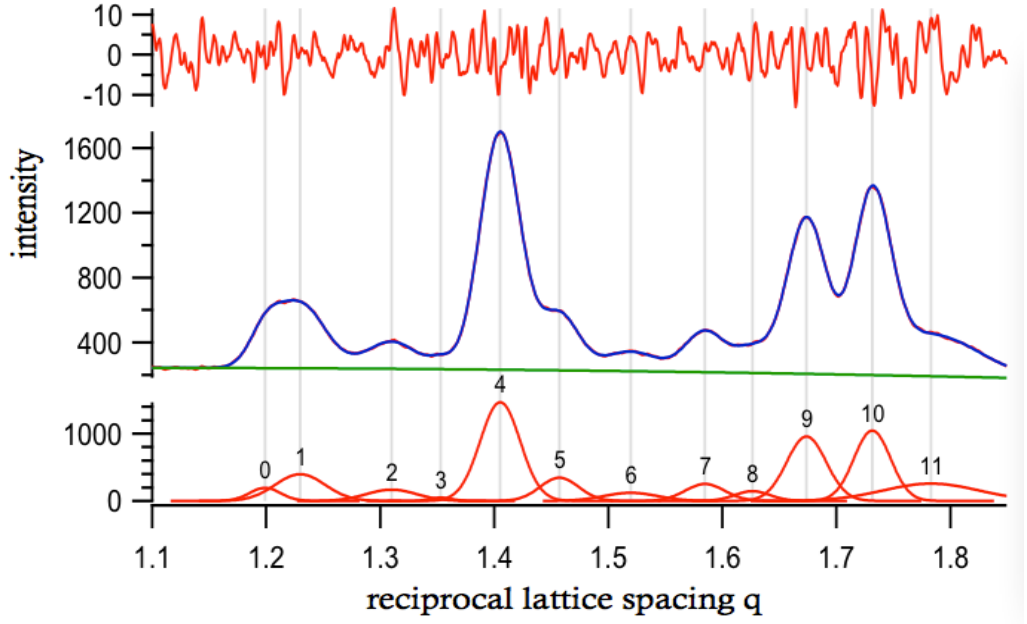

Figure 4 - 3 The fitted Wide Angle Diffraction patterns of β form LLL at -20 °C by Igor Pro.

In Figure 4-3, these three characteristic peaks are peak 4, peak 9 and peak 10. Among all the WAXD patterns of pure materials under different temperatures, there are at least 10 peaks when analyzing with Igor Pro. The upper part of Figure 4-3 shows that the residual

error of the fitting is less than 0.5% at the top of the largest peak. The middle part shows the original wide angle x-ray peaks of β form LLL and the intensity of the peaks. The green line is the base line of the fitting. The lower part shows the fitted wide angle x-ray peaks of β form LLL and the intensity of each peak.

Six main peaks for the β polymorph, which have higher intensity than others, were chosen to reveal the effect of temperature on d-spacing. These stronger peaks would be easier to observe in cases where a small percent of the material is crystalline. These six peaks are compared and discussed according to their general location: 1. Large d-spacing; 2. Medium d-spacing. 3. Small d-spacing.

The changes of the d-spacings with the temperature may not be obvious when plotting the d-spacings of the WAXD peaks versus temperature. Therefore, -20°C was taken as a reference temperature, and the differences of d-spacings at each temperature were calculated by subtracting the d-spacing at -20°C.

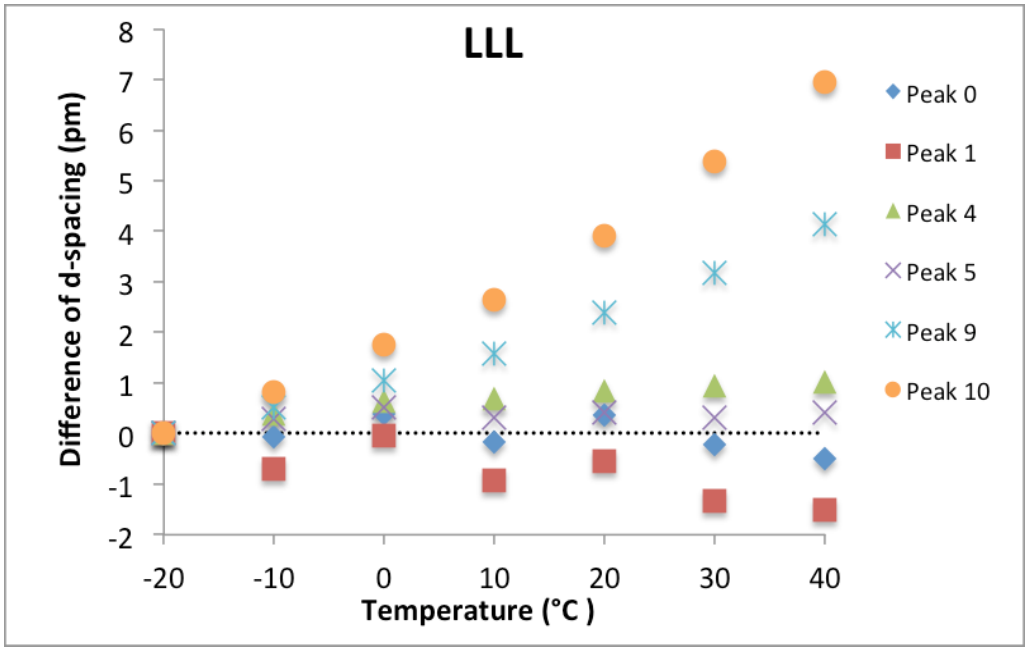

(a)

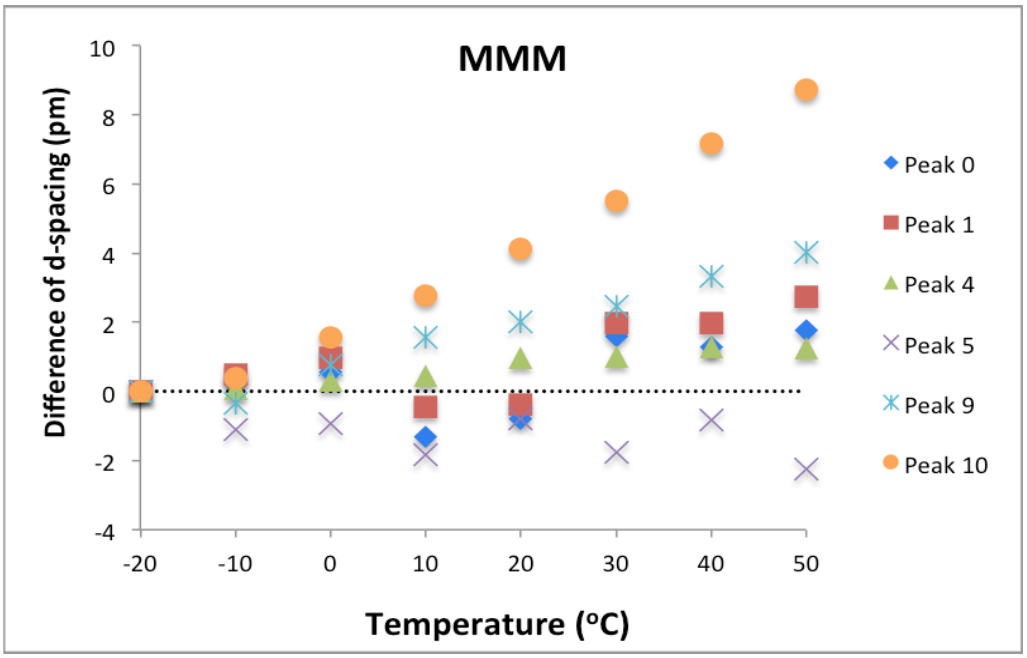
MMM
Difference of d-spacing (pm)
Temperature (°C)
Peak 0
Peak 1
Peak 4
Peak 5
Peak 9
Peak 10

(b)

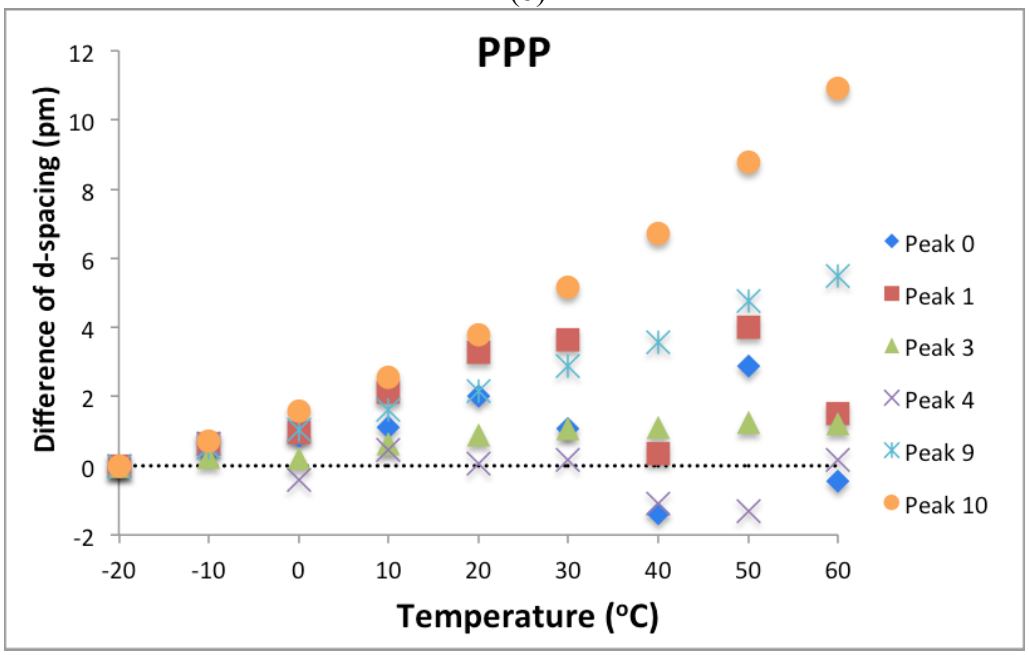
PPP
Difference of d-spacing (pm)
Temperature (°C)
Peak 0
Peak 1
Peak 3
Peak 4
Peak 9
Peak 10

(c)

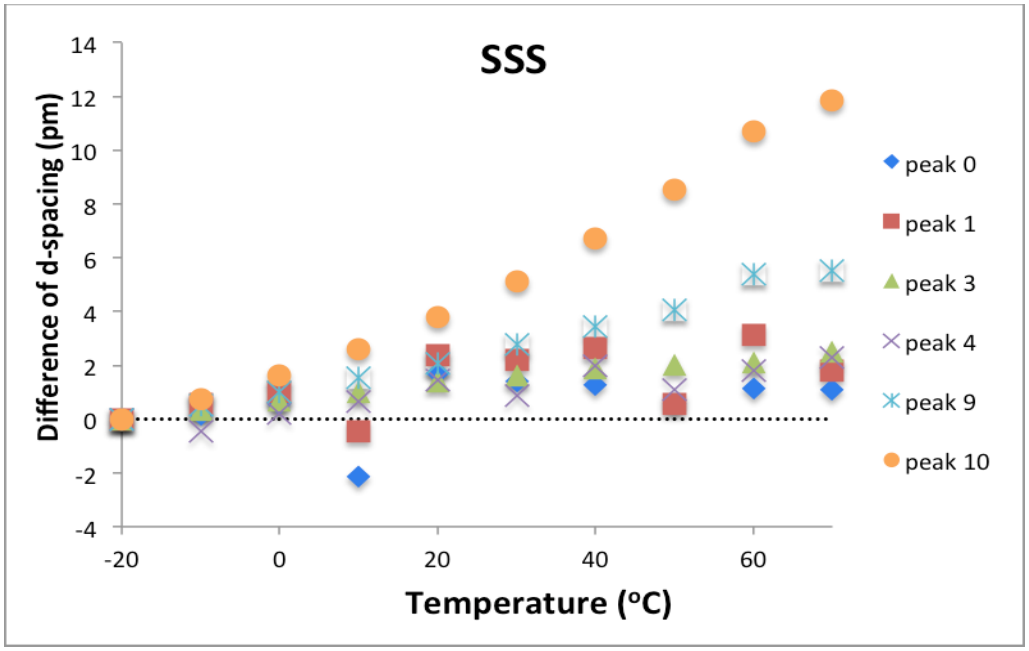

(d)

Figure 4 - 4 Differences of d-spacings with temperature for pure TAGs. (a) LLL. (b) MMM. (c) PPP. (d) SSS.

For the peaks with large d-spacing, when the temperature increases the d-spacings remain almost the same as that under the reference temperature (-20°C). The differences of d-spacings for peak 0 and peak 1 are quite small and can be regarded as 0. This means that the temperature does not affect the d-spacing and therefore the reciprocal lattice spacing q observed is not changed.

For the peaks with medium d-spacing, when the temperature increased to 10°C, the d-spacings are about 1 picometer larger than the original one. When the temperature continues to increase, the increase of the d-spacings is negligible. This means that there is a relaxation limit to these d-spacings trend. It is likely that one of the main reasons that the data points fluctuate from a smooth trend is the difficulty of fitting two peaks that overlap each other: it is hard for the software to separate them in a unique unambiguous way.

For the peaks with small d-spacing, when the temperature increases the d-spacings keep increasing. The effect of temperature on the d-spacings of the peaks with small d-spacing

is much stronger than the effect of temperature on other peaks. This same result is found in the four pure triacylglycerols.

When the temperature increases, the energy distributed between the atoms of the molecules in nanocrystalline triacylglycerols changes. However, it does not have the same effect in all directions. The energy needed to change the position of the peaks with large d-spacing is largest, compared to the energy needed to change other peaks in the wide angle diffraction patterns. The energy needed for changing the position of the peaks with small d-spacing is much smaller than the energy needed to change peaks with large d-spacing, so the d-spacing is easier to change. The energy needed for the peaks with medium d-spacing is between the large d-spacing and the small d-spacing. As the result of an increase in temperature, thermal vibration of the atoms increases. The unit cell expands and causes changes in periodicity d and therefore in 2θ positions of the diffraction lines. If the positions of one or more lines are measured as a function of temperature, the thermal expansion coefficient of the specimen can be determined by x-ray diffraction (Cullity and Stock, 2001)

4.1.2 Effect of Temperature on d-spacing of β' Form WAXD Peaks

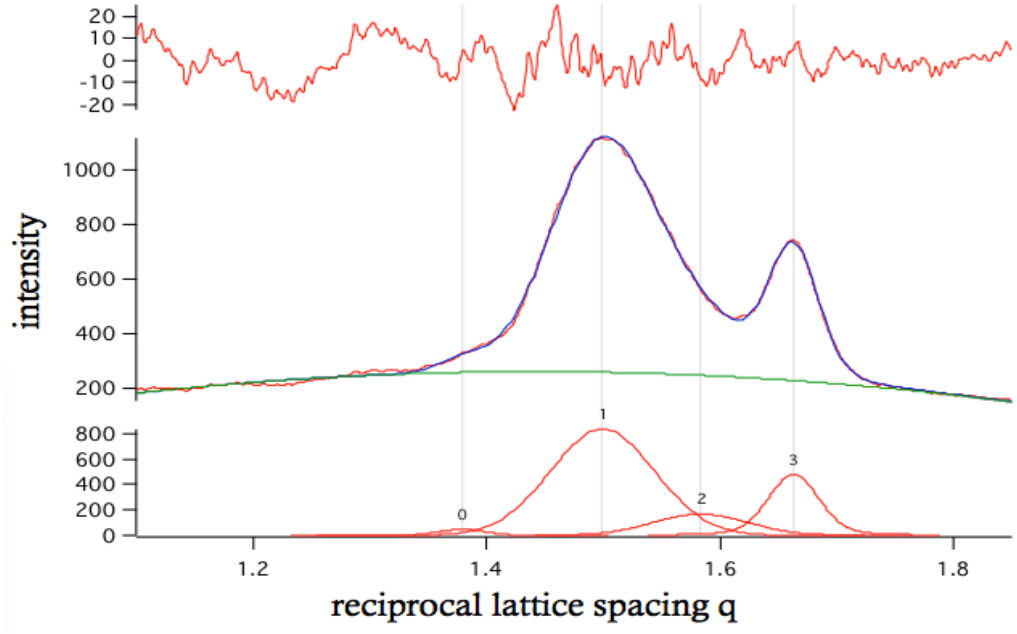

Figure 4 - 5 The fitted Wide Angle Diffraction patterns of β' form PPP by Igor Pro. Broad peaks are often associated with form β' one.

The β' form is identified by an orthorhombic subcell packing, which results in two strong reflections around 4.2 Å and 3.8 Å (Kellens et al., 1990). In Figure 4-5, these two characteristic peaks are peak 1 and peak 3.

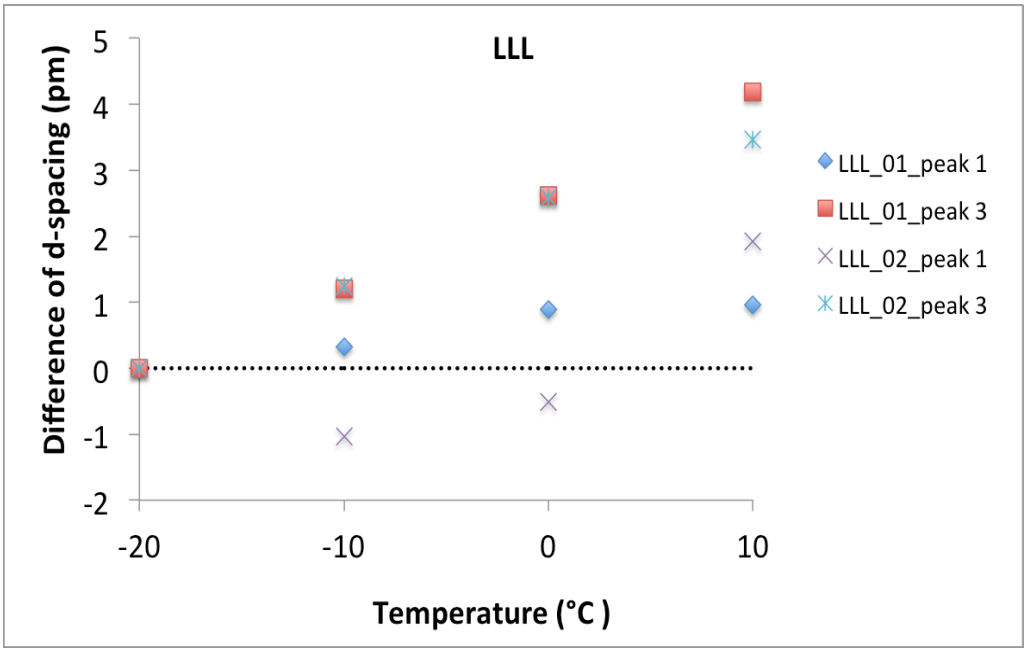

(a)

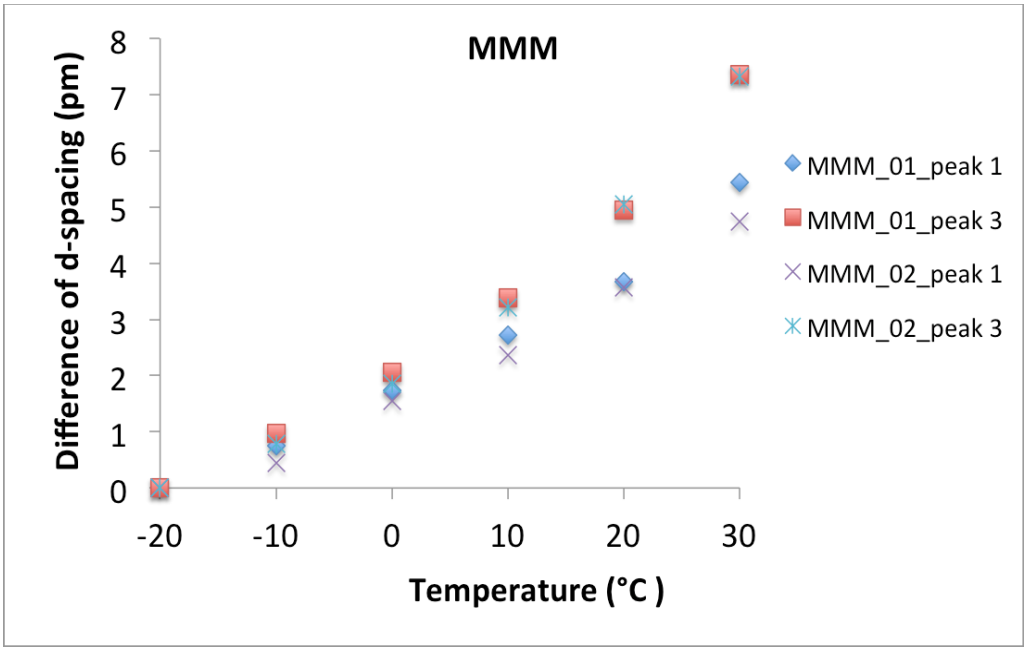
MMM
Difference of d-spacing (pm)
Temperature (°C)
MMM_01_peak 1
MMM_01_peak 3
MMM_02_peak 1
MMM_02_peak 3

(b)

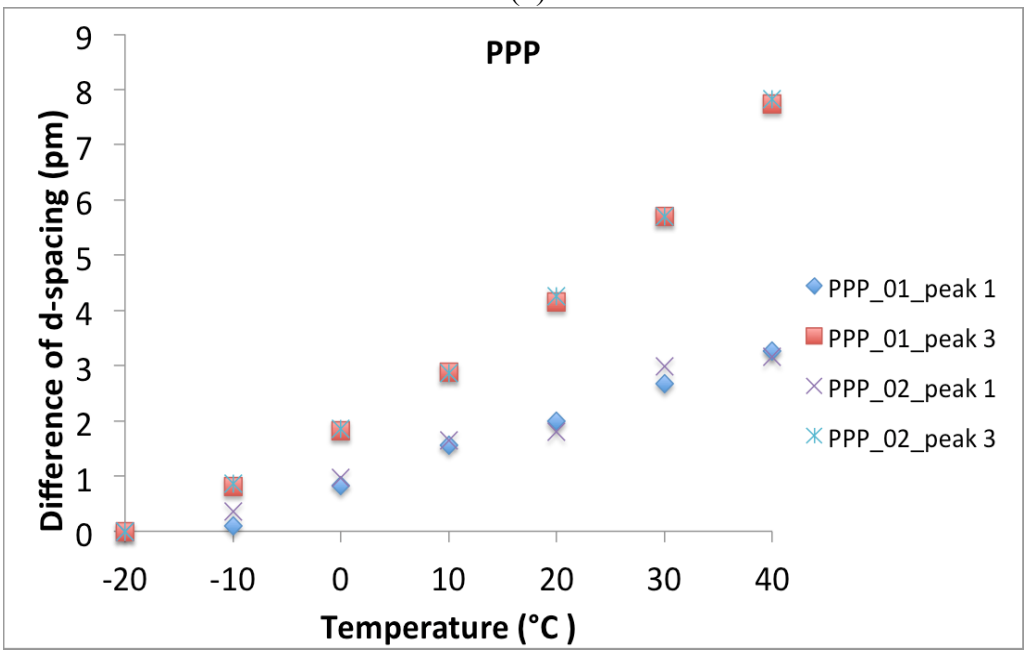
PPP
Difference of d-spacing (pm)
Temperature (°C)
PPP_01_peak 1
PPP_01_peak 3
PPP_02_peak 1
PPP_02_peak 3

(c)

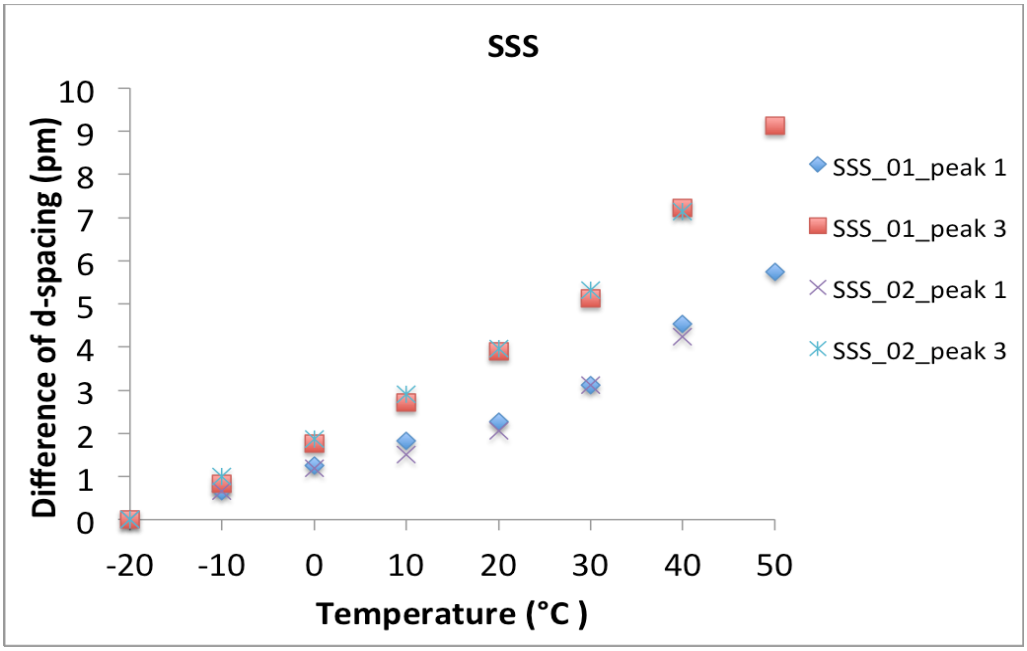

(d)

Figure 4 - 6 Differences of d-spacings with temperature of β' form WAXD Peaks. (a) LLL. (b) MMM. (c) PPP. (d) SSS.

When the temperature increases, the d-spacings of both characteristic peaks of β' form WAXD patterns also increase. Even though the two characteristic peaks of β' form change with temperature, the temperature effect on the peaks with small d-spacing is stronger, and of about the same order as was observed for beta, about 9 pm from -20 to 50 °C. From Figure 4-6 it is obvious that the d-spacings of the peak with small d-spacing (3.8 Å) increase with temperature much faster than the peak with large d-spacing (4.2 Å).

The similarity of this observation with the beta structure suggests that similar intermolecular forces are affected.

4.1.3 Effect of Temperature on d-spacing of α Form WAXD Peaks

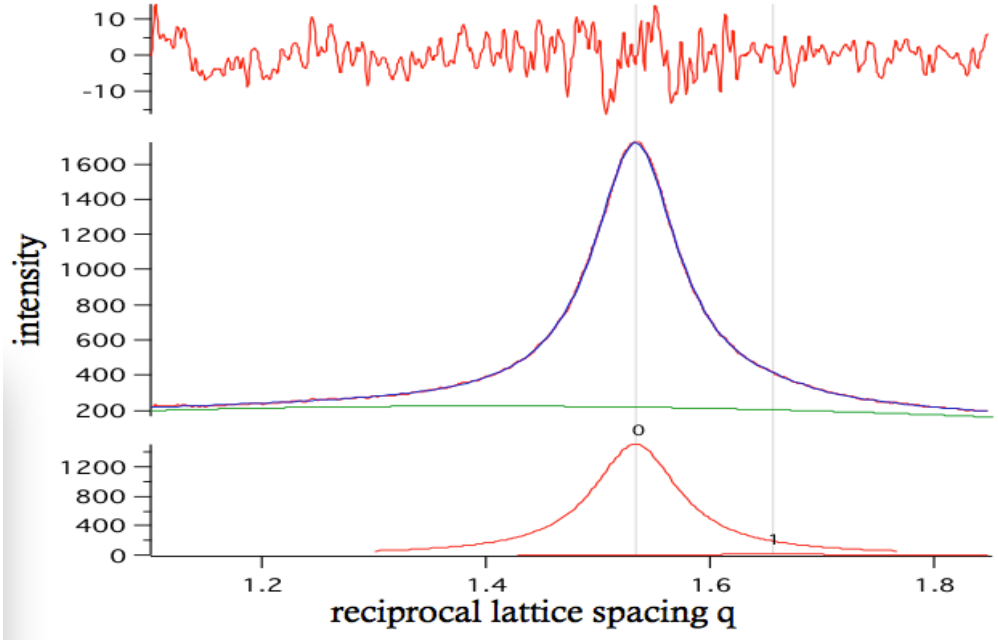

Figure 4 - 7 The fitted Wide Angle Diffraction patterns of α form PPP by Igor Pro.

The α form is characterized by a single strong reflection at 4.15 Å of the hexagonal packing (Kellens et al., 1990). In Figure 4-7, this characteristic peak is peak 0. Since it was hard for LLL to crystallize in α form, just three pure triacylglycerols (MMM, PPP, SSS) were used to produce the WAXD patterns. The α phase peak is very broad because this phase lacks long-range order in the rotational degree of freedom of the molecules about their long axes. The enhanced chain mobility in the metastable hexagonal phase may cause lamellar thickening (Sirota and Herhold, 2000).

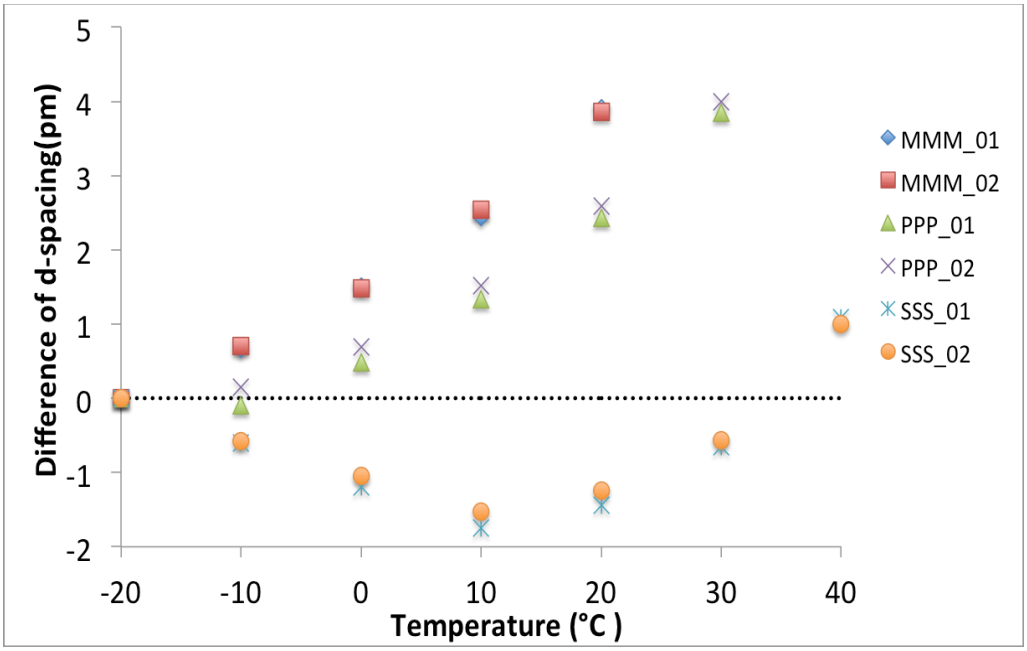

Figure 4 - 8 Differences of d-spacings with temperature of α form WAXD Peaks.

For MMM and PPP, the d-spacings of the characteristic peak increase with the temperature, as was found for β' and β form. However, for SSS, the d-spacings first decrease when the temperature increases from -20 °C to 10 °C. When the temperature keeps increasing from 10 °C to 40 °C, the d-spacings increase. It is not obvious why such behavior would happen, since it would mean that alpha has a negative expansion coefficient in the direction of the hexagonal lattice at temperatures below 10 °C. Since the SAXS have not been measured, it is not possible to know if the overall density of the nanocrystals increased or decreased. A possible reason is that SSS may have formed rather "imperfect" alpha crystals due to the fast cooling rate and its large size, and these crystals annealed to a closer packed lattice as temperature increased. Above 10 °C the lattice may be stable, and it expands with temperature. These conjectures need to be further tested by cooling back the alpha phase formed.

4.2 Reversibility of d-spacing of WAXD Peaks of β Form

In Figure 4-9, d-spacings of the crystallized WAXD peaks show reversibility, especially peaks with small d-spacing. When the temperature increases, the d-spacings keep increasing and when the temperature decreases, the d-spacings go back to their original value. Since the energy needed for the peaks with small d-spacing to change is much smaller, the reversibility is much more obvious than other peaks. In Figure 4-10, for the peaks with small d-spacing (Peak 7 and Peak 9), the differences of d-spacings show the same changing trend with the temperature. The difference of d-spacing is highest when the temperature reaches 40 °C and it is almost back to 0 when the temperature goes back to -20 °C. These results all show that the change of the d-spacing is reversible. The reversibility of d-spacing of WAXD peaks indicates that the temperature effect on the WAXD peaks of nanocrystalline triacylglycerols can occur not just in one single experiment or circumstance. The temperature effect always exists in the experiment and affects the samples. This observation is very important for the intended use of the small d-spacings as potential intrinsic thermometers for experiments of crystallization under shear flow.

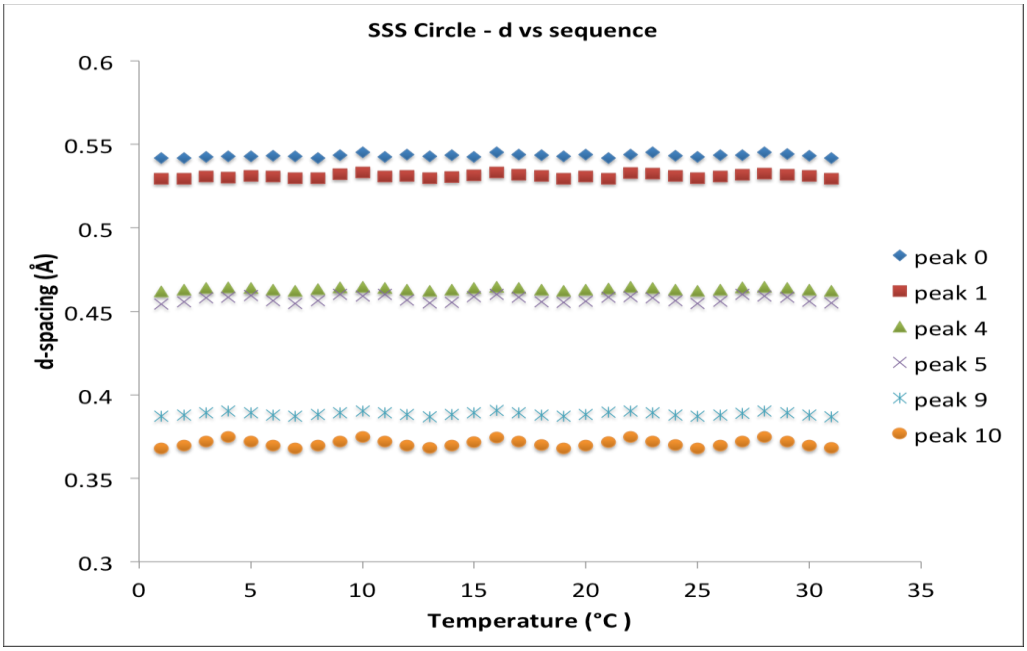

Figure 4 - 9 d-spacings of WAXD peaks versus sequence (SSS).

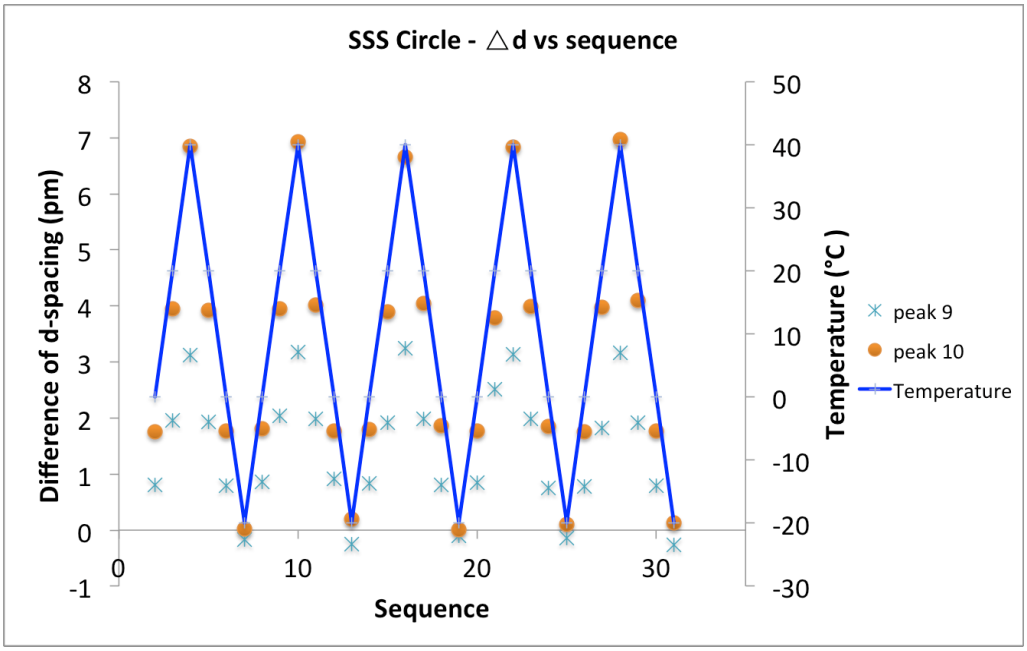

Figure 4 - 10 Differences of d-spacings of WAXD peaks with small d-spacing (SSS).

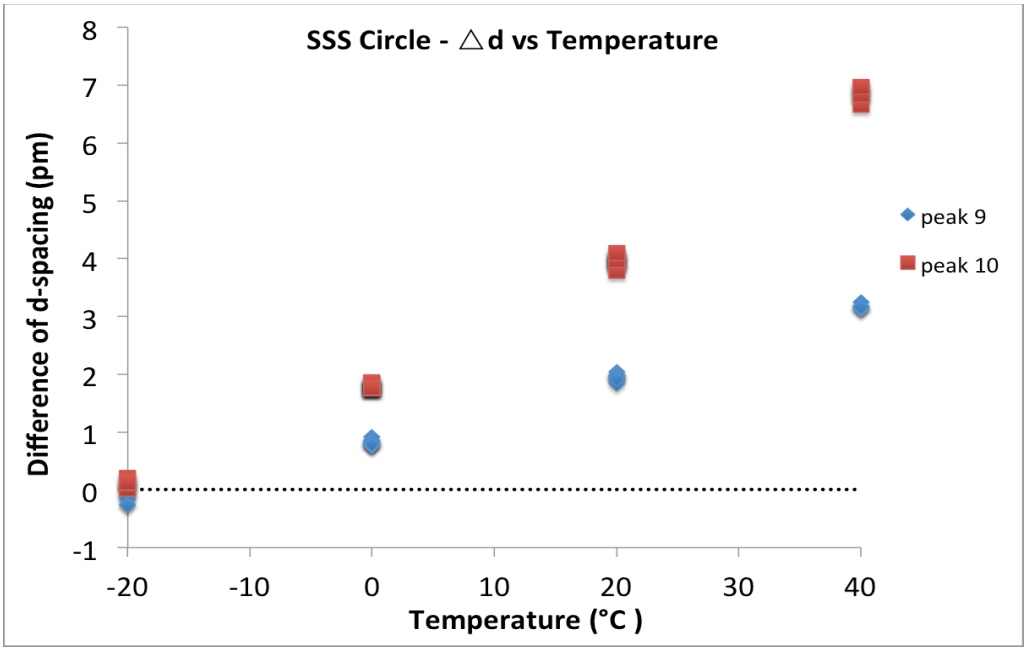

Figure 4 - 11 Differences of d-spacings of WAXD peaks with small d-spacing (SSS) versus temperature in the case where the temperature was cycled up and down.

4.3 Estimation of Temperature from Difference of d-spacing

Since the differences of d-spacings for the peaks with small d-spacing increase as the temperature increases, we can find some mathematical relationship between the difference of d-spacing and the crystallization temperature. After the mathematical relationship between temperature and difference of d-spacing is known, the real sample temperature can be calculated by measuring the difference of the d-spacing using x-ray techniques. In the actual experiment circumstance, there is a gap between the set temperature and the real sample temperature and many factors can affect the sample temperature, such as the interference of the ambient temperature and especially the viscous heat generated. It is hard for experimenters to measure the real sample temperature and it adds difficulty to study the effect of temperature on the crystallization process. Measurement of the small d-spacing change gives researchers a chance to estimate the real sample temperature and make more accurate discussion of the temperature effects. It provides a new way to

monitor and control the temperature of the system under study and the effect of high shear rate on nanocrystalline triacylglycerols crystallization.

As shown in Figure 4-12, there are mathematical relationships between the temperature and the differences of d-spacings for the pure materials. Taking the LLL as example, differences of d-spacings of peak 9 and peak 10 increase with the temperature increase. We can calculate the sample temperature using the equation shown in Figure 4-12 (a). Although the calculated temperature is still an estimated temperature, it is much closer to the real sample temperature and gives us a better understanding for the temperature change of the system and the effect of high shear rate.

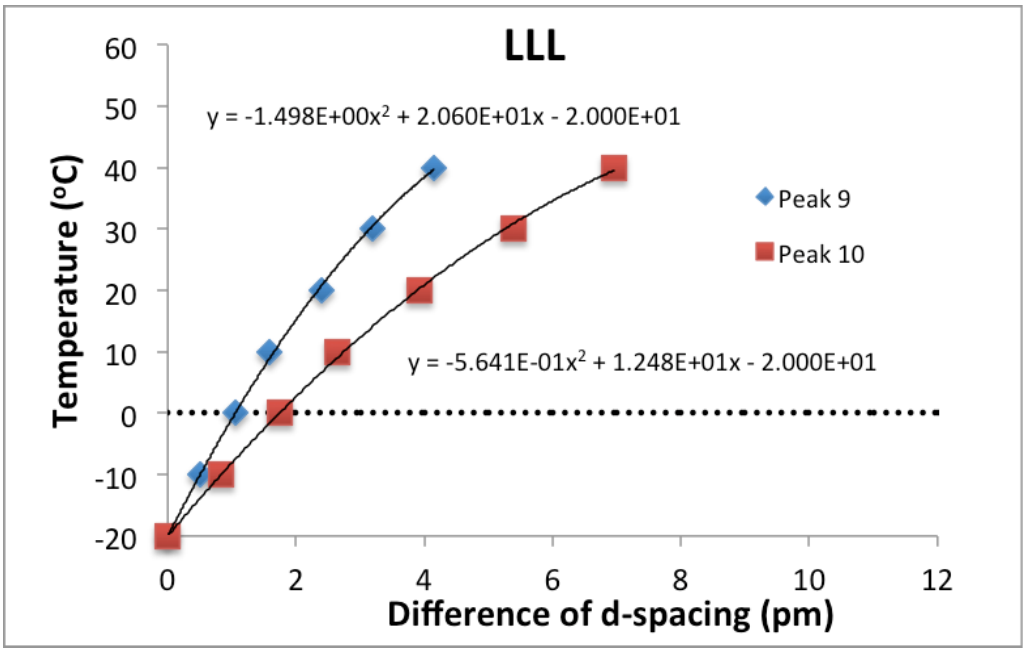

(a)

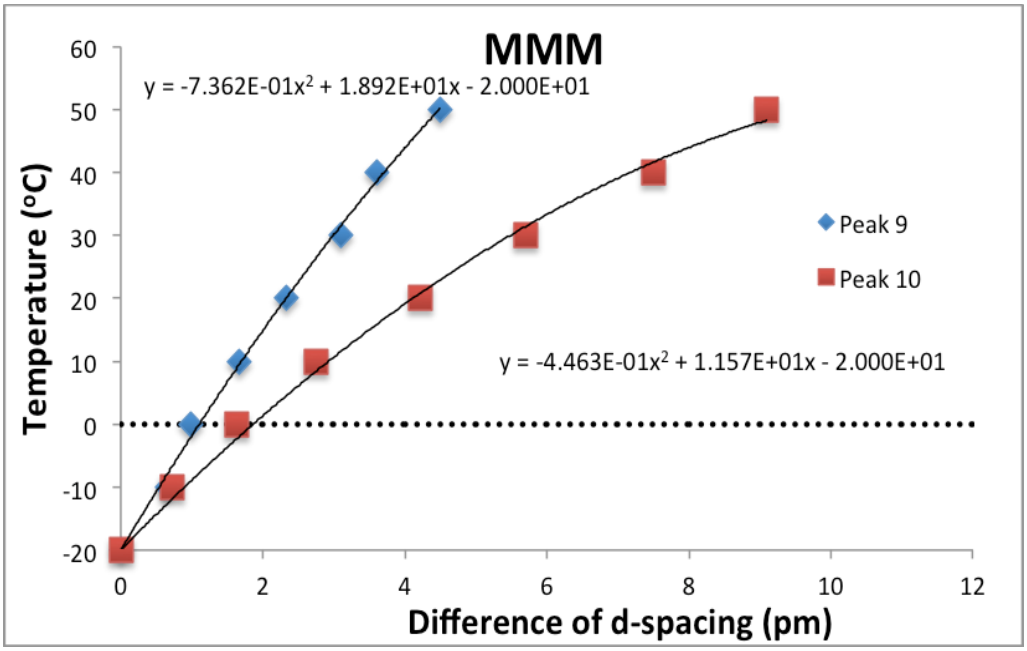
MMM
y = -7.362E-01x² + 1.892E+01x - 2.000E+01
y = -4.463E-01x² + 1.157E+01x - 2.000E+01
Peak 9
Peak 10
Temperature (°C)
Difference of d-spacing (pm)
60
50
40
30
20
10
0
-10
-20
0
2
4
6
8
10
12

(b)

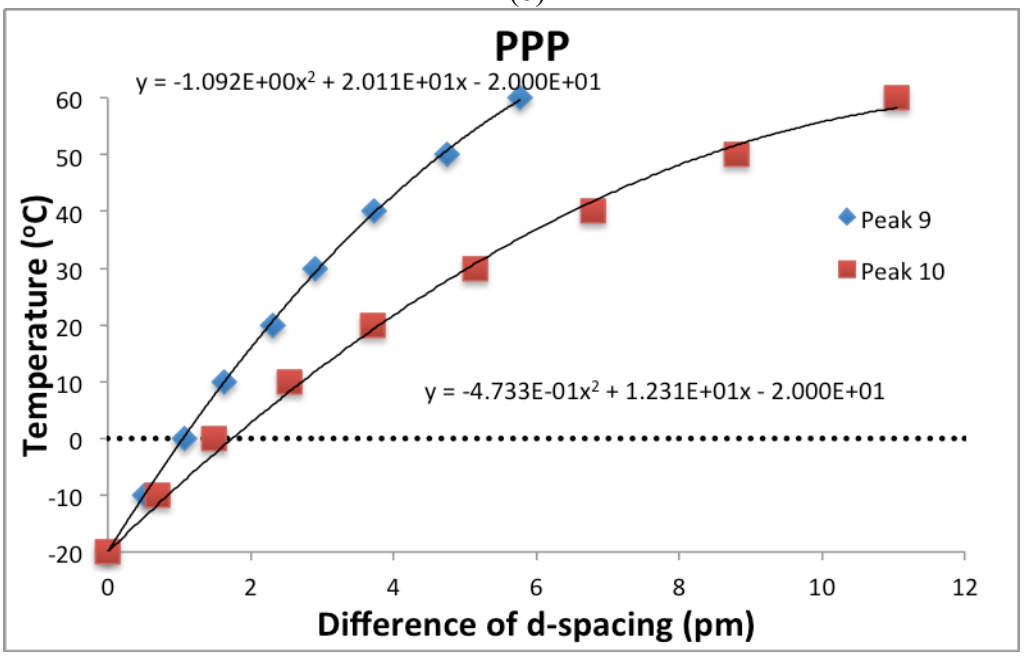
PPP
y = -1.092E+00x² + 2.011E+01x - 2.000E+01
y = -4.733E-01x² + 1.231E+01x - 2.000E+01
Peak 9
Peak 10
Temperature (°C)
Difference of d-spacing (pm)
60
50
40
30
20
10
0
-10
-20
0
2
4
6
8
10
12

(c)

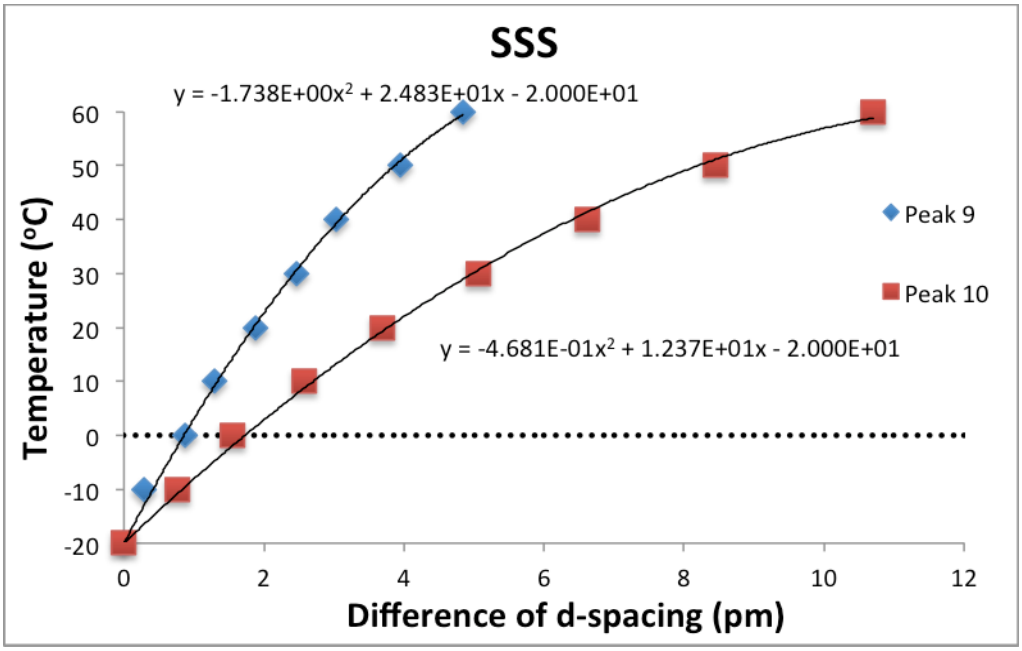

(d)

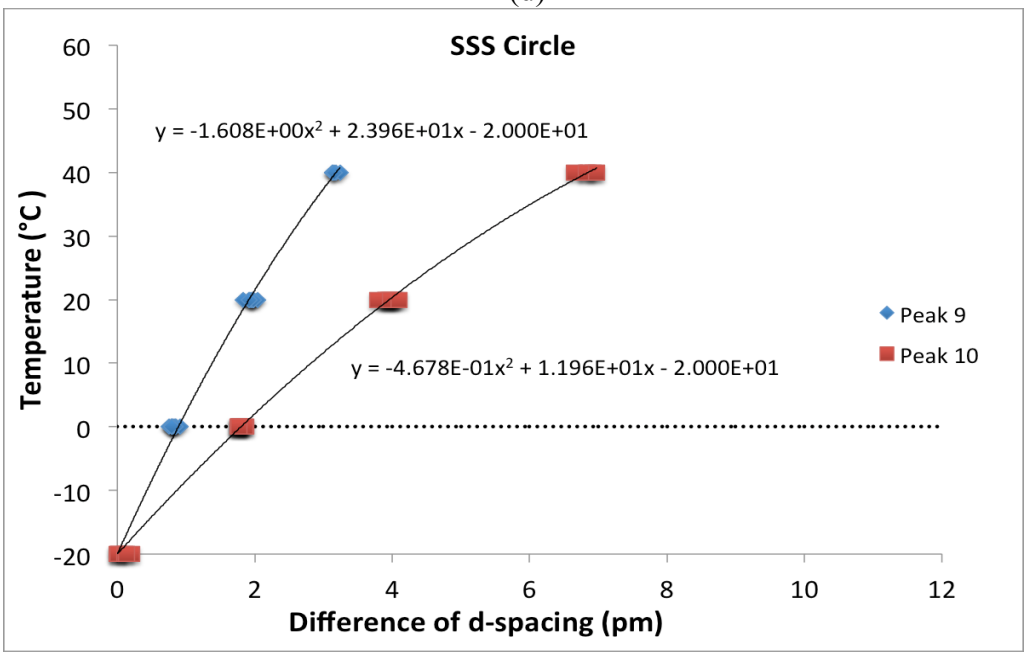

(e)

Figure 4 - 12 Temperature versus differences of d-spacings for peaks with small d-spacing. (a) LLL. (b) MMM. (c) PPP. (d) SSS. (e) SSS Circle.

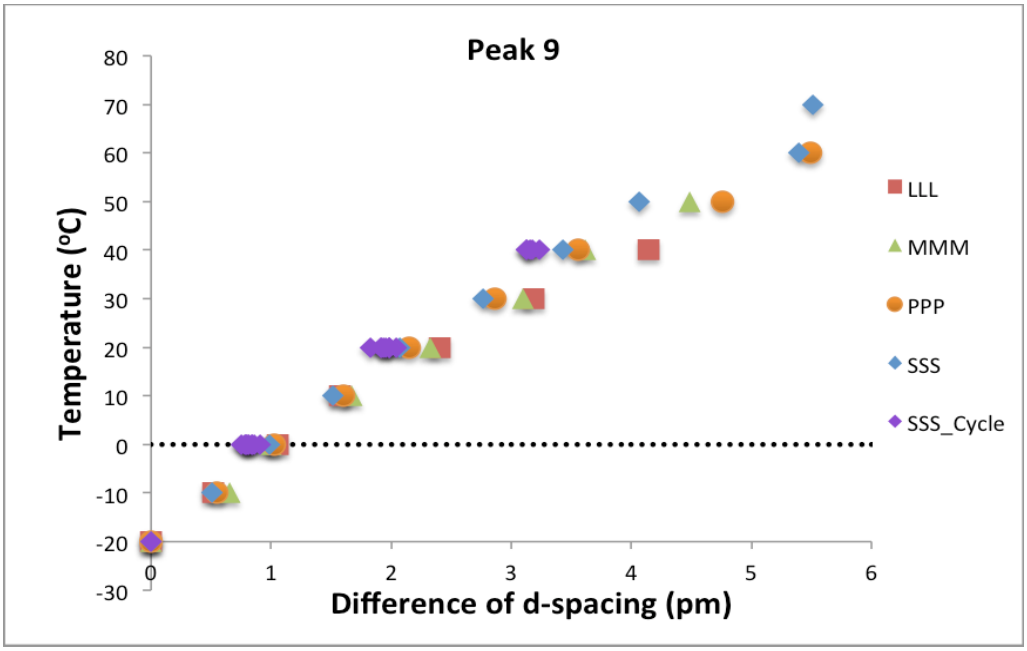
Peak 9
Temperature (°C)
Difference of d-spacing (pm)
LLL
MMM
PPP
SSS
SSS_Cycle

(a)

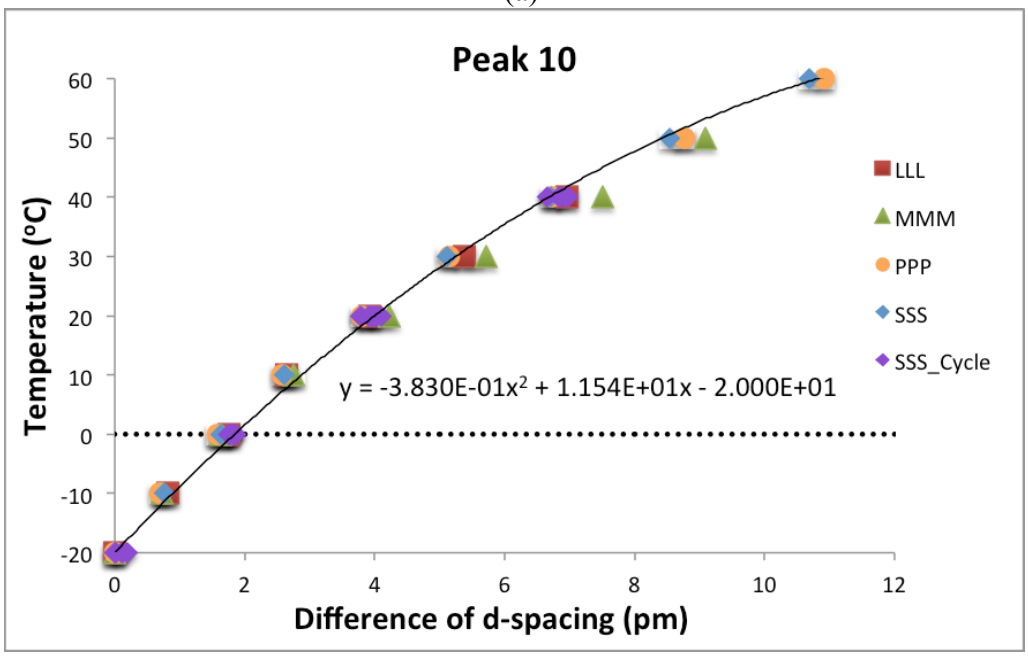
Peak 10
Temperature (°C)
Difference of d-spacing (pm)
y = -3.830E-01x² + 1.154E+01x - 2.000E+01
LLL
MMM
PPP
SSS
SSS_Cycle

(b)

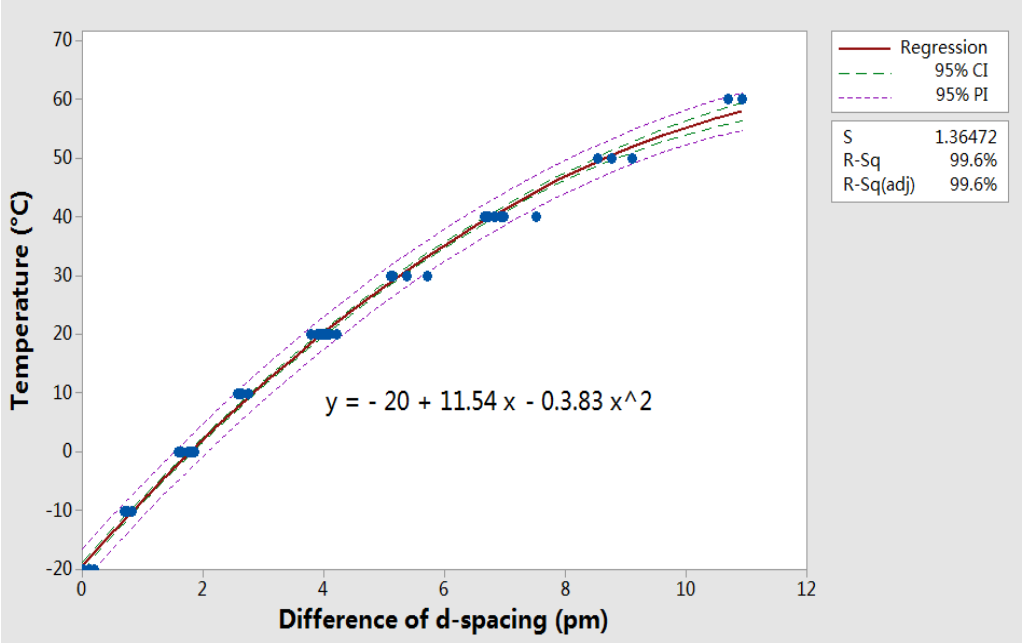

(c)

Figure 4 - 13 Temperature versus differences of d-spacings for peaks with small d-spacing (All β form pure triacylglycerols samples). (a) Peaks with small d-spacing at 3.85 Å. (b) Peaks with small d-spacing at 3.7 Å. (c) Regression of peaks with small d-spacing at 3.7 Å with 95% confidence interval.

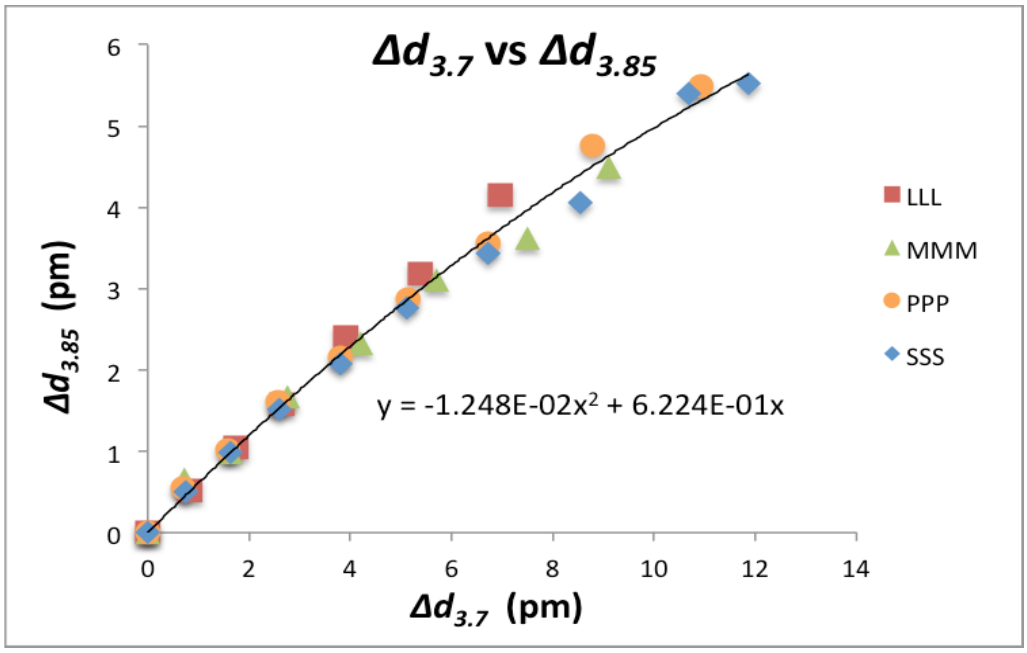

Figure 4 - 14 Δd 3.7 vs Δd 3.85 of four pure TAGs

The trends in the differences of these d-spacings of all the pure triacylglycerol samples versus temperatures show great consistency. It is likely that a single mathematical

function may describe the relationship of d-spacing with temperature, especially the characteristic peak with small d-spacing at 3.7 Å (the red square in Figure 4-12). This means that there may be one mathematical equation or model that can be applied to estimate the temperature of all the four pure triacylglycerol samples. According the confidence interval in Figure 4-13 (c), the equation shows high reliability. The differences of d-spacings for the peaks with small d-spacing at 3.7 Å may be the best peak for β form pure triacylglycerols samples to estimate the real sample temperatures in future studies. In Figure 4-14, for all the four pure triacylglycerol samples, the difference of d-spacings for the peaks with small d-spacing at 3.7 Å change with the difference of d-spacings for the peaks with small d-spacing at 3.85 Å. It indicates the change of one WAXD peak can be estimated from the change of another peak. The dependency means that measuring both peaks could provide a "safeguard" to the estimate of temperature, but one could focus on the 3.7 Å peak exclusively.

4.4 Calculation of Unit Cell Values of β form TAGs from the d-spacings

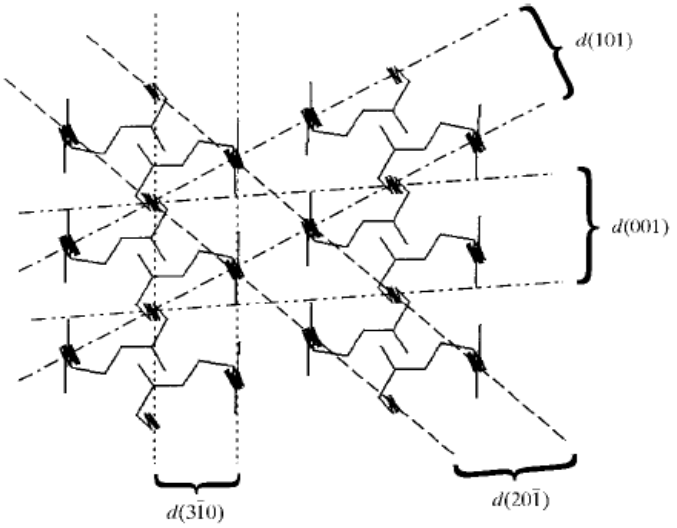

Figure 4 - 15 Crystal structure of β form TAGs with the acyl chains perpendicular to the plane of paper Van Langevelde et al. (1999).

From the d_o in Table 4-1 and the lattice planes shown in Figure 4-15, the change in the peaks with d-spacing at 4.6 Å, 3.85 Å and 3.7 Å in this research corresponds to change of *d(1 0 1)*, *d(2 0 -1)* and *d(3 -1 0)*. In order to understand the reason why the d-spacing of WAXD peaks change in different ways, the unit cell value of β form TAGs needs to be understood.

In Figure 4-4 it can be seen that a change in temperature from -20°C to 60°C represents a change in d 3.7 of 12 pm. To calculate the expansion percentage, the increase of d-spacing is divided by the original d-spacing for each peak. This is approximately 12/0.37 = 3.3%. The change for the 3.85 peak can be estimated from Figure 4-4 5.5 pm. Thus 5.5/0.385 = 1.4 %. The change for the 4.6 peak is very small, around 1 pm 1/0.46 = 0.2%.

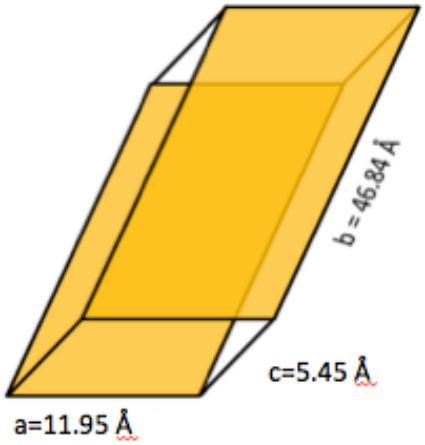

Figure 4 - 16 Triclinic unit cell of β form PPP with the acyl chains, with the cell values from Van Langevelde et al. (1999)

Using the equation (5) to (12) in Part 2.2.1, the value of d, the distance between adjacent planes in the set (*hkl*), of β form crystals can be calculated. The results are shown in Table 4-1. After comparing with the d_0 in the literature, d-spacing of peak 3.75 Å, peak 3.8 Å and peak 4.58 Å expand 3.30%, 1.27% and 0.101% respectively. In order to get how the *a, b, c* parameters change, the Excel solver is applied and the percentages of change are set for each peak: 3.0%, 1.5% and 0.1%. The result (Table 4-2) shows *a* parameter

increases about 3.5% and the increase of *b* parameter even exceeds the limit set. But the *c* parameter decreases slightly. It means in *a* and *b* direction, the crystal expands but in *c* direction the crystal contracts a little bit. Since we lack small angle x-ray diffraction data, how much *b* parameter really change remains unknown.

The change in volume is 6.9 %, and the average expansion coefficient of this crystal would be

$$\boldsymbol{\beta} = \frac{\partial\left(\frac{\Delta V}{V}\right)}{\partial T} = 8.6 \text{ E-04 } K^{-1}$$

This expansion coefficient values are similar to those of many organic liquids, but are orders of magnitude larger than those of urea (~10^{-5}) or benzophenone (~10^{-7}) (Hammond et al, 2005). Thus it seems that the relative strength of the forces holding the TAGs molecules together are much weaker than those of smaller organic crystals (Templin, 1956).

Table 4 - 1 Characteristic d-spacing (Å) for the β TAGs

	d(1 0 1)	***d(2 0 -1)***	***d(3 -1 0)***
h	1	2	3
k	0	0	-1
l	1	-1	0
d_o	4.5844	3.8131	3.6387
d_{cal}	4.5890	3.8615	3.7587
Ratio of change (%)	1.01E-03	1.27E-02	3.30E-02
Target change (%)	1.00E-03	1.50E-02	3.00E-02

d_o is the *d spacing* from Van Langevelde et al. (1999).

Table 4 - 2 Cell parameters of β TAGs

	Cell parameters from Van Langevelde et al. (1999)	Cell parameters calculated using Excel Solver	% Expansion
a (Å)	11.95	12.2626	2.616
b (Å)	46.84	48.7136	4.000 (limit set)
c (Å)	5.4514	5.4437	-0.142
V(Å^3)	2581.0	2750.6	6.571

CHAPTER 5 RESULTS AND DISCUSSION – II - EFFECT OF TEMPERATURE ON WAXD OF TRIACYLGLYCEROLS MIXTURES

5.1 Effect of Temperature on d-spacing of WAXD Peaks

5.1.1 Effect of Temperature on d-spacing of β Form WAXD Peaks (Dry Blends)

Figure 5-1 shows the original wide angle x-ray peaks of β form 3L7M and the intensity of the peaks, as they were fitted using Igor Pro. The very strong reflection at about 4.6 Å and the other two strong reflections at about 3.85 Å and 3.7 Å show that 3L7M had crystallized in β form. The green line is the base line of the fitting. The upper part shows the error of the fitting is less than 0.5%. The lower part shows the fitted wide angle x-ray peaks of β form 3L7M and the intensity of each peak.

There are six or seven main peaks in the WAXD patterns which have higher intensity than others. To reveal the effect of temperature on d-spacings of dry blend samples, for the β polymorph, these peaks are also compared and discussed according to their locations: 1. Large d-spacing; 2. Medium d-spacing. 3. Small d-spacing.

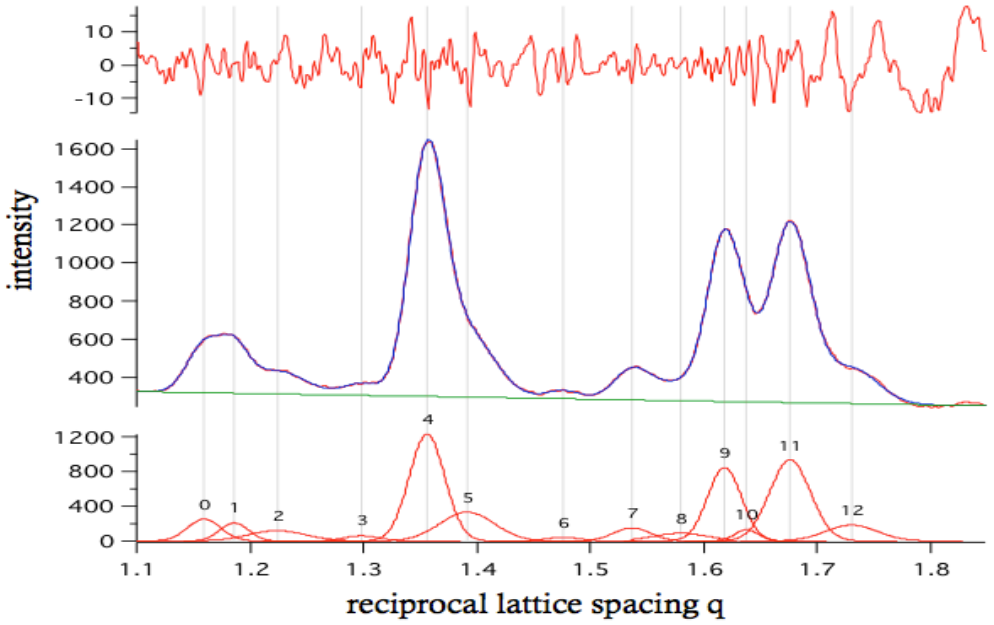

Figure 5 - 1 The fitted wide angle diffraction patterns of β form 3L7M by Igor Pro.

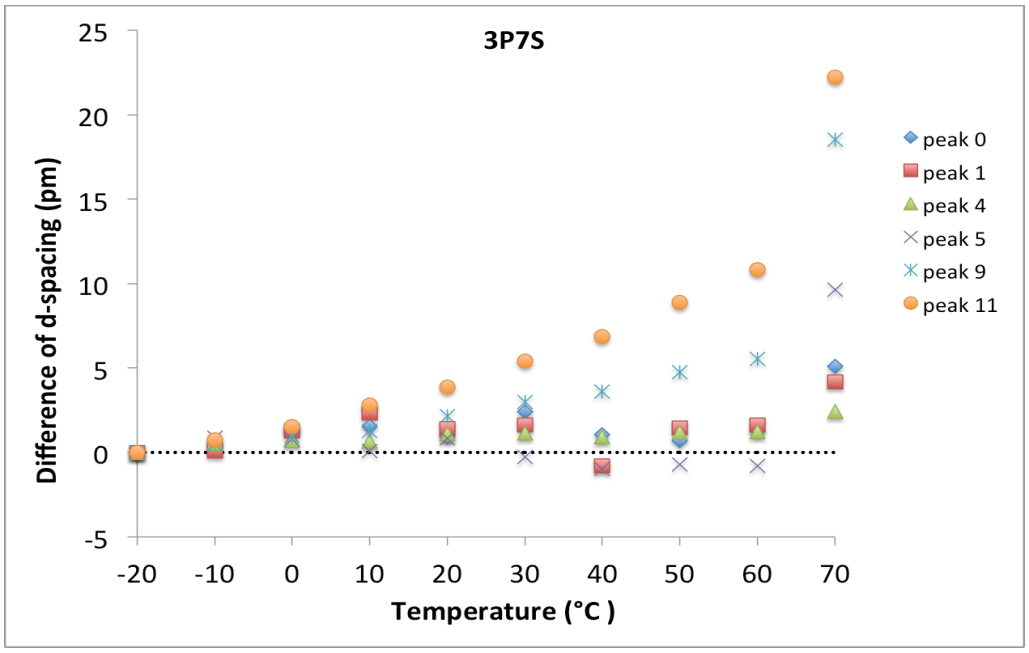

(a)

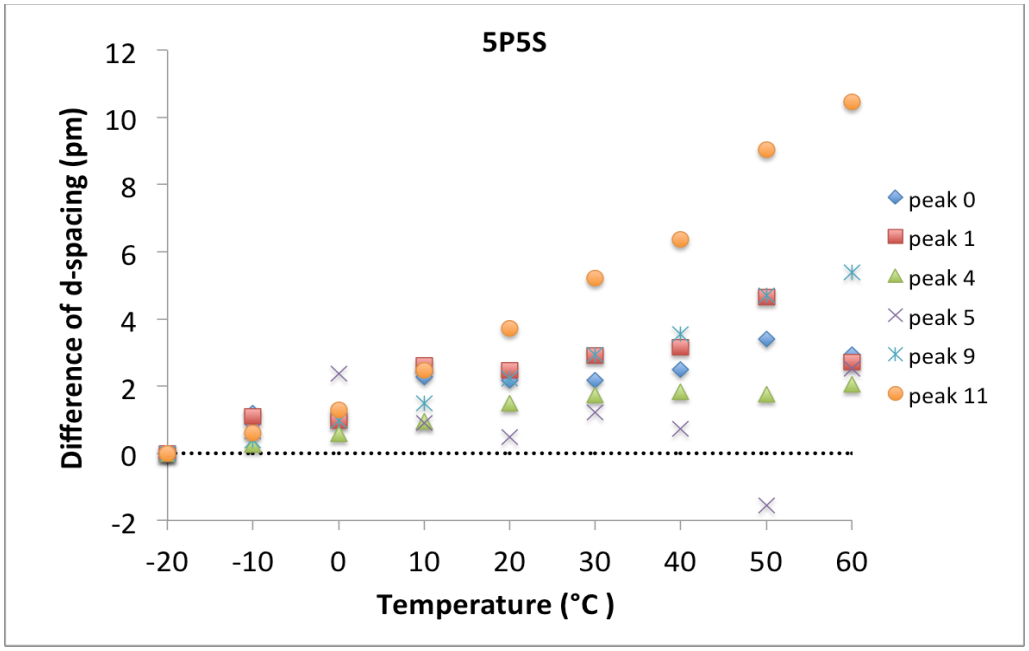

(b)

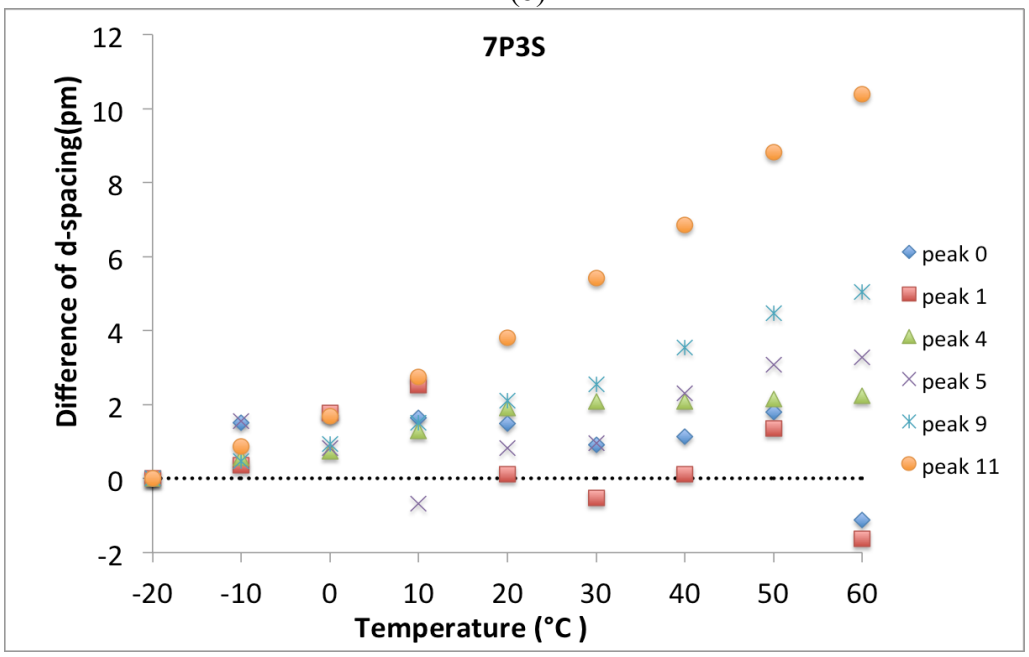

(c)

Figure 5 - 2 Differences of d-spacings with temperature. (a) 3P7S. (b) 5P5S. (c) 7P3S.

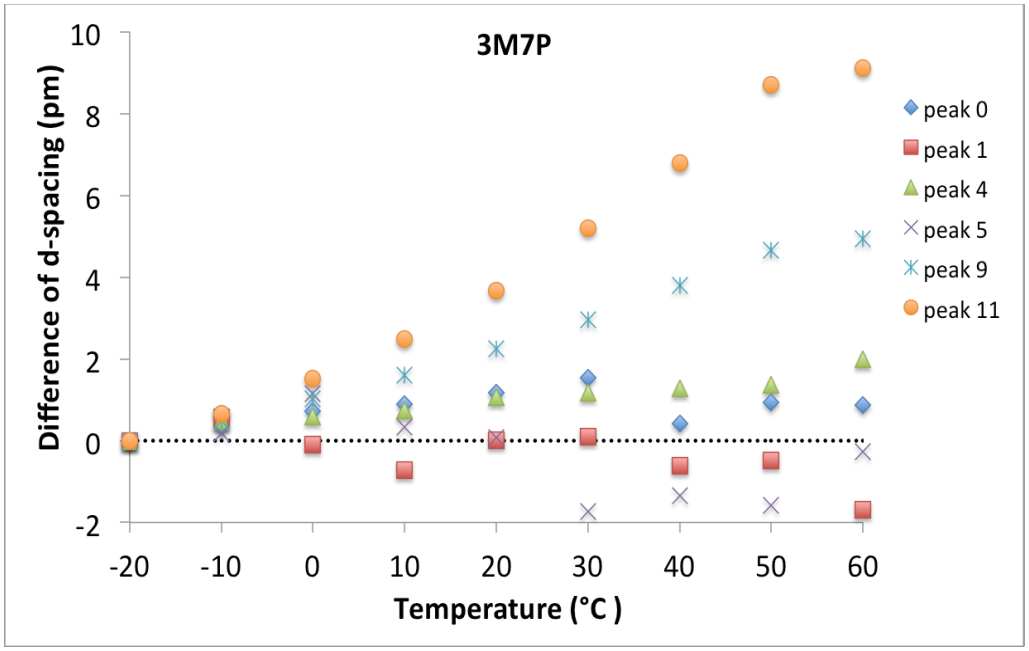
3M7P
Difference of d-spacing (pm)
Temperature (°C)
peak 0
peak 1
peak 4
peak 5
peak 9
peak 11

(a)

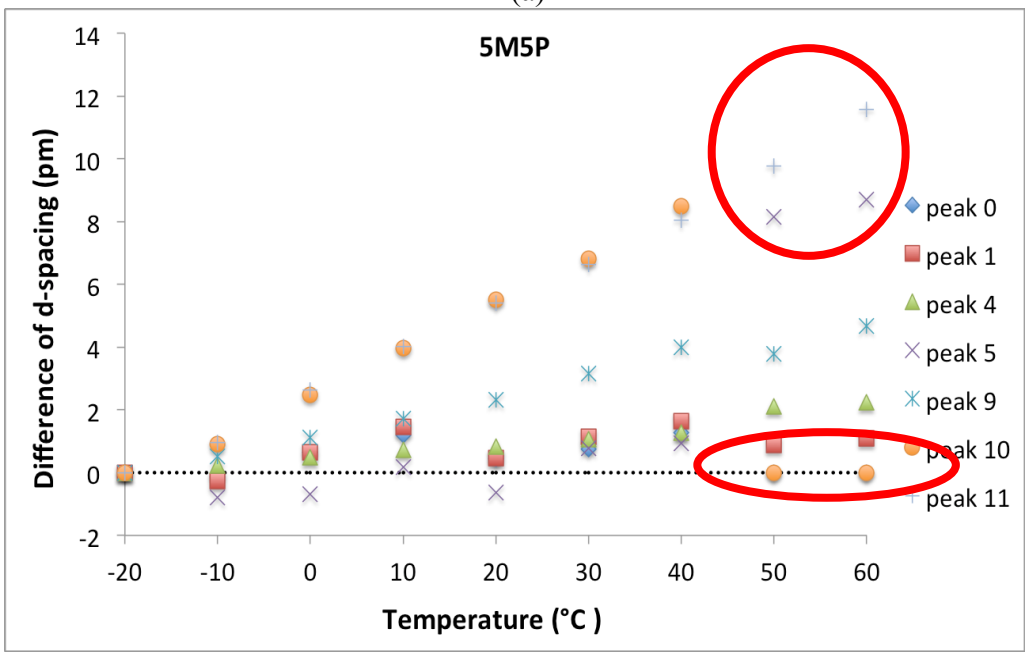
5M5P
Difference of d-spacing (pm)
Temperature (°C)
peak 0
peak 1
peak 4
peak 5
peak 9
peak 10
peak 11

(b)

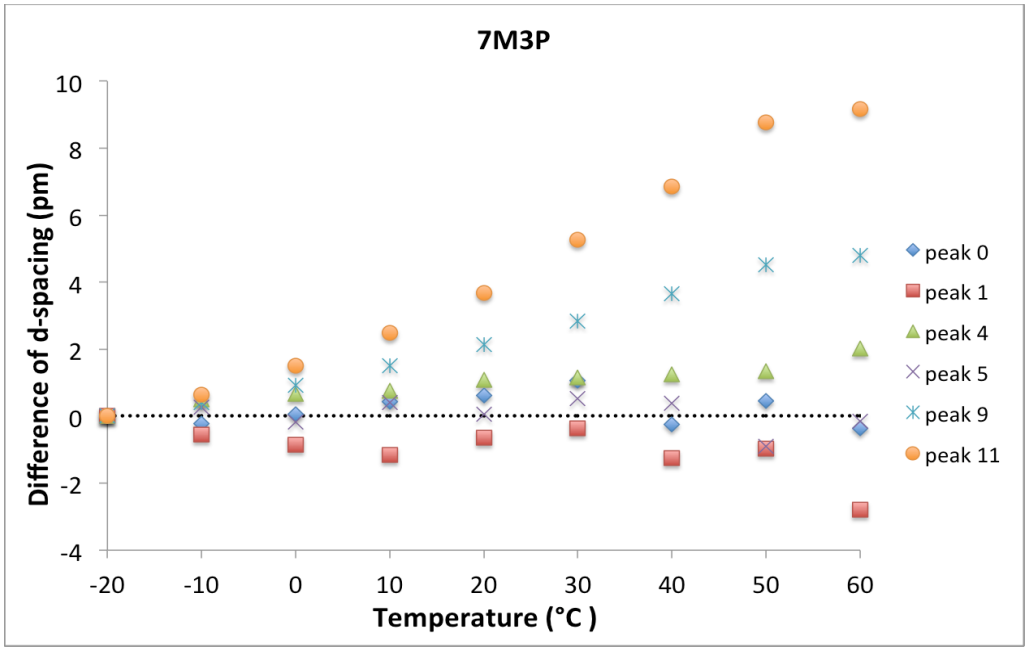

(c)

Figure 5 - 3 Differences of d-spacings with temperature. (a) 3M7P. (b) 5M5P. (c) 7M3P.

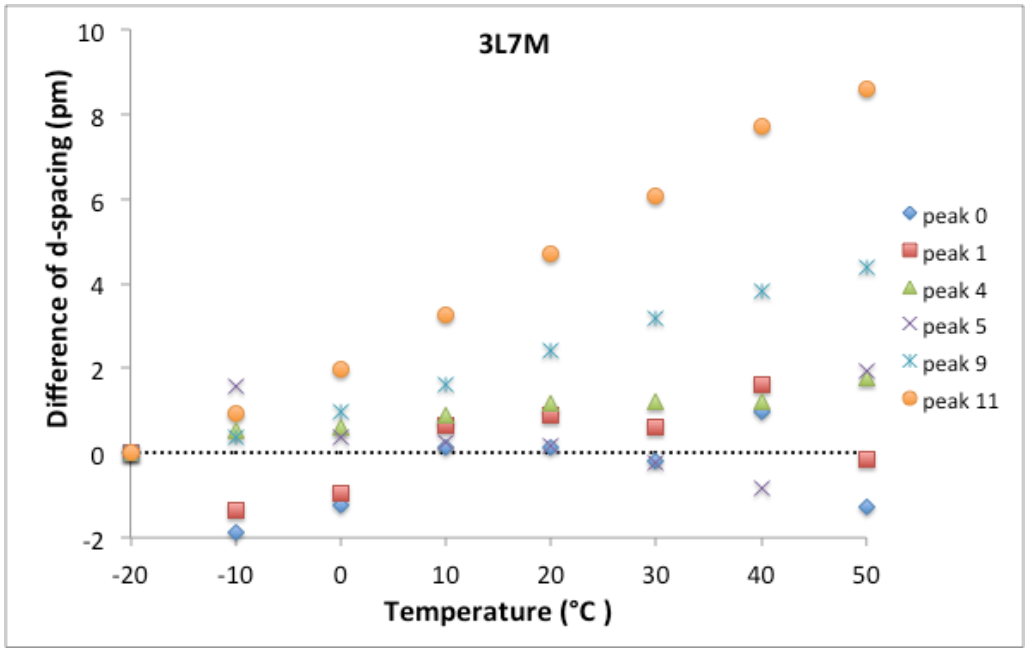

(a)

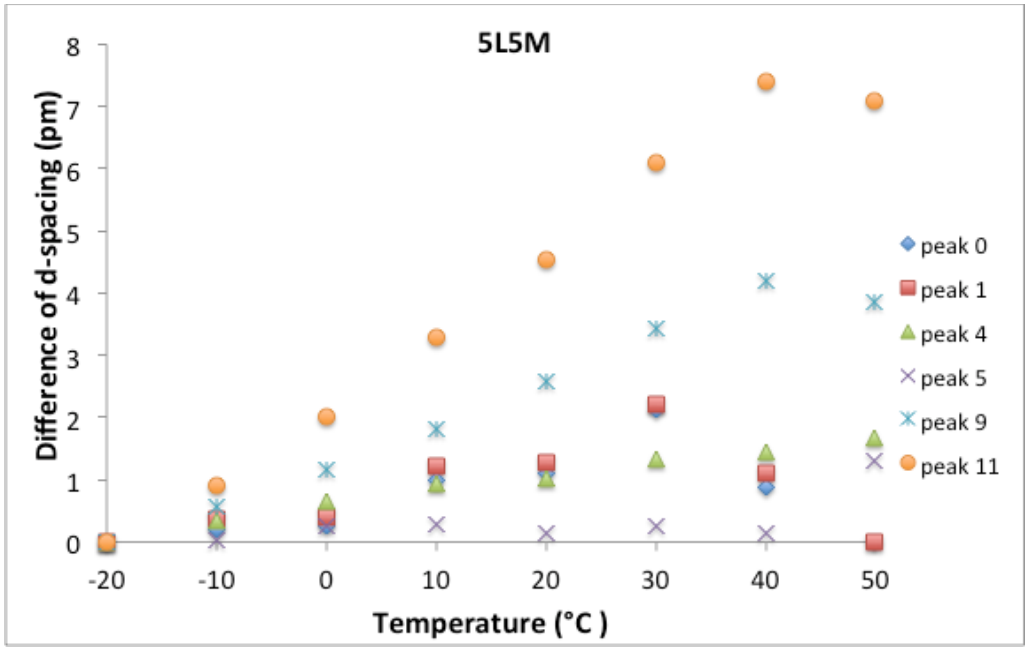

(b)

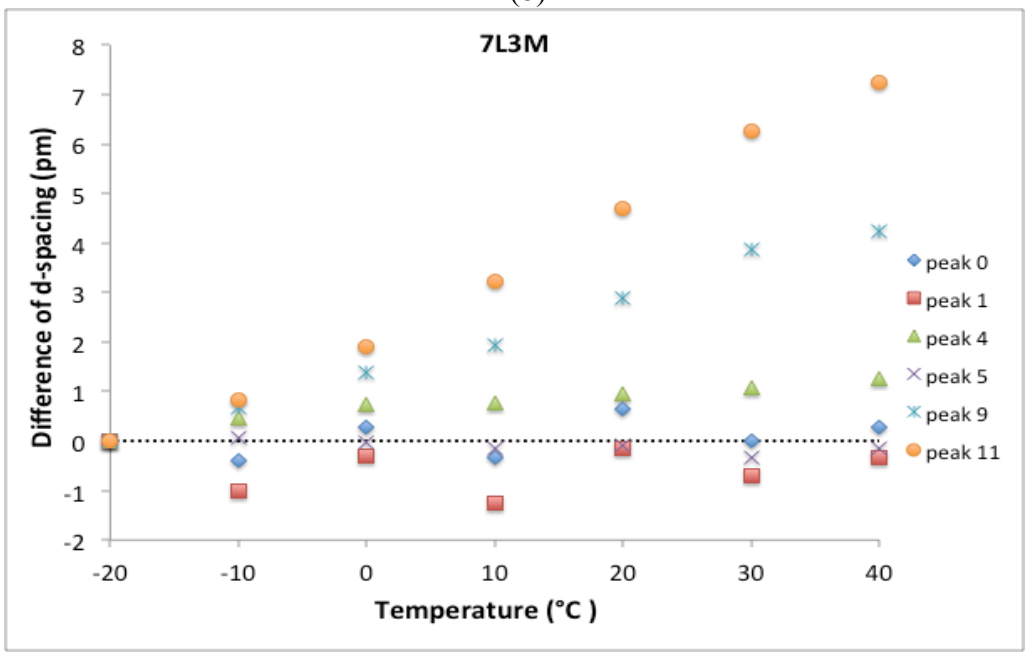

(c)

Figure 5 - 4 Difference of d-spacing with temperature. (a) 3L7M. (b) 5L5M. (c) 7L3M.

The same results are found in triacylglycerol mixtures as in the pure triacylglycerols. For the peaks with large d-spacing, when the temperature increases the d-spacing remains essentially the same as that under the reference temperature (-20°C).

For the peaks with medium d-spacing, when the temperature increased to 10°C, the d-

spacing is about 1 pm larger than the original one. When the temperature continues to increase, the increase of the d-spacings stops. The peak with d-spacing 4.6 Å is formed by two peaks overlapping each other so it is hard for Igor Pro to separate them, and the points of these two peaks in Figure 5-2, 5-3, 5-4 fluctuate a little bit.

For the peaks with small d-spacing, when the temperature rises the d-spacing keeps increasing. The position of the peaks with small d-spacing is affected by temperature much more than other peaks. This result can apply to all triacylglycerols mixtures (dry blends).

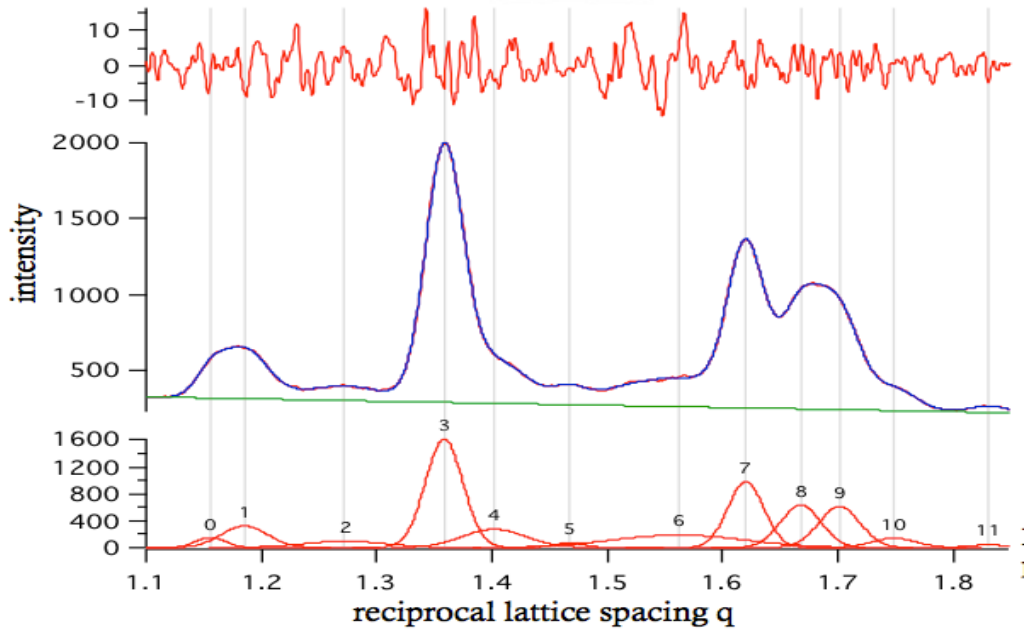

Figure 5 - 5 The fitted Wide Angle Diffraction patterns of β form 5L5S by Igor Pro.

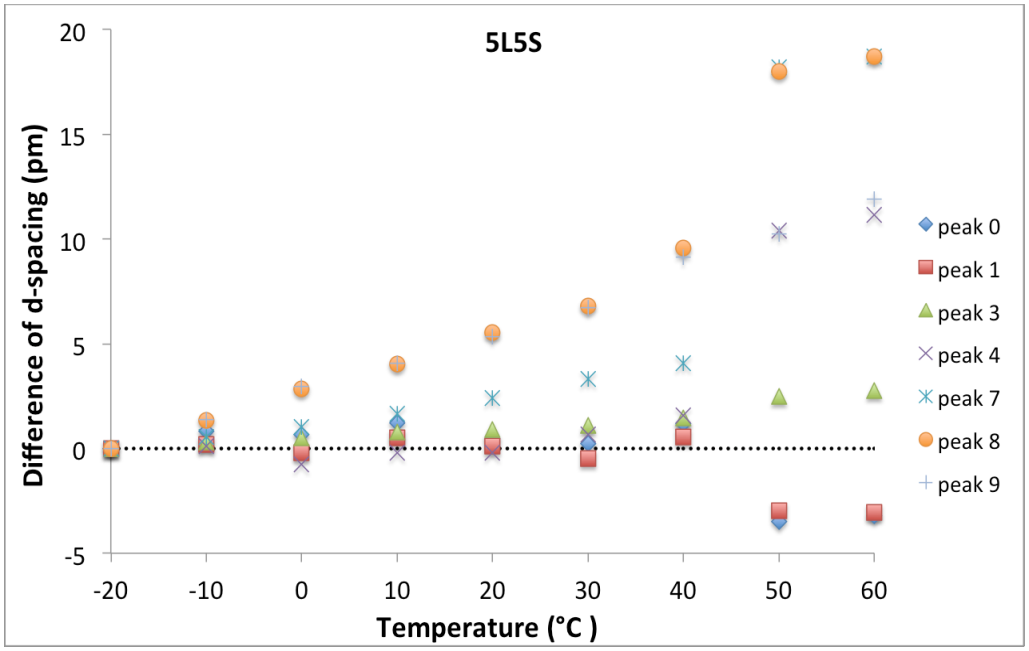

Figure 5 - 6 Difference of d-spacing with temperature of 5L5S.

There is a difference between the fitted WAXD patterns of 5L5S and 5M5P and the fitted WAXD patterns of other dry blend samples. In 5L5S and 5M5P (Figure 5-6 and Figure 5-3 (b)), one of the peaks with small d-spacing is combined by two peaks. And when the temperature exceeds the melting point of composition with lower melting point, 45.7°C for LLL and 57.1°C for MMM, one of the peaks disappears and the fitted WAXD patterns become the same as other dry blend samples.

.

5.1.2 Effect of Temperature on d-spacing of β Form WAXD Peaks from Complex Triacylglycerols Mixtures.

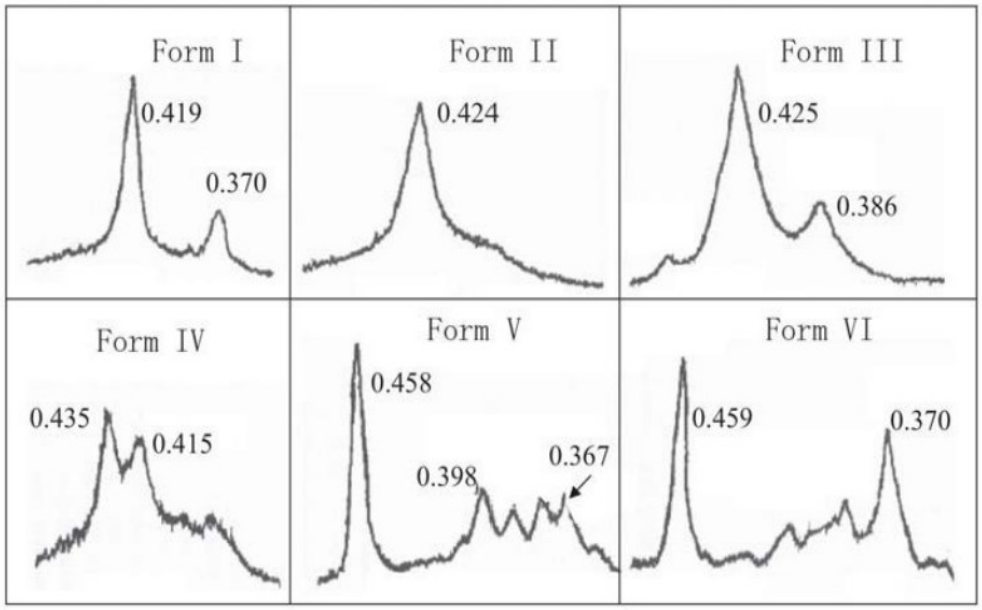

Figure 5 - 7 Wide Angle x-ray Diffraction Patterns (short spacing) of six polymorphs of cocoa butter (Garti and Widlak. 2012).

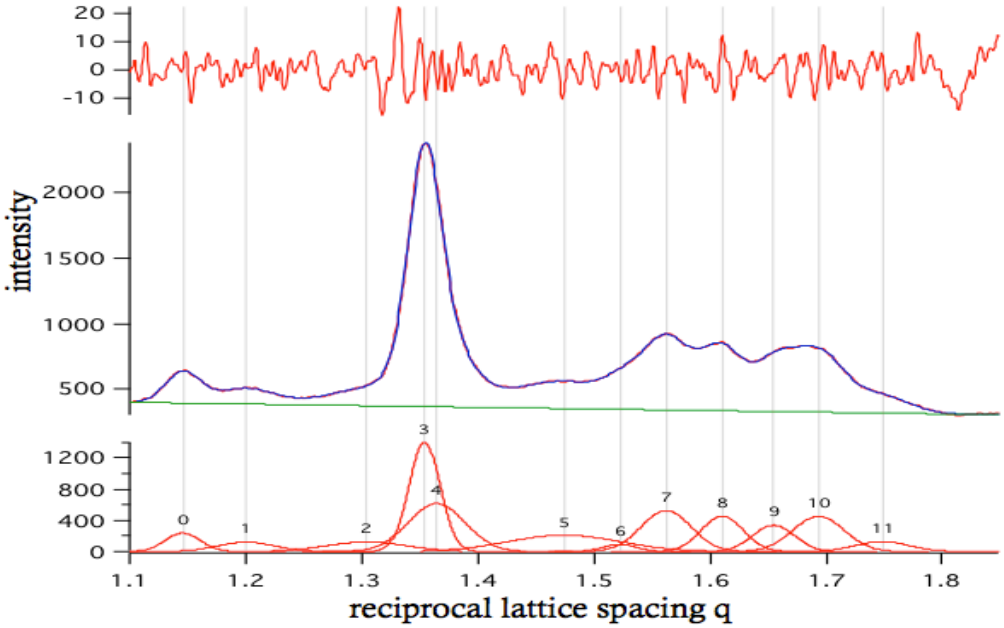

Figure 5 - 8 The fitted Wide Angle Diffraction patterns of β form cocoa butter by Igor Pro.

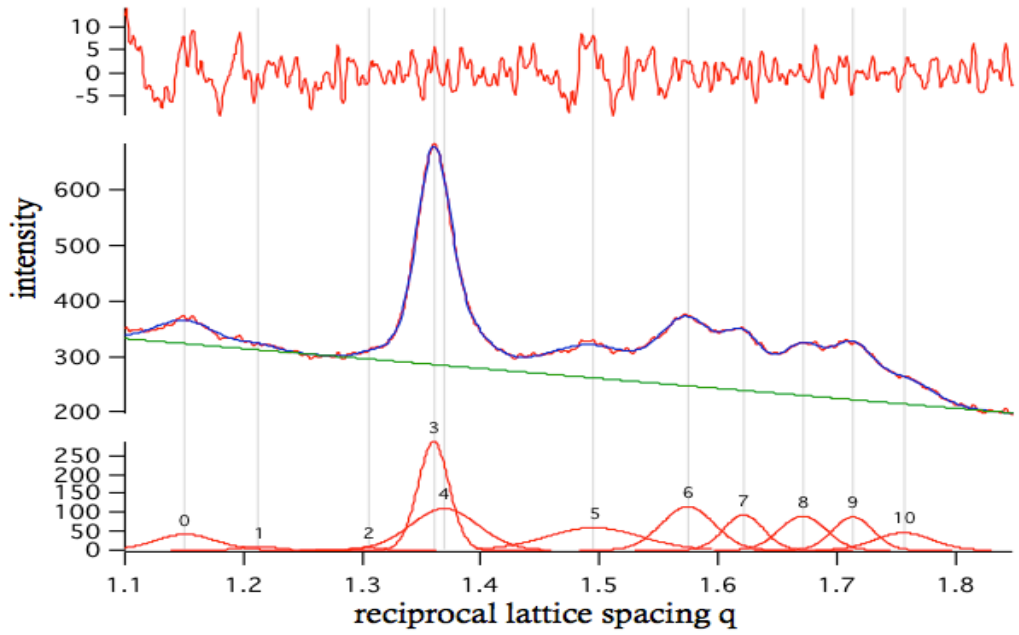

Figure 5 - 9 The fitted Wide Angle Diffraction patterns of β form 99% dark chocolate by Igor Pro.

After calculating the d-spacing of the peaks of cocoa butter and 99% dark chocolate and comparing with the WAXD patterns of six polymorphs of cocoa butter shown in Figure 5-8, the samples crystallized as β form (form V) with d-spacings of the characteristic peaks at 0.458 Å, 0.398 Å and 0.367 Å. As described by Guthrie et al. (2005), when examining lower-sugar content dark chocolates (i.e. with sugar content less than 30%), the intensity of the cocoa butter peaks in the wide angle region can be observed directly since the peaks are distinct from nearby sucrose diffraction peaks. Thus it is unnecessary to remove the sugar in order to observe these peaks (Guthrie et al, 2005).

Given the complexity of the triacylglycerol composition of cocoa butter, it is much harder to see the change of d-spacings than in other samples studied here, even without the interference of sugar or other minor compounds. The WAXD patterns of cocoa butter and chocolate are much more complex than the WAXD patterns of pure triacylglycerols and dry blend samples.

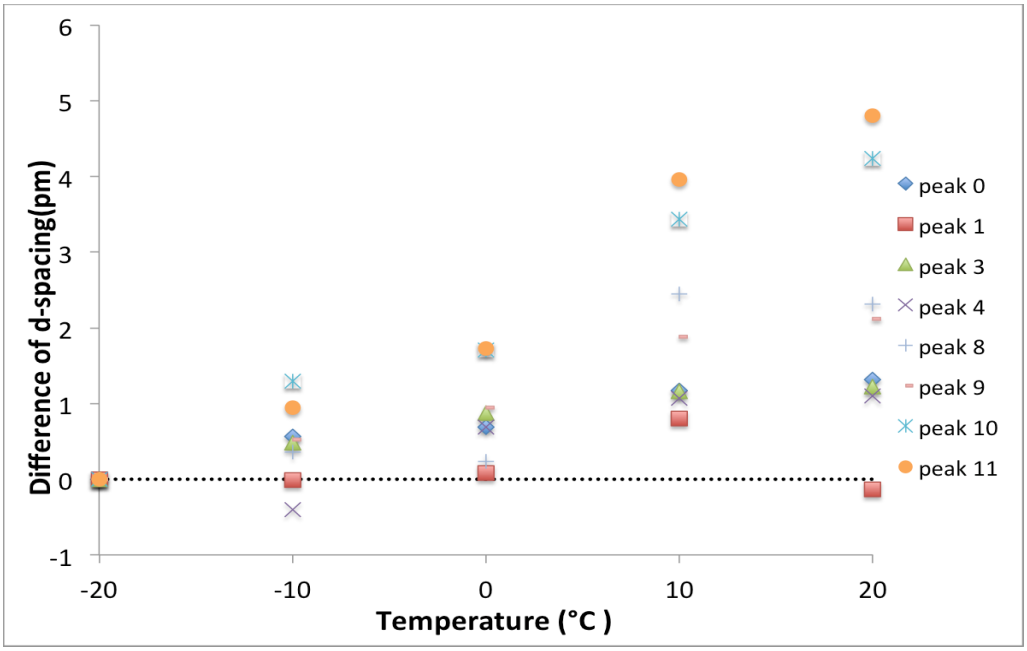

Figure 5 - 10 Difference of d-spacing with temperature (Cocoa butter).

Consistently with the methodology of this study, three kinds of peaks for cocoa butter were chosen to study the temperature effect on the WAXD patterns: the peaks with large d-spacing (peak 0 and peak 1), the peaks with medium d-spacing (peak 3 and peak 4) and the peaks with small d-spacing (peak 8, peak 9, peak 10 and peak 11). For the peaks with large and medium d-spacing, when the temperature increases, the increase of d-spacings is less than 1 pm. The differences of d-spacings of peak 1, peak 3 and peak 4 are about 1 pm and the differences of d-spacings of peak 0 are close to 0. Temperature does not have significant influence on the peaks with large and medium d-spacing. For the peaks with small d-spacing, the difference of d-spacing for all the four peaks get higher when the samples were heated up. But the increase of d-spacings for peak 8 and peak 9 is smaller than the increase of d-spacings for peak 10 and peak 11.The magnitude of the change from -20 °C to 20 °C is similar to that observed in pure triglycerides and dry blends, of the order of 5 pm.

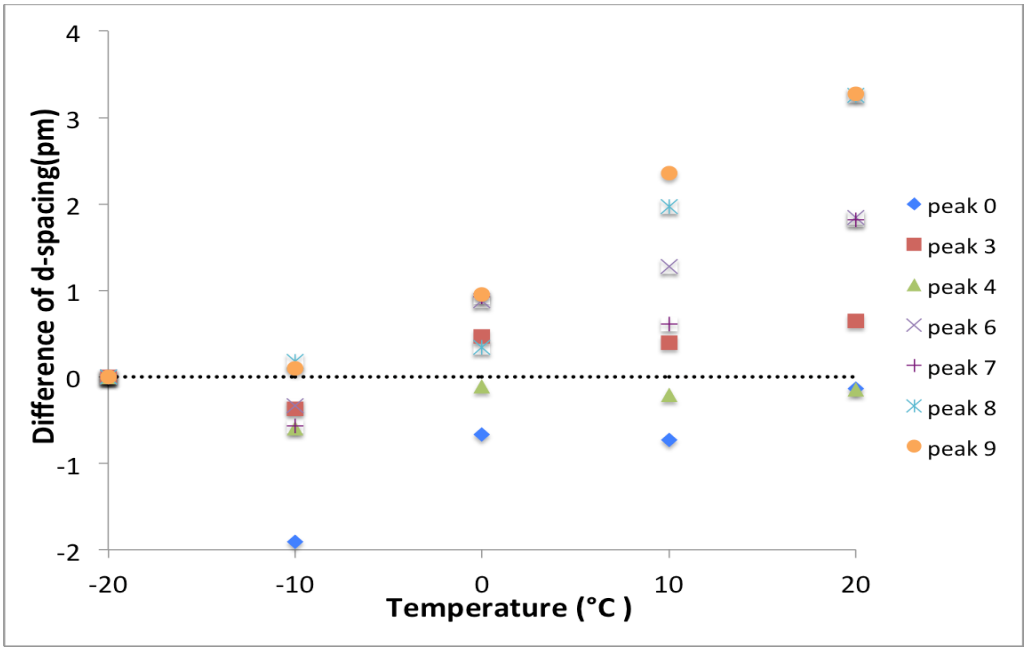

Figure 5 - 11 Differences of d-spacings with temperature (99% dark chocolate).

For 99% dark chocolate, the peaks to be compared are selected by the same way as cocoa butter. The d-spacings of peak 3 and peak 4 are about 1 pm larger than the d-spacing under the reference temperature and the differences of d-spacings of peak 0 is close to 0. As in the result of cocoa butter, temperature does not have significant influence on the peaks with large and medium d-spacing. For the peaks with small d-spacing (peak 6, peak 7, peak 8 and peak 9), the differences of d-spacings for all the four peaks get higher when the samples were heated up. But the increase of d-spacings for peak 6 and peak 7 is smaller than the increase of d-spacings for peak 8 and peak 9. Peak 8 and peak 9 depend much more strongly on temperature than other peaks. It is shown that temperature affects the WAXD patterns of 99% dark chocolate in the same way as the temperature effect on cocoa butter. However, the observed increase in Δd is smaller than in the other materials, between 3 and 4 pm.

5.2 Estimation of Temperature from Difference of d-spacing

As with pure triacylglycerols, we can estimate the real sample temperature of the triacylglycerol mixtures using the differences of d-spacings for the peaks with small d-spacing.

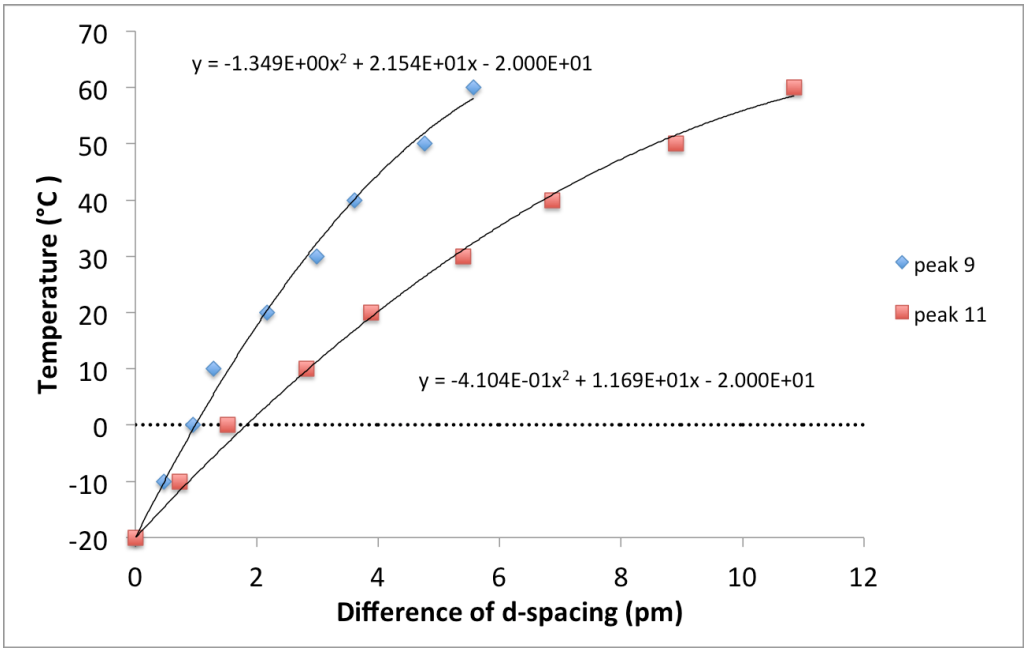

Figure 5 - 12 Temperature versus differences of d-spacings for peaks with small d-spacing (3P7S).

For the dry blends, taking the 3P7S as example, differences of d-spacings of peak 7 and peak 8 increase with the temperature increase. We can calculate the sample temperature using the polynomial equations showed in Figure 5-12. Though the calculated temperature is still an estimated temperature, it is much closer to the real sample temperature. We expect, thus, to gain a better understanding of the temperature effects by monitoring the temperature of sheared systems.

Using the differences of d-spacing to estimate the real sample temperature can be applied to most of the dry blend samples except 5M5P and 5L5S. Taking 5L5S as example, when temperature reaches 50°C, peak 7 disappear and the d-spacings of peak 8 become much

larger than the d-spacings at previous temperature. The mathematical equations for differences of d-spacings for peak 7 and peak 8 found in this situation are not accurate to calculate the sample temperature.

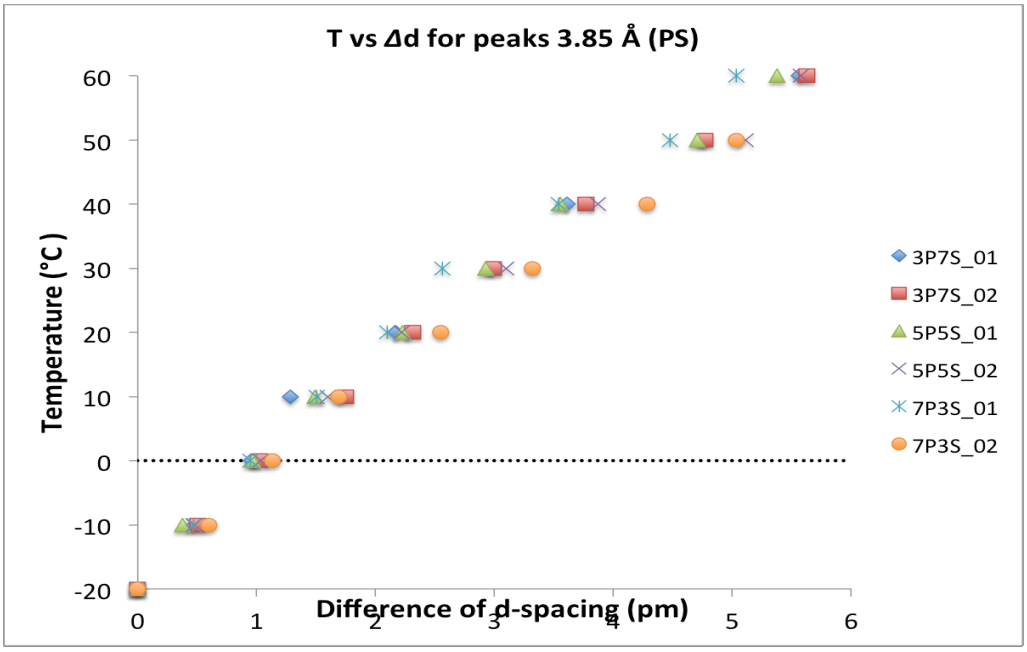

(a)

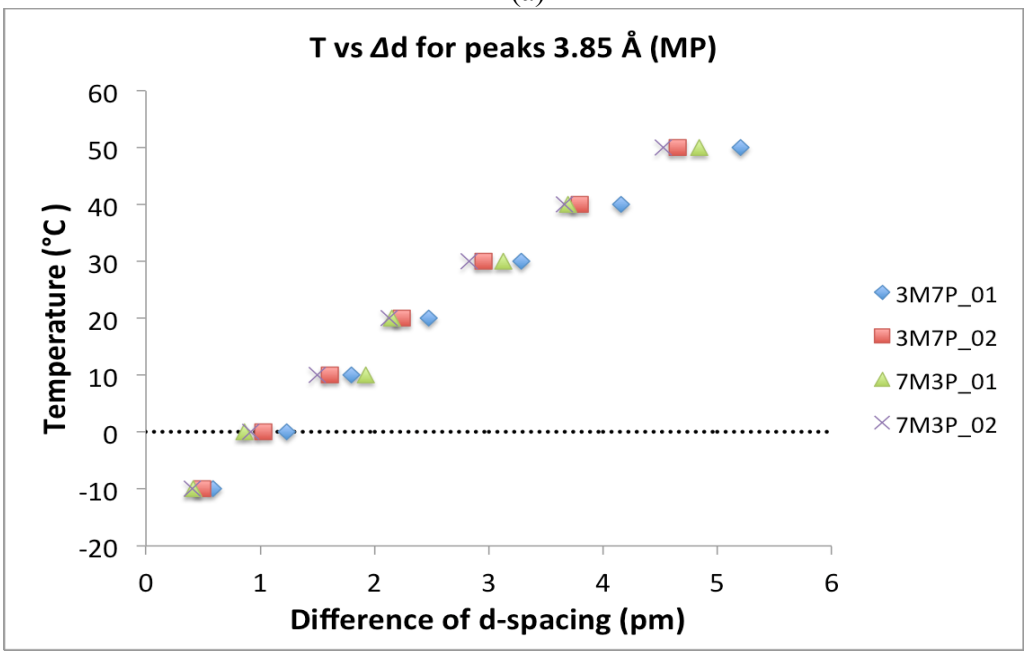

(b)

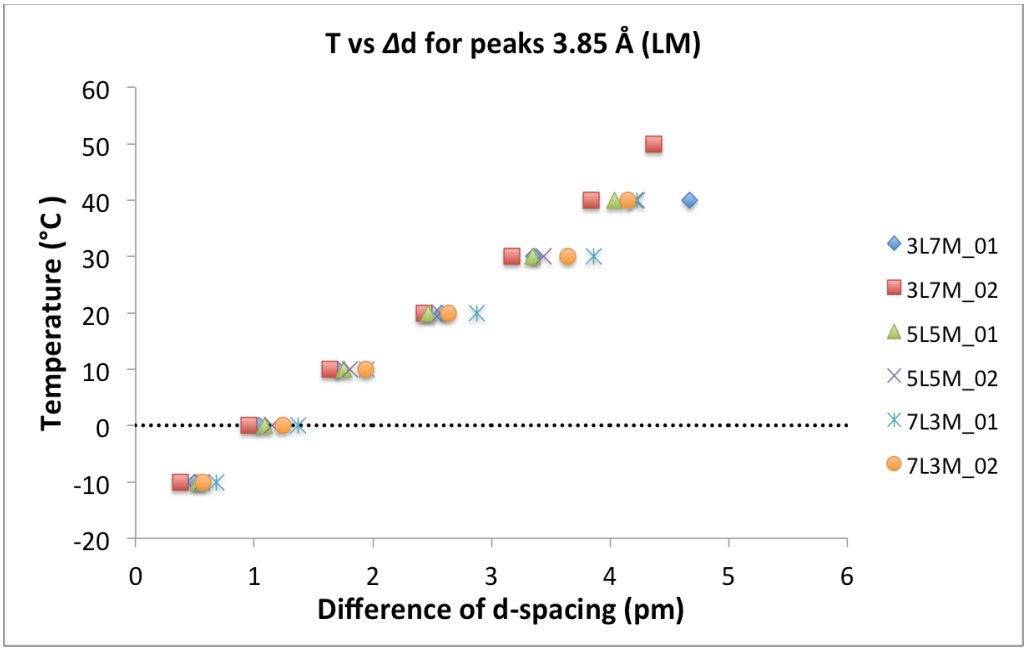

(c)

Figure 5 - 13 Temperature versus differences of d-spacings for peaks with small d-spacing at 3.85 Å. (a) Triacylglycerol mixture composed by PPP and SSS. (b) Triacylglycerol mixture composed by MMM and PPP. (c) Triacylglycerol mixture composed by LLL and MMM.

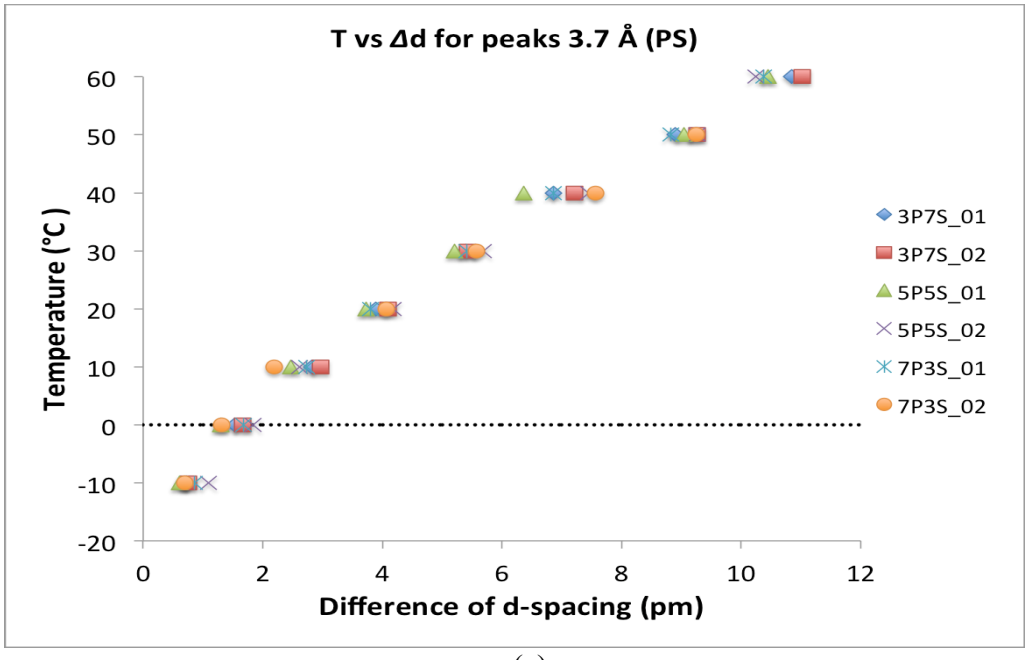

(a)

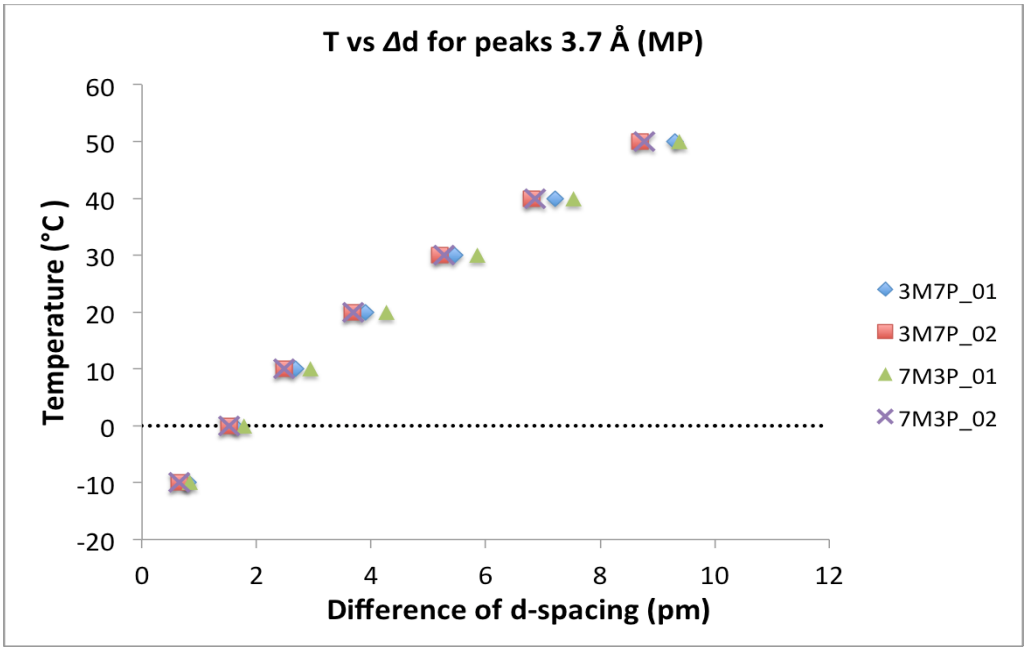

(b)

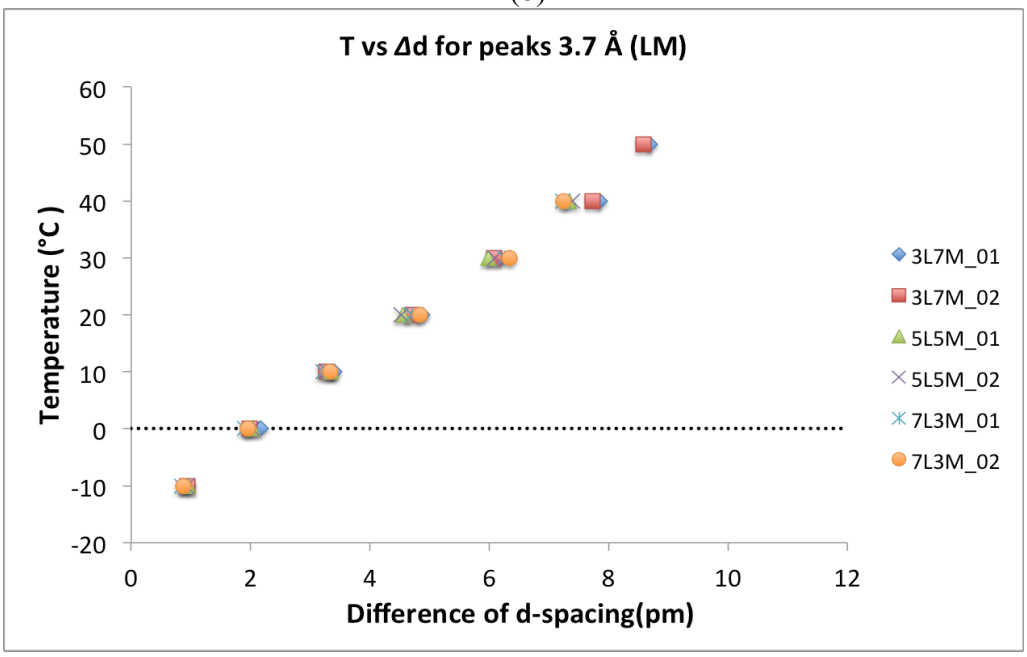

(c)

Figure 5 - 14 Temperature versus differences of d-spacings for peaks with small d-spacing at 3.7 Å. (a) Triacylglycerol mixture composed by PPP and SSS. (b) Triacylglycerol mixture composed by MMM and PPP. (c) Triacylglycerol mixture composed by LLL and MMM.

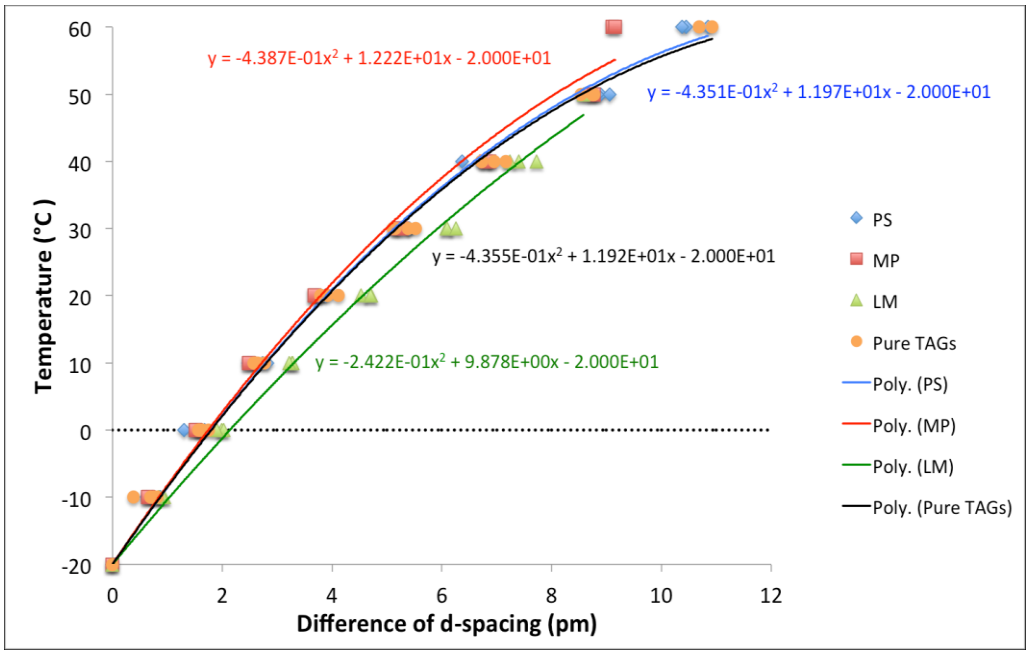

Figure 5 - 15 Temperature versus differences of d-spacings for peaks with small d-spacing at 3.7 Å (all dry blend samples and pure TAGs).

In order to have a better understanding of the estimation of temperature from the differences of d-spacings for the peaks with small d-spacing of the triacylglycerol mixtures, the differences of d-spacings for the peaks with small d-spacing versus temperature from the samples with the same composition but different proportion are plotted together in Figure 5-13 and Figure 5-14. These figures show that the peaks with smaller d-spacing have greater consistency. After plotting the differences of d-spacings for peaks with small d-spacing (3.85 Å) (blue diamonds in Figure 5-10, 5-11 and 5-12) into one graph (Figure 5-13), it is clear that the mathematic equation changes a little bit with the change of the sample composition. For the peak with small d-spacing (3.7 Å) (red squares in Figure 5-10, 5-11 and 5-12), the mathematic equations present higher consistency. For the samples with the same composition but different proportion, it is reliable to have one mathematic equation to estimate the real sample temperature using the differences of d-spacings of the characteristic peak (3.7 Å). In Figure 5-15, the mathematic equations of dry blends with different composition and the pure

triacylglycerols also show good consistency, except the dry blend samples composed by LLL and MMM.

CHAPTER 6 RESULTS AND DISCUSSION – III - EFFECT OF TEMPERATURE ON WAXD OF TRIACYLGLYCEROLS MIXTURES UNDER SHEAR FLOW

6.1 Effect of Temperature on d-spacing of WAXD Peaks

6.1.1 Effect of Temperature on d-spacing of β Form WAXD Peaks without Shear in the Mini Couette Cell

In Figure 6-1, peak 4, peak 7 and peak 8 show that PPP crystallized in β form in the mini Couette cell and the large peak 1 shows the solvent BBB is still in liquid form. The large liquid peak makes the peak fitting much harder since it easily affects the peak position, amplitude, width and the baseline.

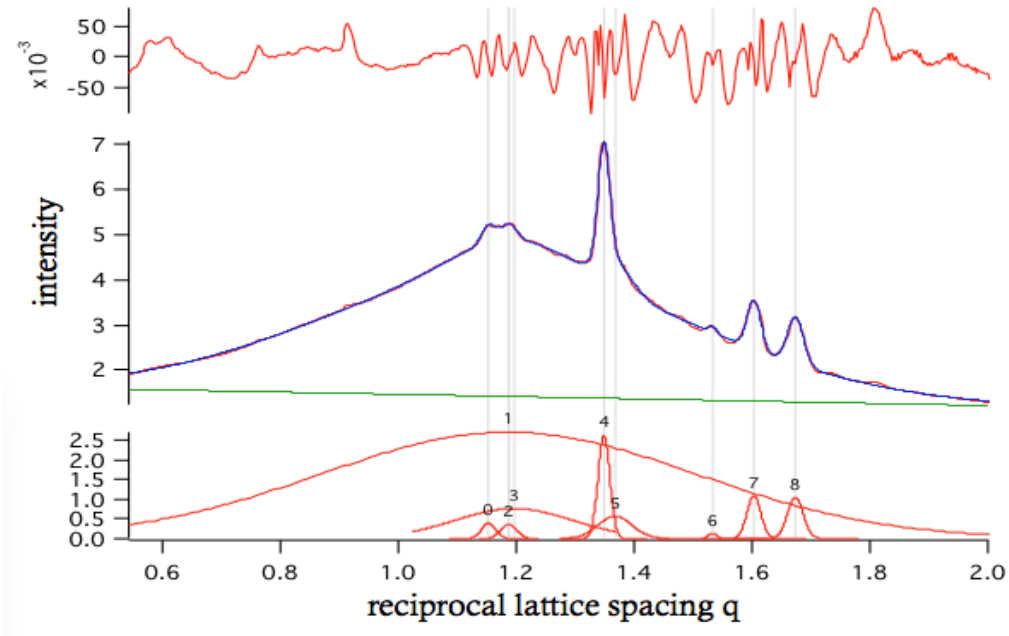

(a)

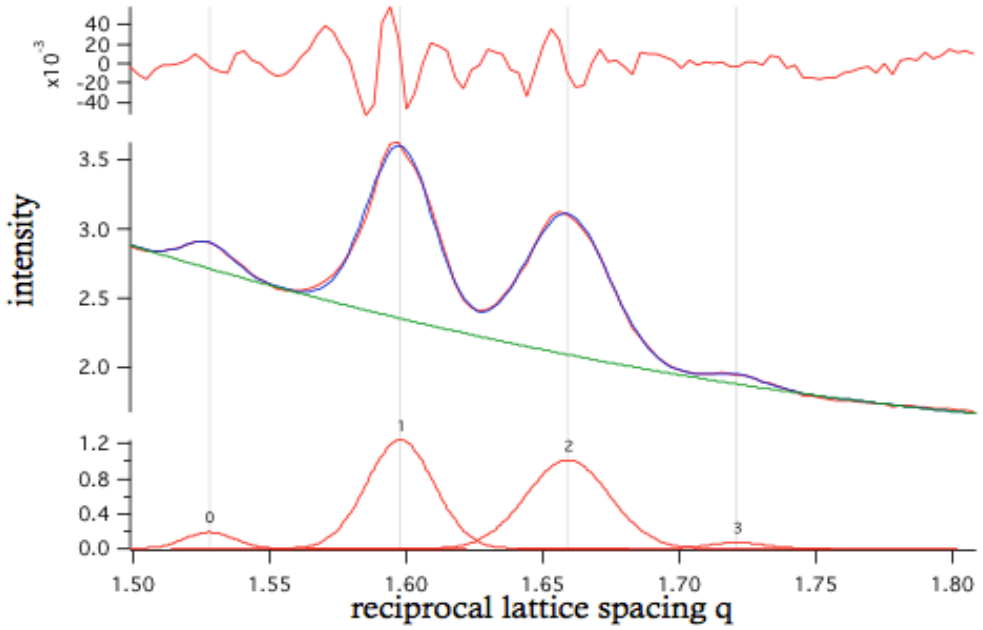

(b)

Figure 6 - 1 The fitted Wide Angle Diffraction patterns of 6B4P without shear by Igor Pro. (a) Whole diffraction patterns. (b) Re-fitting for peak 7 and peak 8 at the reciprocal lattice spacing range from 1.5 to 1.8.

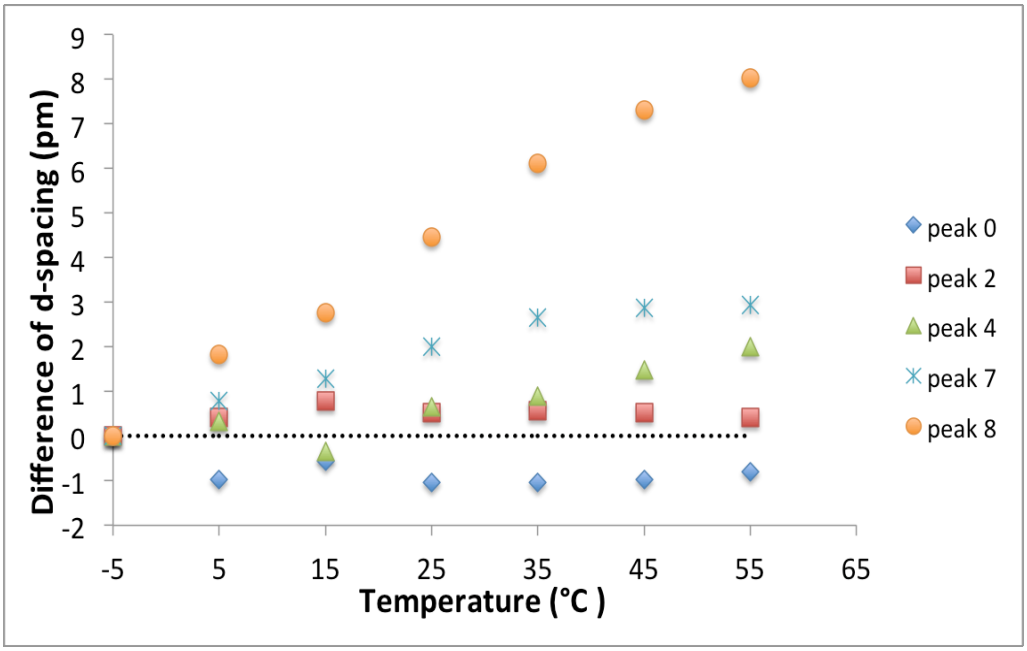

Figure 6 - 2 Differences of d-spacings with temperature (6B4P without shear).

Since the minimum temperature that the water bath in APS can reach is -5°C the results of Δd are presented in this chapter using -5°C as the reference temperature, i.e. the

differences of d-spacings are calculated by subtracting the d-spacing under -5°C.

From Figure 6-2, the differences of d-spacing for the peaks with large d-spacing (peak 0 and peak 2) scarcely change when the temperature increases. For the peak with medium d-spacing (peak 4), the d-spacings increase only minimally when the temperature increases. It is hard to tell how d-spacings of peak 5 changes with temperature because of the fitting of peak 5. The overlapping with peak 4 and the large liquid peak makes it hard to get an accurate d-spacing of peak 5. For the peaks with small d-spacing (peak 7 and peak 8), the differences of d-spacing keep increasing when the temperature increases. But the increase of peak 7 is much smaller than the increase of peak 8. The general trends of results of 6B4P in the mini Couette cell without shear are similar to the results from pure triacylglycerols in capillary cells using in-house x-rays. This means that the d-spacings of the crystallized samples change in the same way using different experimental setups.

6.1.2 Effect of Temperature on d-Spacing of β Form WAXD Peaks with 40 r/s Rotational Speed

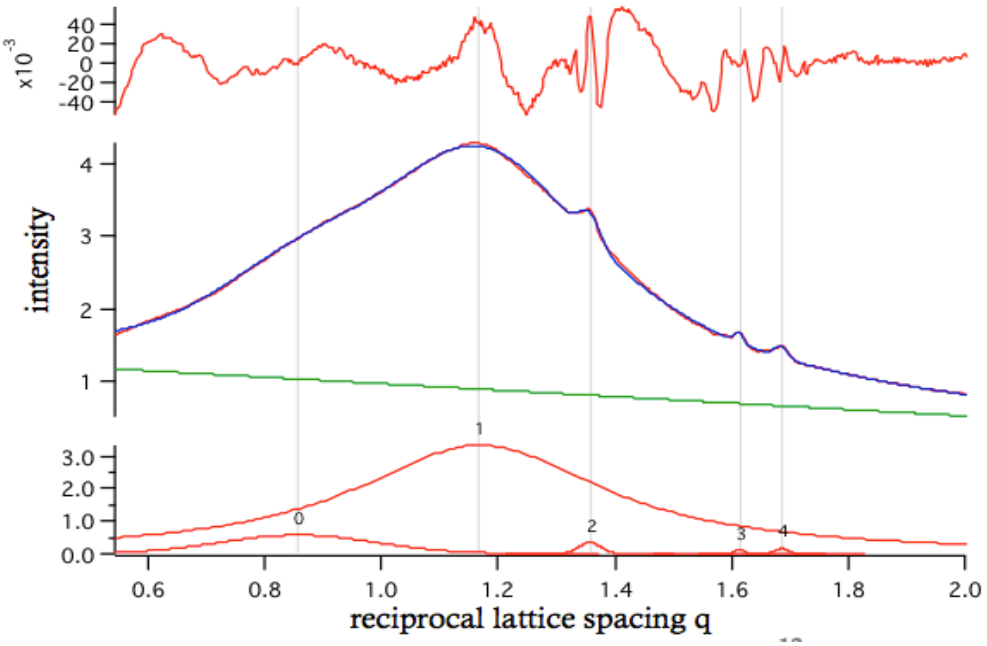

(a)

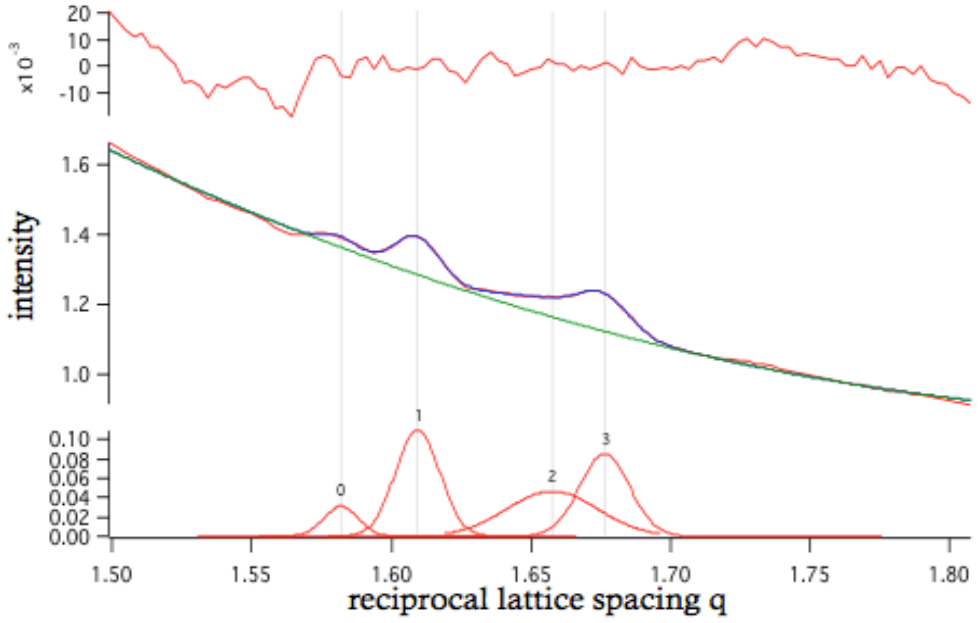

(b)

Figure 6 - 3 The fitted Wide Angle Diffraction patterns of 6B4S under 40 r/s rotational speed at 0 °C by Igor Pro. (a) Whole diffraction patterns. (b) Re-fitting for peak 3 and peak 4 Re-fiting for peak 7 and peak 8 at the reciprocal lattice spacing range from 1.5 to 1.8.

Following the same temperature profile as 6B4P, the WAXD patterns of 6B4S were

captured under rotational speed 40 revolution per second (r/s) which yields an approximate average shear rate of 940 s^{-1}. Compared to the 6B4P without shear flow, Figure 6-3 shows the 6B4S crystallized but the degree of crystallization is small and the intensity of the crystal peaks is much lower. BBB as solvent did not crystallize so there is a broad liquid peak (peak 1). After calculating the d-spacings of peak 2, peak 3 and peak 4, it indicates SSS crystallized in β form. Fitting the WAXD patterns from the reciprocal lattice spacing 1.5 to 1.8 can avoid artificial peak shifting due to the large amorphous peaks.

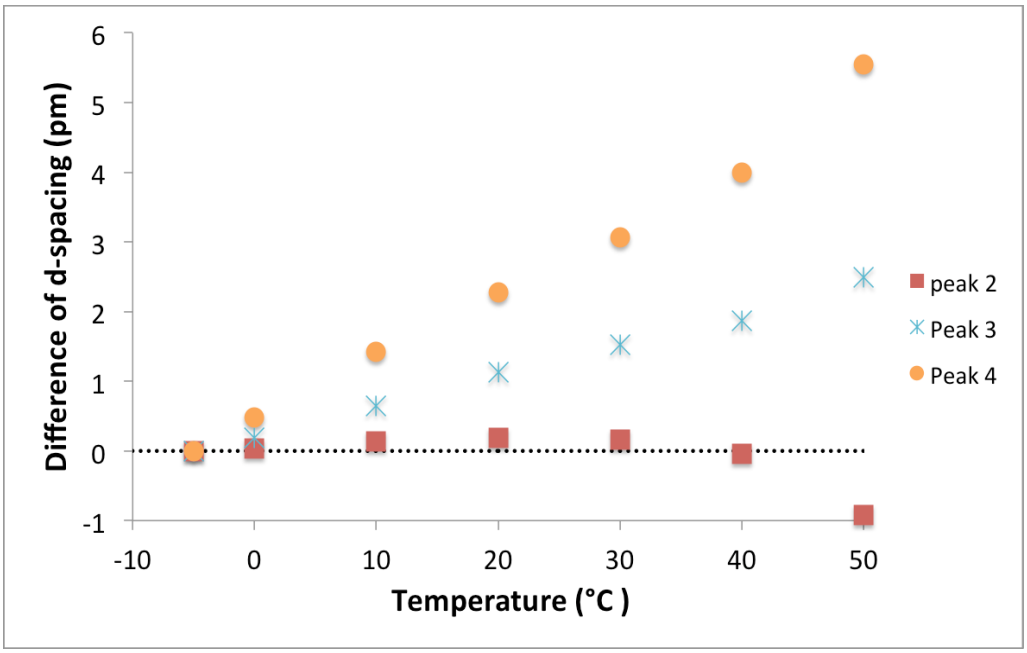

Figure 6 - 4 Difference of d-spacing with temperature (6B4S with 40r/s rotational speed)

The differences of d-spacings of peak 2 are approximately 0 when the temperature increases from -5°C to 50°C. This indicates the d-spacings remain the same as that under reference temperature (-5°C). The differences of d-spacings of peak 3 and peak 4 keep increasing when the temperature is getting higher and the differences of d-spacing of peak 4 is increasing much faster than the differences of d-spacing of peak 3. Under the same temperature, the change of d-spacings of peaks with small d-spacing is larger than the

peaks with large d-spacing.

6.1.3 Effect Of Temperature on d-spacing of β Form WAXD Peaks with 50 r/s Rotational Speed

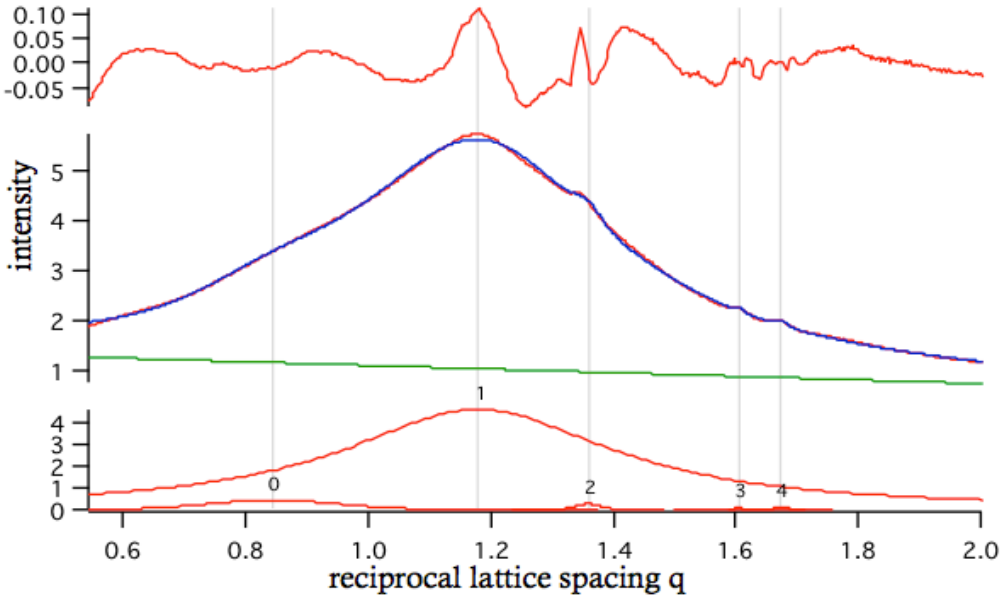

(a)

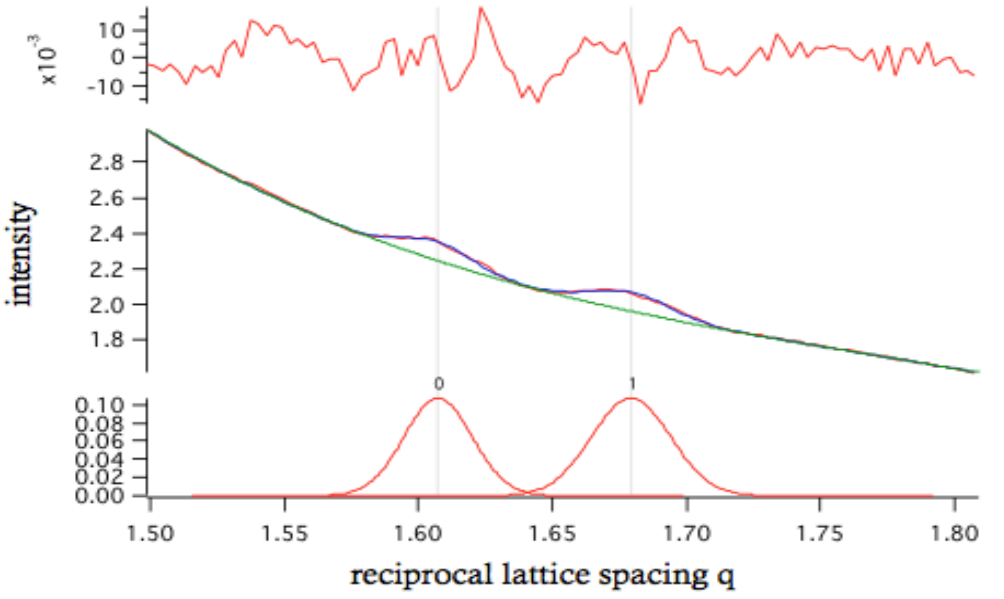

(b)

Figure 6 - 5 The fitted Wide Angle Diffraction patterns of 6B4S with 50 r/s rotational speed at 0 °C by Igor Pro. (a) Whole diffraction patterns. (b) Re-fitting for peak 3 and peak 4 Re-fiting for peak 7 and peak 8 at the reciprocal lattice spacing range from 1.5 to 1.8.

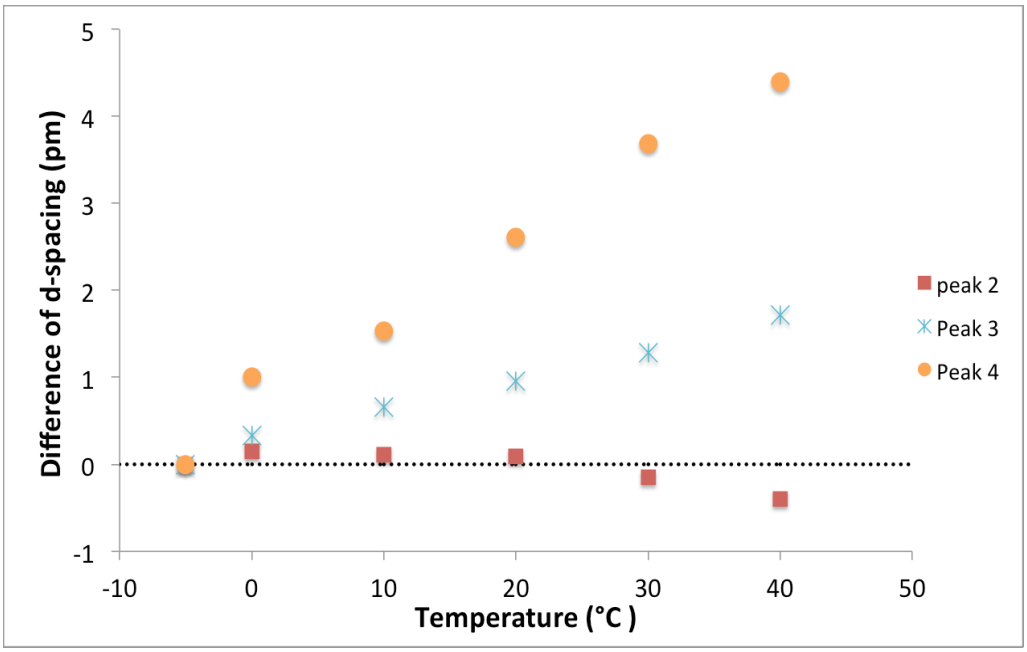

Figure 6 - 6 Difference of d-spacing with temperature (6B4S with 50r/s rotational speed)

From Figure 6-5, the fitted wide angle diffraction pattern of 6B4S with 50 r/s rotational speed which yields an approximate average shear rate of 1200 s^{-1} by Igor Pro, is similar with that at 40 r/s rotational speed. Peak 1 is a large liquid peak and shows that BBB as solvent did not crystallize. The d-spacings of peak 2, peak 3 and peak 4 is calculated from the reciprocal lattice spacing q and show SSS crystallized in β form. But compared to the WAXD pattern of 6B4S with 40 r/s rotational speed, there is less crystal formed under 50 r/s rotational speed. The crystal peaks are much harder to identify for fitting and the d-spacings of the WAXD peaks is harder to determine.

The differences of d-spacing of peak 2 is close to 0 when the temperature rises from -5°C to 50°C. This indicates that the d-spacings remain the same as that under reference temperature (-5°C). The differences of d-spacings of peak 3 and peak 4 keep increasing when the temperature increases and the differences of d-spacing of peak 4 increase much faster than the difference of d-spacing. Under the same temperature, the change of d-

spacings of peaks with small d-spacing is larger than the peaks with large d-spacing. These results are similar as that at 40 r/s rotational speed described in Section 7.1.2.

6.2 Estimation of Temperature from Difference of d-spacing

At high shear rate a lot of factors will affect the temperature of the samples, such as viscous heat, the temperature of the sample in the mini Couette Cell is always higher than the set temperature. Because of the configuration of the mini Couette Cell System, it is hard to measure and record the sample temperature using a thermistor. Both temperature and shear can have a great influence on fat crystallization so it is difficult to study the real effect of different shear rates on the fat crystallization when the temperature cannot be determined. It is necessary to find a way to measure or estimate the real sample temperature under shear. Only after that, the effect of shear flow on the fat crystallization can be understood.

The same as the pure materials crystallized in the capillary cells, for the sample 6B4P without applying shear, the differences of d-spacings of peak 7 and peak 8 increase as the temperature increases. We can calculate the sample temperature in the mini Couette System using the equations shown in Figure 6-7. Even though the calculated temperature is still an estimated temperature, it gives us a better understanding for the temperature of the mini Couette system without applying shear flow.

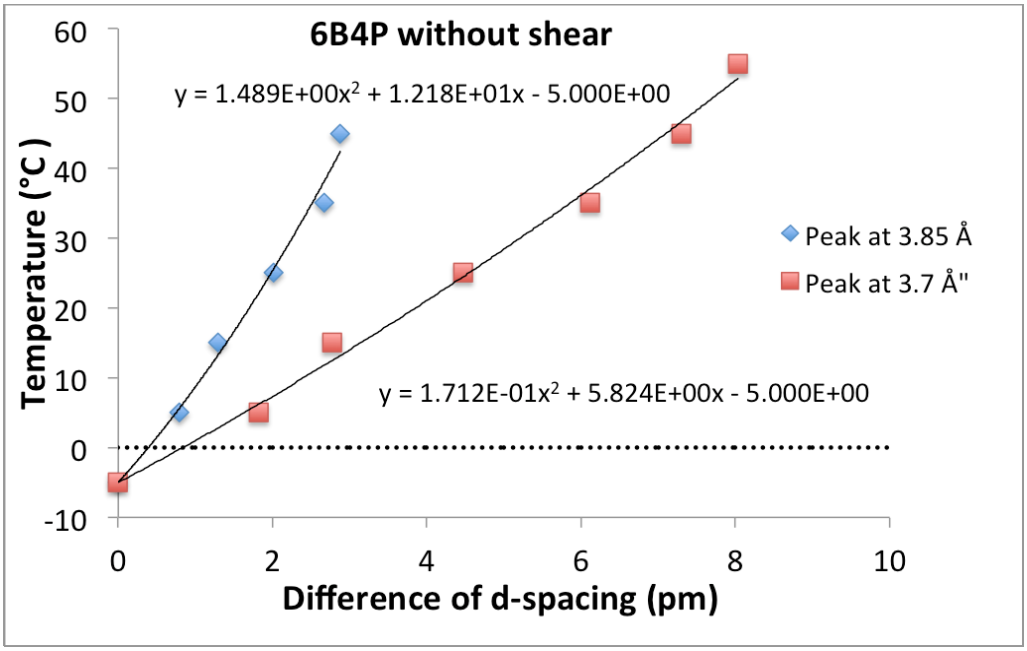
6B4P without shear
y = 1.489E+00x² + 1.218E+01x - 5.000E+00
y = 1.712E-01x² + 5.824E+00x - 5.000E+00
Peak at 3.85 Å
Peak at 3.7 Å"
Temperature (°C)
Difference of d-spacing (pm)
60
50
40
30
20
10
0
-10
0
2
4
6
8
10

(a)

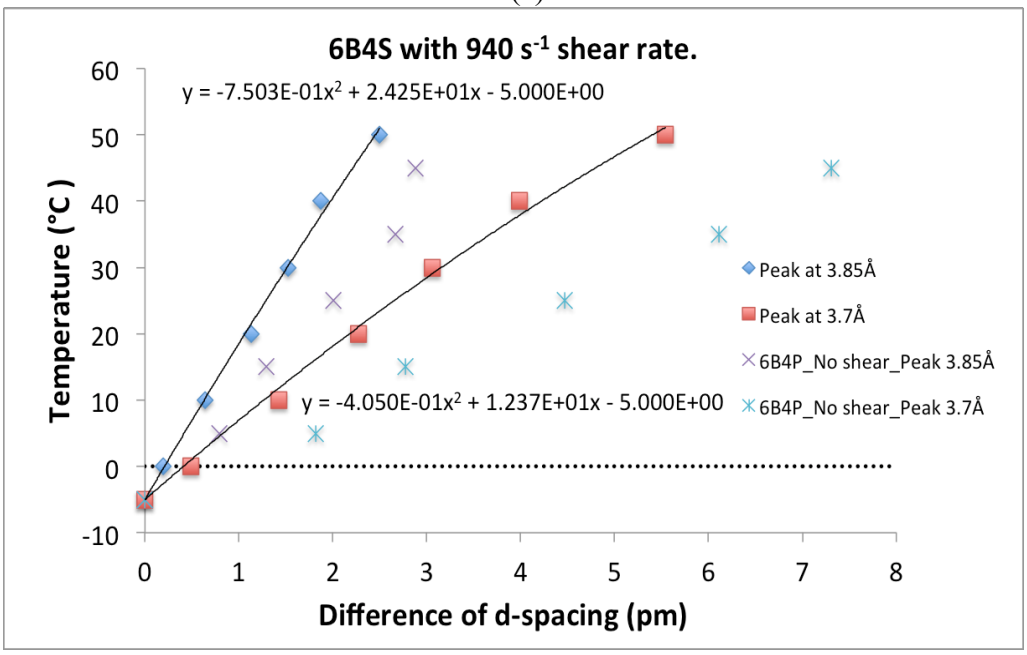
6B4S with 940 s-1 shear rate.
y = -7.503E-01x² + 2.425E+01x - 5.000E+00
y = -4.050E-01x² + 1.237E+01x - 5.000E+00
Peak at 3.85Å
Peak at 3.7Å
6B4P_No shear_Peak 3.85Å
6B4P_No shear_Peak 3.7Å
Temperature (°C)
Difference of d-spacing (pm)
60
50
40
30
20
10
0
-10
0
1
2
3
4
5
6
7
8

(b)

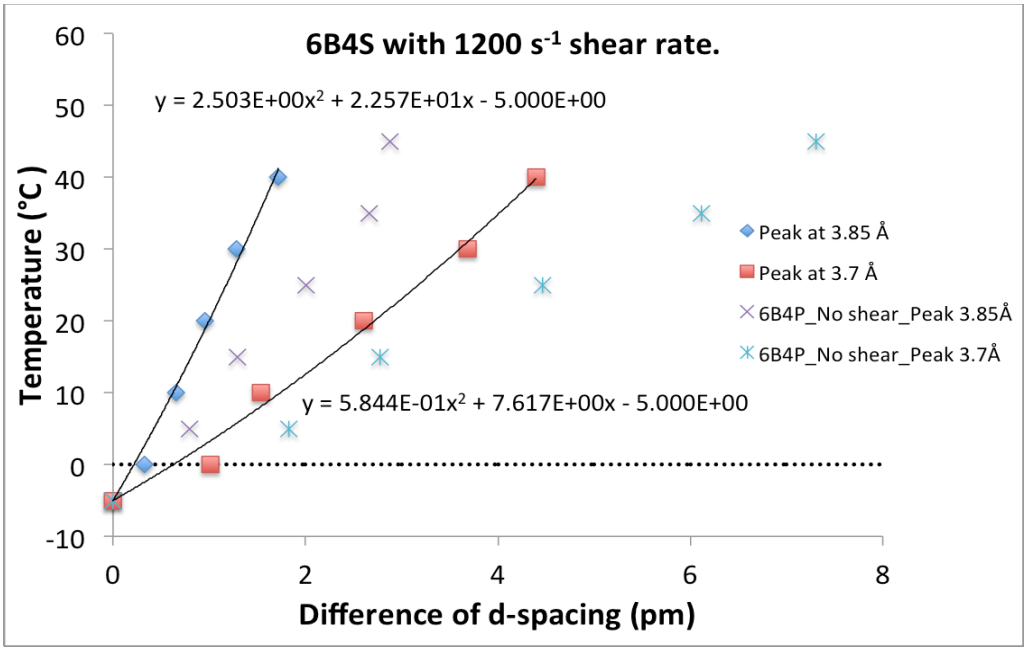

(c)

Figure 6 - 7 Temperatures versus differences of d-spacings for peaks with small d-spacing. (a) 6B4P without shear. (b) 6B4S with 940 s^{-1} shear rate (40r/s rotational speed). (c) 6B4S with with 1200 s^{-1} shear rate (50r/s rotational speed).

For the sample 6B4S with 40 r/s and 50 r/s rotational speed, the sample temperature can also be estimated by calculating the temperature from the differences of d-spacings for the peaks with small d-spacing, which the d-spacing is 3.85 Å and 3.7 Å. As shown in Figure 6-7, the real sample temperature can be calculated from the differences of d-spacings of peak 3 and peak 4.

6.3 Comparison of the Difference of d-spacing with Different Shear Rate

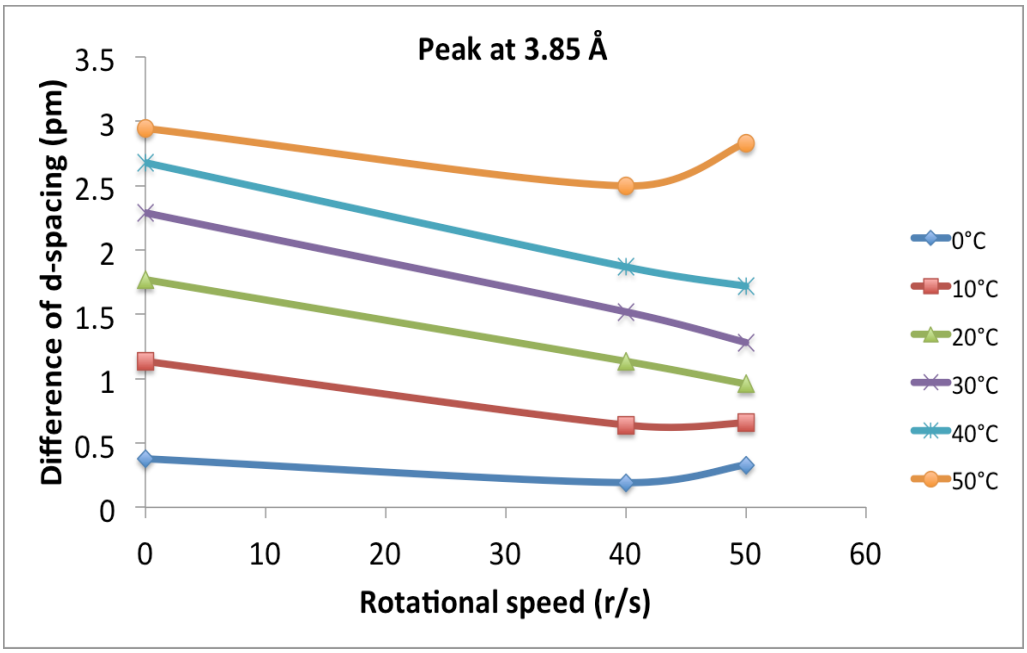

(a)

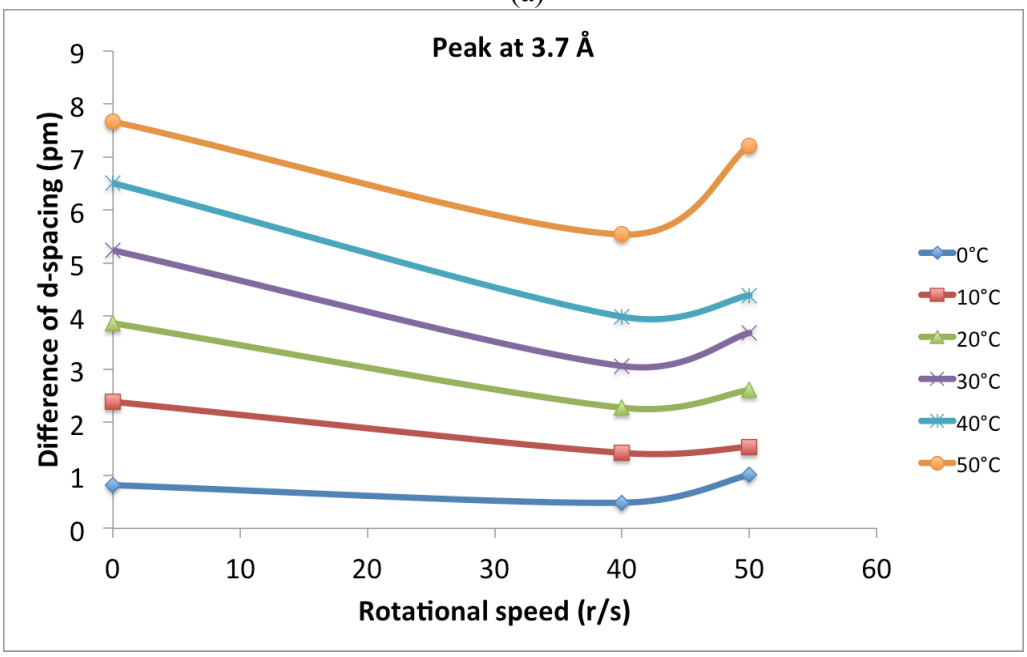

(b)

Figure 6 - 8 Difference of d-spacings versus rotational speed for peaks with small d-spacing. (a) Peak with small d-spacing at 3.85 Å. (b) Peak with small d-spacing at 3.7 Å

To compare the change of d-spacing with different shear rates, the differences of d-spacings under six experiment temperatures are plotted versus shear rates in Figure 6-8. For the WAXD peaks at 3.7 Å (Figure 6-8 (b)), the differences of d-spacings are larger at

higher shear rate under the same temperature. The difference of d-spacing at 50 r/s rotational speed is higher than the difference of d-spacing at 40 r/s rotational speed. For the WAXD peaks at 3.85 Å (Figure 6-8 (a)), the change of the d-spacings is not as obvious as the peaks at 3.7 Å with different shear rates since the temperature effect on *d(2 0 -1)* is weaker than *d(3 -1 0)* in the triacylglycerol crystals. At the temperature 20°C to 40°C, the difference of d-spacing with 50 r/s rotational speed is smaller than the difference of d-spacing with 40 r/s rotational speed. But at the lower temperature (0°C and 10°C) and the high temperature (50°C), the difference of d-spacing changes in an opposite way. From Figure 6-8, the differences of d-spacings without shear are largest and when the shear flow is applied to the sample, the differences of d-spacings decrease. But since the lack of data of lower shear rate, it is hard to draw a conclusion about how different shear rate affect the d-spacing at the same experiment temperature.

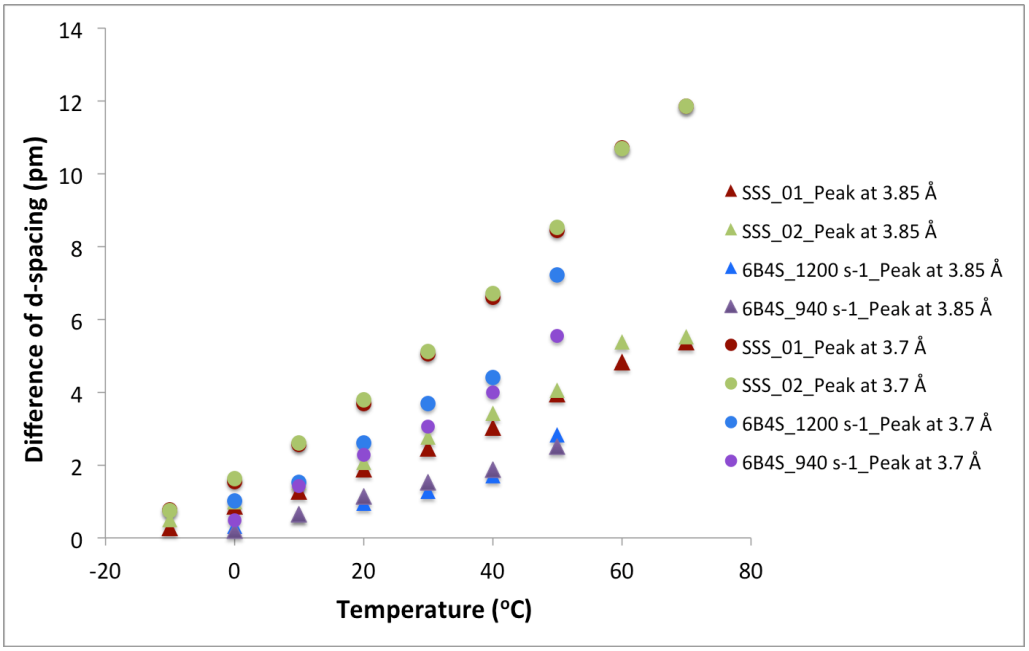

Figure 6 - 9 Change of difference of d-spacing with temperature using in-house x-ray and synchrotron x-ray.

In order to compare the shear effect on the d-spacings of WAXD patterns, the differences of d-spacings obtained using the in-house x-ray and synchrotron x-ray are compared in

Figure 6-9. According to the d-spacings of WAXD peaks, peak 7 of SSS using in-house x-ray without shear is corresponding to peak 3 using synchrotron x-ray with shear flow. Peak 8 of SSS using in-house x-ray without shear is corresponding to peak 4 using synchrotron x-ray with shear. The differences of d-spacings of 6B4S peak 3 with 40 r/s and 50 r/s are smaller than the differences of SSS peak 7 without shear. The same result can be found by comparing the differences of d-spacings of 6B4S peak 4 with 40 r/s and 50 r/s and the differences of SSS peak 8 without shear.

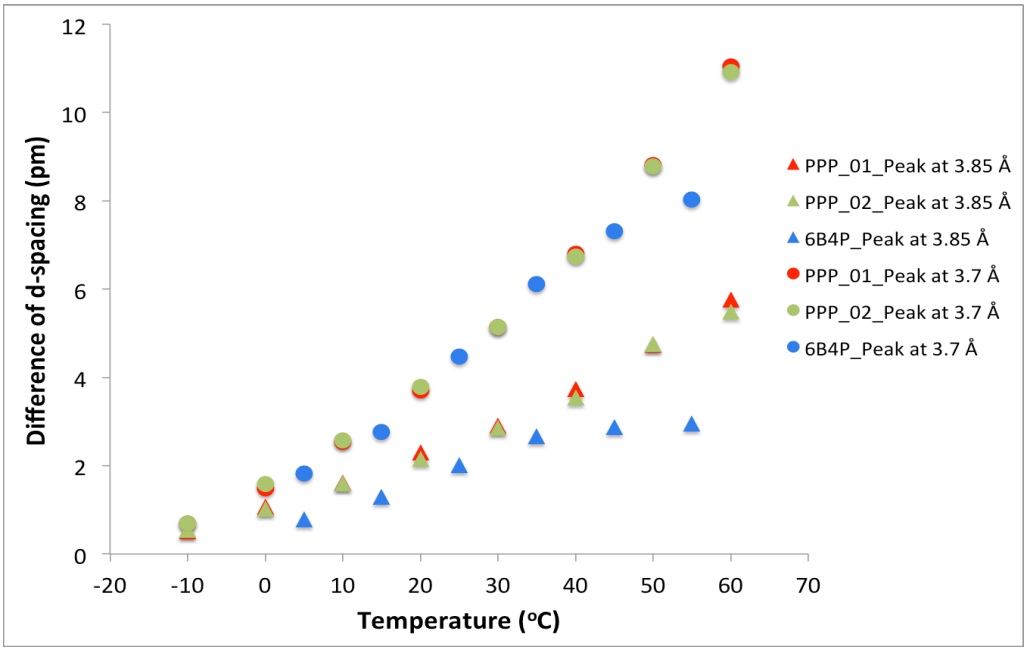

Figure 6 - 10 Change of difference of d-spacing with temperature with and without shear.

The experimental results obtained by using the synchrotron x-ray are compared in Figure 6-10. Since all the experiments with and without shear were done in the mini-Couette System and using the synchrotron x-ray, the error caused by using different sample holding systems and experiment setups can be minimized. According to the d-spacings of WAXD peaks, peak 7 of 6B4S without shear is corresponding to peak 3 using with shear. Peak 8 of 6B4S without shear is corresponding to peak 4 using with shear. As we could see in Figure 6-10, the differences of d-spacings of 6B4S peak 3 with 40 r/s and 50 r/s are

smaller than the difference of 6B4P peak 7 without shear. The same result can be found by comparing the differences of d-spacings of 6B4S peak 4 with 40 r/s and 50 r/s and the differences of 6B4P peak 8 without shear. Both Figure 6-9 and Figure 6-10 lead to the same conclusion: the differences of d-spacings under shear are smaller than that without shear, especially at the higher temperature.

CHAPTER 7 CONCLUSION AND FUTURE WORK

The primary goal of this research was to investigate the temperature effect on the WAXD patterns of the nanocrystalline triacylglycerols, especially the effect on the d-spacings. The secondary purpose was to conduct preliminary tests for its use as intrinsic thermometers in shear cell. Pure triacylglycerols and triacylglycerol mixtures were crystallized in a desired polymorph in capillaries or mini Couette system, under different temperatures and shear rates. The WAXD patterns were obtained using in-house x-ray and synchrotron radiation x-ray at a beamline in APS. How the d-spacings of WAXD peaks of the nanocrystalline triacylglycerols changed with the different temperatures and shear rates was studied and compared in detail.

The materials are described in section 3.1 in this thesis. Four kinds of samples were studied, including the pure triacylglycerols, dry blends by mixing two pure triacylglycerols with different proportions, complex triacylglycerols mixtures and pure triacylglycerols dissolved in BBB.

For the samples under static environment, when the temperature increases the d-spacings for the peaks with small d-spacing increase. In the β form, for the peaks at 3.7 Å, the d-spacings increased by 7 pm to 12 pm for different triacylglycerol samples. For the peaks at 3.85 Å, the d-spacings increased by 4 pm to 6 pm as well. However, the d-spacings for other peaks remain unchanged or just have very small changes. This result can be found in β, β' and α polymorphs of triacylglycerols. It means that the energy between the molecules in nanocrystalline triacylglycerols changes but not in the same way in all directions. The positions and d-spacings of WAXD peaks are reversible with temperature. The reversibility of d-spacings of WAXD peaks indicates that the temperature effect on the WAXD peaks of nanocrystalline triacylglycerols can occur not just in one single

experiment or circumstance. For the complex triacylglycerol mixtures like cocoa butter and 99% dark chocolate, these phenomena can also be observed. Due to the complexity of cocoa butter and chocolate the changes of d-spacings are harder to distinguish than the pure triacylglycerols and dry blends.

The unit cell values of β form TAGs from the d-spacings are calculated using the Miller indices to understand the reason why the d-spacing of WAXD peaks change in different ways. It shows in *a* and *b* direction, the crystal expands but in *c* direction the crystal contracts a little bit. Due to the lack of small angle x-ray diffraction data, how much *b* parameter really change remains unknown.

The intrinsic temperature of the triacylglycerol can be estimated from the differences of the d-spacings. It provides a new way to monitor and control the temperature of the system under study and the effect of high shear rate on nanocrystalline triacylglycerols crystallization. This will be useful to calculate the temperature of the triacylglycerol samples in different researches, especially the experiments applied high shear rate where the sample temperature is affected greatly by the viscous heat. It is particularly remarkable that the temperature dependency of Δd at 3.7 Å is identical for all the pure samples and for most of the dry blends. A simple quadratic function has been used to describe this relationship, as shown in Figure 4-13 and Figure 5-15. It is also useful that Δd at 3.85 Å depends on Δd at 3.7 Å. This can improve the quality of the fit of the peaks, since the relative position of the peaks can be estimated.

For the samples under shear flow, d-spacings of the peaks with small d-spacing also show a great dependence on temperature. The d-spacings keep increasing when the temperature increases. But at higher shear rate, the crystallization is not as obvious as that at lower shear rate.

The differences of d-spacings under static environment were compared with Δd obtained under shear flow. The differences of d-spacings under shear flow are smaller than that under static environment. When the shear flow is applied to the sample, the differences of d-spacings decrease. After comparing the differences of d-spacing under different shear rate, the differences of d-spacings are larger at higher shear rate under the same temperature, especially the WAXD peaks at 3.7 Å. But since the lack of data of lower shear rate, it is hard to draw a conclusion about how different shear rate affect the d-spacing at the same experiment temperature. The differences of d-spacings at 50 r/s shear rate are higher than the differences of d-spacings at 40 r/s shear rate. This can be used to estimate the increase in temperature. This is a considerable progress, even though it is necessary to improve the method.

As what has been found under static environment, when the shear is applied to the crystallized samples, the temperature is a function of the differences of d-spacings of the peaks with small d-spacing mathematically. It provides a new way to estimate the temperature and the effect of high shear rate on nanocrystalline triacylglycerols crystallization.

From the experiment data, it is clear that not only d-spacing, but also the FWHM of WAXD peaks change with temperature. In order to get a better understanding of the temperature effect on WAXD peaks, deeper study on the FWHM of WAXD peaks must be done in the future. To reveal how the TAG crystal lattices expand, more experiments using the small angle of x-ray diffraction must be done as well in the future. With the combination of wide and small angle x-ray diffraction, the change of different structure parameters of TAG crystal lattices can be fully understood. This temperature dependence studies will shed additional light on the nanostructural characteristics of these crystalline

materials.

BIBLIOGRAPHY

Acevedo, N. C. & Marangoni, A.G. (2010). Characterization of the Nanoscale in Triacylglycerol Crystal Networks. *Crystal Growth & Design,* Vol. 10, No. 8: 3327–3333.

Adam-Berret, M., Rondeau-Mouro, C., Riaublancb, A. & Mariette, F. (2008). Study of triacylglycerol polymorphs by nuclear magnetic resonance: effects of temperature and chain length on relaxation parameters. *Magnetic Resonance in Chemistry.* 46: 550–557.

Arishima, T., Sugimoto, K., Kiwata, R., Mori, H., & Sato, K. (1996). 13C cross-polarization and magic-angle spinning nuclear magnetic resonance of polymorphic forms of three triacylglycerols. *Journal of the American Oil Chemists' Society.* 73:1231-1236.

Bragg, W. L. (1913). The Structure of Some Crystals as Indicated by Their Diffraction of x-rays. *Proceedings of the Royal Society of London.* 89 (610): 248.

Cullity, B. D., & Stock, S. R. (2001). Geometry of Crystals. *Elements of x-ray diffraction 3rd edition.* Upper Saddle River, NJ: Prentice Hall. Chapter 2.

De Jong, S. & Van Soest, T. C. (1978). Crystal structures and melting points of saturated triglycerides in the β -2 phase. *Acta Cryst*. B34, 1570–1583.

Dhonsi, D., & Stapley, A. G. F. (2006). The effect of shear rate, temperature, sugar and emulsifier on the tempering of cocoa butter. *Journal of Food Engineering.* 77: 936–942.

Garti, N. & Widlak, N. R. (2012). Polymorphism and Mixing Phase Behavior of Major Triacylglycerols of Cocoa Butter. *Cocoa butter and related compounds.* Urbana, IL: AOCS Press. Chapter 6.

Gibon, V., Blanpain, P., Norberg, B. & Durant, F. (1984). New Data About Molecular Structure of β-Trilaurin. *Bull. Soc. Chim. Belg.* 93, 27-34.

Guthrie, S. E., Mazzanti, G., & Idziak, S. H. J. (2005). X-ray phase identification of chocolate is possible without the removal of sugar. *Eur. J. Lipid Sci. Technol.* 107: 656–659.

Hagemann, J. W., & Rothfus, J. A. (1993). Transitions of saturated monoacid triglycerides: Modeling conformational change at glycerol during α → β' → β transformation. *Journal of the American Oil Chemists' Society*. v70 n3: 211-217.

Hammond, R., Pencheva, K., Roberts, K. J., Mougin, P., & Wilkinson, D. (2005). An examination of the thermal expansion of urea using high-resolution variable-temperature X-ray powder diffraction. *Journal of Applied Crystallography.* 38: 1038–1039.

Himawan, C., Starov, V. M., & Stapley, A. G. F. (2006). Thermodynamic and kinetic aspects of fat crystallization. *Science Advances in Colloid and Interface.* 122: 3-33.

Idziak, S. H. J. (2003) Orientation and phase transitions of fat crystals under shear. Crystal *Growth and Design*. 3(5): 721–725.

Jensen, L. H., & Mabis, A. J. (1966). Refinement of the Structure of β-Tricaprin. *Acta Cryst*. 21: 770-781.

Kellens, M., Meeussen, W., Riekel, C., & Reynaers, H. (1990). "Time resolved x-ray diffraction studies of the polymorphic behaviour of tripalmitin using synchrotron radiation." Chemistry and Physics of Lipids. 52: 79—98.

Kellens, M., Meeussen, W., & Reynaers, H. (1991). Crystallization and phase transition studies of tripalmitin. *Chemistry and Physics of Lipids*. 55: 163—178.

Koberl, M., Hinz, H. J., & Rapp, G. (1998). Temperature scanning simultaneous small- and wide-angle x-ray scattering studies on glycolipid vesicles: areas, expansion coefficients and hydration. *Chemistry and Physics of Lipids*. 91: 13–37.

Larsson, K. (1971). Hydrocarbon Chain Conformation in Fats. *Chemica Scripta*. 1: 21-23.

Li, M. (2011). *Rheo-NMR and synchrotron x-ray diffraction characterization of nanostructures of triglycerides crystallizing from solutions.* Dalhousie Univerisity.

MacMillan, S. D. & Roberts, K. J. (2002). In Situ Small Angle x-ray Scattering (SAXS) Studies of Polymorphism with the Associated Crystallization of Cocoa Butter Fat Using Shearing Conditions. *Crystal Growth & Design.* Vol. 2, No. 3: 221-226.

MacMillan, S. D. & Roberts, K. J. (2003). Identification of the Initial Nucleating Form Involved in the Thermal Processing of Cocoa Butter Fat as Examined Using Wide Angle x-ray Scattering (WAXS). *Crystal Growth & Design*. Vol. 3, No. 2: 117-119.

Marangoni, A.G., & Rousseau, D. (1999). Plastic Fat Rheology Is Governed by the Fractal Nature of the Fat Crystal Network and by Crystal Habit. P*hysical Properties of Fats, Oils, and Emulsifiers*. AOCS Press, Champaign. 96–111.

Marangoni, A. G., & Wesdorp, L. H. (2013) "Nucleation and Crystalline Growth Kinetics". *Structure and properties of fat crystal networks.* CRC Press. Chapter 2.

Mazzanti, G., Guthrie, S. E., Sirota, E. B., Marangoni, A. G., & Idziak, S. H. J. (2004). Novel Shear-Induced Phases in Cocoa Butter. *Crystal Growth and Design*. 4(3): 409–411.

Mazzanti, G., Guthrie, S. E., Sirota, E. B., Marangoni, A. G., & Idziak, S. H. J. (2004). A Conceptual Model for Shear-Induced Phase Behavior in Crystallizing Cocoa Butter. *Crystal Growth and Design*. 7(7): 1230–1241.

Mazzanti, G., Marangoni, A. G., & Idziak, S. H. J. (2005). Modeling phase transitions during the crystallization of a multicomponent fat under shear. *Physical Review*. E71, 041607.

Mazzanti, G., Welch, S. E., Sirota, E. B., Marangoni, A. G., & Idziak, S. H. J. (2005). Crystallization of bulk fats under shear. *Soft Materials Structure and Dynamics*. N.Y., Marcel Dekker, Inc. Chapter 3.

Mazzanti, G., Mudge, E. M., & E. Y. Anom (2008). In Situ Rheo-NMR Measurements of Solid Fat Content. *Journal of American Oil Chemists' Society* 85: 405-412.

Mazzanti, G., Marangoni, A. G., & Idziak, S. H. J. (2009). Synchrotron study on crystallization kinetics of milk fat under shear flow. *Food Research International*. 42: 682–694.

Mazzanti, G., Li, M., Marangoni, A. G., & Idziak, S. H. J. (2011). Effects of Shear Rate Variation on the Nanostructure of Crystallizing Triacylglycerols. *Crystal Growth and Design*. 11: 4544–4550.

Narine, S. S., Marangoni, A.G. (1999). Relating structure of fat crystal networks to mechanical properties: a review. *Food Research International*. 32: 227-248.

Riiner, U. (1970). Investigation of the phase behavior of Cruciferae seed oils by temperature programmed x-ray diffraction. *Journal of the American Oil Chemists' Society*. 47(4): 129-133.

Sato, K. (1993). Polymorphic transformations in crystal growth. *Journal of Physics. D: Applied Physics.* 27: B77-B84.

Sato, K. (2001). Crystallization behaviour of fats and lipids - a review. *Chemical Engineering Science.* 56: 2255-2265.

Sato, K. (2001). Molecular Aspects in Fat Polymorphism. *Crystallization and solidification properties of lipids.* Conference publication: English. Chapter 1.

Sato, K. & Ueno, S. (2005). Polymorphism in Fat and Oils. *Bailey's Industrial Oil and Fat Products*. F.B. Shahidi, Editor, Wiley Interscience, New York. Chapter 3.

Shimazu, A., Miyazaki, T., & Ikeda, K. (2000). Interpretation of d-spacing determined by wide angle x-ray scattering in 6FDA-based polyimide by molecular modeling. *Journal of Membrane Science.* 166: 113–118.

Sirelli, L., Pereira, R. A., Perez, C. A., & Dias, M. L. (2006). Thermal Behavior of Poly(ethylene terephthalate) Crystalline and Amorphous Phases by Wide Angle x-ray Scattering. *Journal of Macromolecular Science.* Part B: Physics, 45:343–359.

Sirota, E. B., & Herhold, A. B. (2000). Transient rotator phase induced nucleation in *n*-alkane melts. *Polymer.* 41: 8781-8789.

Skoda, W., Hoekstra, L. L., Van Soest, T. C., Bennema, P. & Van den Tempel, M. (1967). Structure and morphology ofβ-crystals of glyceryl tristearate *Kolloid Z. Z. Polym.* 219, 149-156.

Stapley, A. G. F., Tewkesbury, H., & Fryer, P. J. (1999). "The Effects of Shear and Temperature History on the Crystallization of Chocolate." Journal of American Oil Chemists' Society 76: 677-685.

Takeuchi, M., Ueno, S., & Sato, K. (2003). Synchrotron Radiation SAXS/WAXS Study of Polymorph-Dependent Phase Behavior of Binary Mixtures of Saturated Monoacid Triacylglycerols. *Crystal Growth and Design.* 3(3): 369.

Templin, P. R. (1956). Coefficient of Volume Expansion for Petroleum Waxes and Pure n-Paraffins. *Industrial & Engineering Chemistry*. v48 n1: 154-161.

Toro-Vazquez, J. F., Dibildox-Alvarado, E., Herrera-Coronado, V., & Charó-Alonso, M. A. (2001). Triacylglyceride Crystallization in Vegetable 0ils: Application of Models, Measurements, and Limitations. *Crystallization and solidification properties of lipids.* Conference publication: English. Chapter 5.

Toro-Vazquez, J. F., Dibildox-Alvarado, E., Charó-Alonso, M., Herrera-Coronado, V., & Gómez-Aldapa, C. A. (2002). The Avrami Index and the Fractal Dimension in Vegetable Oil Crystallization. *JAOCS*. Vol.9, no. 9: 855–866.

Van Langevelde, A., van Malssen, A. K.. Hollander, F., Peschara, R. & Schenk, H. (1999). Structure of mono-acid even-numbered b-triacylglycerols. *Acta Cryst.* B55: 114-122.

Vand, V. & Bell, I. P. (1951). A direct determination of the crystal structure of the β form of trilaurin. *Acta Cryst*. 4: 465-469.

Wang, F. C., Johnson, M. B. & Mazzanti, G. (2011). Viscous heating in a mini-Couette cell used in Rheo-XRD and Rheo-NMR research.

Wright, A. J., Hartel, R. W., Narine, S. S., & Marangoni, A. G. (2000). The Effect of Minor Components on Milk Fat Crystallization. *JAOCS*, Vol. 77, no. 5: 463-475.

APPENDIX A WAXD PATTERN FITTINGS AND CALIBRATIONS

Centering the capillary

After putting the capillary into the holder, we need to center the capillary to make sure it is in the middle of the detector to get the most accurate image.

First, move the detector to where the x-ray beam pass through and immobilize the detector. Turn on the detector and adjust the voltage to the level of 9000V.

Second, use the instruction code “so” to turn on the x-ray shutter, generate the x-ray and get the graph of x-ray intensity, shown as Figure A-A-1. The position where we get the lower intensity of the x-ray is the center of the capillary.

Third, after we get the center of the capillary, use the instruction code “umv” to move the motor to the center of the capillary.

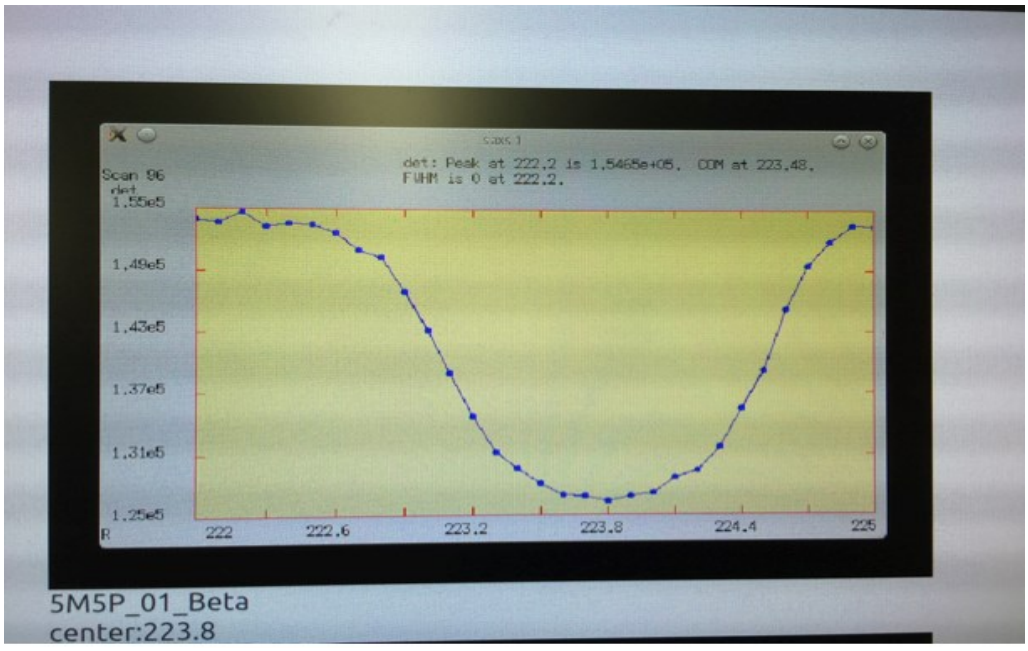

Figure A - 1 Center of the capillary of β form 5M5P.